CHEMICAL REVIEWS

Review

pubs.acs.org/CR

Amyloid β Protein and Alzheimer's Disease: When Computer Simulations Complement Experimental Studies

Jessica Nasica-Labouze,[†] Phuong H. Nguyen,[†] Fabio Sterpone,[†] Olivia Berthoumieu,[‡] Nicolae-Viorel Buchete,[§] Sébastien Coté,[∥] Alfonso De Simone,[⊥] Andrew J. Doig,[#] Peter Faller,[‡] Angel Garcia,[▽] Alessandro Laio,[○] Mai Suan Li,[◆,¶] Simone Melchionna,[⬠] Normand Mousseau,[§] Yuguang Mu,[▲] Anant Paravastu,[◇,⊕] Samuela Pasquali,[†] David J. Rosenman,[●] Birgit Strodel,[△] Bogdan Tarus,[†] John H. Viles,[▼] Tong Zhang,[†,▲] Chunyu Wang,[◇] and Philippe Derreumaux*[,†,□]

[†]Laboratoire de Biochimie Théorique, Institut de Biologie Physico-Chimique (IBPC), UPR9080 CNRS, Université Paris Diderot, Sorbonne Paris Cité, 13 rue Pierre et Marie Curie, 75005 Paris, France

[‡]LCC (Laboratoire de Chimie de Coordination), CNRS, Université de Toulouse, Université Paul Sabatier (UPS), Institut National Polytechnique de Toulouse (INPT), 205 route de Narbonne, BP 44099, Toulouse F-31077 Cedex 4, France

[§]School of Physics & Complex and Adaptive Systems Laboratory, University College Dublin, Belfield, Dublin 4, Ireland

[∥]Département de Physique and Groupe de recherche sur les protéines membranaires (GEPROM), Université de Montréal, C.P. 6128, succursale Centre-ville, Montréal, Québec H3C 3T5, Canada

[⊥]Department of Life Sciences, Imperial College London, London SW7 2AZ, United Kingdom

[#]Manchester Institute of Biotechnology, University of Manchester, 131 Princess Street, Manchester M1 7DN, United Kingdom

[▽]Department of Physics, Applied Physics, & Astronomy, and [●]Department of Biology, Rensselaer Polytechnic Institute, Troy, New York 12180, United States

[○]The International School for Advanced Studies (SISSA), Via Bonomea 265, 34136 Trieste, Italy

[◆]Institute of Physics, Polish Academy of Sciences, Al. Lotnikow 32/46, 02-668 Warsaw, Poland

[¶]Institute for Computational Science and Technology, SBI Building, Quang Trung Software City, Tan Chanh Hiep Ward, District 12, Ho Chi Minh City, Vietnam

[⬠]Instituto Processi Chimico-Fisici, CNR-IPCF, Consiglio Nazionale delle Ricerche, 00185 Roma, Italy

[▲]School of Biological Sciences, Nanyang Technological University, 60 Nanyang Drive, 637551 Singapore

[◇]Department of Chemical and Biomedical Engineering, Florida A&M University-Florida State University (FAMU-FSU) College of Engineering, 2525 Pottsdamer Street, Tallahassee, Florida 32310, United States

[⊕]National High Magnetic Field Laboratory, 1800 East Paul Dirac Drive, Tallahassee, Florida 32310, United States

[△]Institute of Complex Systems: Structural Biochemistry (ICS-6), Forschungszentrum Jülich GmbH, 52425 Jülich, Germany

[▼]School of Biological and Chemical Sciences, Queen Mary University of London, London E1 4NS, United Kingdom

[□]Institut Universitaire de France, 75005 Paris, France

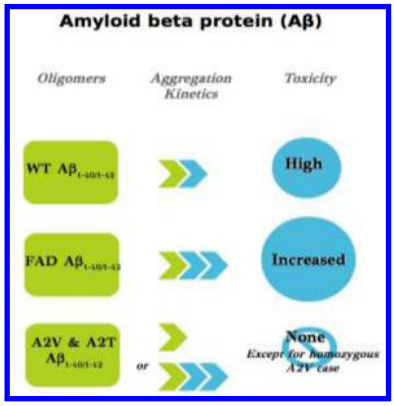

CONTENTS

Received: November 7, 2014
Published: March 19, 2015

DOI: 10.1021/cr500638n
Chem. Rev. 2015, 115, 3518−3563

1. INTRODUCTION

Alzheimer's disease (AD) challenges our society with an annual estimated cost of $1.08 trillion in the United States alone by 2050.[1] AD is a progressive irreversible neurological disorder with marked atrophy of cerebral cortex and loss of cortical and subcortical neurons, which is characterized pathologically by accumulation of amyloid plaques and numerous neurofibrillary tangles formed from filaments of microtubule-associated highly phosphorylated Tau proteins.[2] The pathogenesis of AD includes other factors such as cholinergic malfunction and oxidative stress.[3]

The major constituents of the senile plaques are amyloid β (Aβ) peptides of 39−43 amino acids. Aβ derives from cleavage of the transmembrane amyloid precursor protein (APP), located in chromosome 21, by β-secretase (BACE1), producing a 99 amino acid fragment (C99) that is further cleaved by the γ-secretase.[4] The human Aβ1−42 wild-type (WT) sequence is DAEFRHDSGYEVHHQKLVFFAEDVGSNKGAIIGLM-VGGVVIA. Five drugs are currently available for AD. These include four cholinesterase inhibitors, donepezil, reminyl, razadyne, and rivastigmine, and the *N*-methyl-D-aspartate (NMDA) receptor antagonist memantine. However, they are only effective for 6−12 months and for half of the patients with milder forms of Alzheimer's.[5] Scientists are developing novel benzopolycyclic amines with increased NMDA receptor antagonist activity[6] and are targeting BACE1[7] and Tau and Aβ proteins.[8,9] Despite many in vitro and in vivo studies, drug after drug has failed to slow the progression of AD for several reasons.

First, while oligomers such as dimers, trimers, and 12-mers (Aβ*56) are the most critical players in the pathology of AD[10,11a,b] and larger aggregates and fibril fragmentation are toxic as well,[12,13] there is currently little information on their rate and extent of formation. Experimental and theoretical studies showed that Aβ1−40/1−42 peptides self-assemble into amyloid fibrils by a nucleation−condensation polymerization mechanism. However, while master equations allow interpretation of the experimental sigmoidal kinetic profiles of amyloid formation by means of primary and/or secondary (fragmentation or lateral) nucleation processes,[14−16] they do not provide any information on the 3D topology and size of the primary nucleus. Overall, probing the conformational changes of Aβ aggregation is challenging owing to the vast heterogeneity of the aggregates, the number of substates for each aggregate, and the sensitivity of the process to pH, agitation, temperature, concentration, ionic strength, surfactants, sample preparation, and the sequence (Aβ1−40 vs Aβ1−42).[17−19]

Second, standard tools of structural biology have failed to provide the 3D structures of the monomers and the oligomers of the Aβ1−40/1−42 peptides in aqueous solution. Aβ monomer is described as a random coil by solution nuclear magnetic resonance (NMR)[20] and circular dichroism (CD).[21] Due to their heterogeneity and high propensity to aggregate, the low molecular weight Aβ oligomers are not amenable to NMR and X-ray crystallography. As a result, only low-resolution structural data from CD, ion mobility mass spectrometry (IM-MS), electron microscopy (EM), transmission electron microscopy (TEM), and atomic force microscopy (AFM) measurements are available.[11,20−26] At the end of the reaction, the fibrils are insoluble, and we are left with complicated experiments using isotopic labeling to propose models. These experiments revealed that fibrils of synthetic Aβ1−42 peptides have U-shaped conformations with β-strands at residues L17−F20 and I31−V40 with the 16 N-terminal residues disordered, while fibrils of synthetic Aβ1−40 peptides have β-strands at Y10−D23 and A30−G38 with the 9 N-terminal residues disordered.[27,28] Fibrils made of AD-brain-derived Aβ1−40 peptides show, however, deformed U-shaped conformations, with a twist in residues F19−D23, a kink at G33, and a bend at G37−G38 and a more ordered N-terminus.[29] Overall, the final products are very sensitive to the nature of the sample (synthetic or brain-derived Aβ peptides). Fibril formation is also under kinetic control rather than thermodynamic control, adding further complexity to the determination of the physical factors governing Aβ1−40/1−42 amyloid fibril formation.[17,30]

Third, because of their presence in the brain, the metal ions Cu^{2+}, Zn^{2+}, and Fe^{3+} and the cell membrane have to be considered. A full dynamic and thermodynamic picture of the interactions of Aβ1−40/1−42 oligomers with metal ions or the membrane is very difficult, but recent progress has been made.[31,32]

Fourth, it is important to better understand the molecular interactions of Aβ oligomers with the proteins colocalized in the brain and notably human serum albumin,[33] the most abundant protein in cerebral spinal fluid, and the prion protein (PrP), concentrated at the synaptic terminals with a high affinity for Aβ.[34,35] Mapping all partners that bind to Aβ oligomers is a daunting task because disparate results can emerge from experiments depending on the initial state of the protein, its source, and its stoichiometry.[36] In addition, as functional genomics has taught us,[37] biomolecules are involved in a network of interactions, so toxicity is likely to be multifactorial and to result from interactions of Aβ with multiple partners. Three recent papers illustrate this fea-

DOI: 10.1021/cr500638n
Chem. Rev. 2015, 115, 3518−3563

ture.[38−40] Murine-paired immunoglobulin-like receptor B and its human orthologue leukocyte immunoglobulin-like receptor B2 were identified as receptors for Aβ oligomers, with nanomolar affinity.[38] Aβ oligomers also induce synaptic damage via Tau-dependent microtubule severing by tubulin-tyrosine-ligase-like-6 and spastin,[39] and Aβ oligomer−PrP complexes generate metabotropic glutamate receptor 5-mediated increases of intracellular calcium.[40] Finally, among the apolipoprotein E (apoE) isoforms, apoE4 increases the risk of AD. While transporting cholesterol is its primary function, apoE regulates Aβ metabolism, aggregation, and deposition and competes with Aβ for cellular uptake through apoE receptors.[41] Overall, our current structural knowledge of Aβ oligomers with receptors is still in its infancy.

Fifth, the summer of 2012 was plagued by the release of bad news from clinical trials of two drugs targeting Aβ, bapineuzumab and solanezumab.[42] The general consensus for a couple of years has been that the drugs are given too late.[43] Scientists have failed to provide the structures of Aβ monomers or Aβ oligomers with known inhibitors of Aβ aggregation in vitro and toxicity, a prerequisite to develop more specific drugs with optimal affinities for Aβ oligomers.[44]

In addition, working on the most abundantly produced species, Aβ1−40, and the far less abundant but more aggregation prone and toxic form, Aβ1−42, is a simplification as the γ-secretase generates peptides from Aβ1−36 to Aβ1−43.[45] Several truncated variants are also observed in the amyloid plaques with various populations. These include Aβ4−42 and Aβ5−42,[46] Aβ1−26 and Aβ1−30,[40] and post-translational modifications of Aβ peptides: isomerization at D1, phosphorylation at S26, a dityrosine covalent bond at Y10, and proteolytic removal of D1 and A2 and the subsequent cyclizing of E3 and E11 to a pyroglutamate (designated Aβ3(pE) and Aβ11(pE)), among others.[47−49] The Aβ(pE) species in vivo consist of Aβ3(pE)-40/42 and Aβ11(pE)-40/42, with Aβ3-(pE)-42 being the most abundant. Aβ(pE) is more cytotoxic and aggregates more rapidly than conventional Aβ, and a recent study raises the possibility that Aβ3(pE)-42 formation acts at a primary step in AD pathogenesis.[50]

Finally, while most Alzheimer's disease is sporadic, i.e., not the result of inheritance (familial AD (FAD) represents 5% of the cases), we have learned a large amount about the genetic risk factors that predispose an individual to contract the disease. One of the major risk factors for AD is mutation in the APP gene, though many mutations in two presenilin genes have also been reported and are constantly discovered.[51] Mutant APP may be more likely to be proteolytically cleaved into the Aβ form, which generates the amyloid plaques. Some familial mutations, including H6R (English), D7H (Taiwanese), D7N (Tottori), A21G (Flemish), E22Q (Dutch), E22G (Artic), E22Δ (Osaka), and D23N (Iowa), change aggregation and toxicity and lead to different phenotypes.[52,53] Two recent FAD mutations, however, turn that inheritance pattern on its head. The A673V mutation in APP or A2V in Aβ is associated with AD, but the inheritance pattern is recessive; i.e., a patient needs two mutant alleles to acquire the disease risk. In combination with the WT allele, A673V does not cause AD. Furthermore, the presence of the mutant peptide prevents the WT peptide from forming amyloid fibrils, even under very favorable in vitro conditions.[54] The second striking result comes from the coding variants in APP in a set of whole-genome sequence data from 1795 Icelanders and the discovery that the mutation A673T in APP or A2T in Aβ protects against AD in both homozygous and heterozygous patients. Though A2T reduces the cleavage of APP by 40%, how the mixing of Aβ1−40 A2T and Aβ1−40 WT protects patients from AD remains to be determined.[55]

Overall, a full understanding of AD within the amyloid cascade hypothesis requires the development and use of innovative biophysical techniques. Along with standard approaches, e.g., Fourier transform infrared spectroscopy (FTIR), CD, X-ray powder diffraction, TEM, AFM, solid-state nuclear magnetic resonance (ss-NMR), dynamic light scattering (DLS), and IM-MS, new techniques are being applied. These include, notably, pulsed hydrogen/deuterium exchange coupled with mass spectrometry analysis,[56] which unlike fluorescence methods, does not require labeling with a fluorophore, photonic crystal-based approaches,[57] single-molecule imaging techniques,[58] and specific isotope labeling with electron paramagnetic resonance (EPR), advanced hyperfine sublevel correlation (HYSCORE), and electron−nuclear double resonance (ENDOR) methods.[59,60]

Experimental studies alone are not sufficient, however, since they generally give time- and space-averaged properties. Computer simulations by exploring different time and length scales can complement experiments. Simulations are very challenging due to the inherent flexibility and heterogeneous ensemble of the Aβ1−40/1−42 monomers and oligomers and the impact of a crowded environment. As a result, we need to develop and/or use various protein representations ranging from all-atom and coarse-grained (CG) to mesoscopic models and improve sampling techniques to converge rapidly to equilibrium and explore the dynamics over a wide range of time scales.[44,61]

In summary, we provide an in-depth review on the contribution of biophysical and biochemical studies and computer simulations to characterize the molecular structures of Aβ1−40/1−42 monomers, oligomers, protofibrils, and amyloid fibrils in aqueous solution. We then focus on our current knowledge of the Aβ1−40/1−42 nucleus and the structures and dynamics of Aβ1−40/1−42 oligomers in proximity of or at the membrane. We summarize what is known about the interactions of Aβ monomers and oligomers with ion metals, cellular partners, and potential inhibitors. We also report the main findings of the simulations on FAD mutations and conclude by offering a perspective on the future of the field and the major questions that need to be addressed to discover drugs with much higher efficacy.

2. MOLECULAR STRUCTURES OF Aβ1−40 AND Aβ1−42 FIBRILS TO MONOMERS FROM EXPERIMENTS

Experimental characterization of amyloid fibril structures has been the topic of extensive research for decades, producing remarkable molecular-level insights.[62−65] Nonfibrillar monomer and oligomer structures, in contrast, are not well understood. We summarize the major findings on Aβ1−40/1−42 molecular structure from monomers to fibrils with emphasis on the most recent results. Structural understanding of Aβ fibrils and insights into the self-assembly process establish a basis for addressing the challenges associated with determining the structures of Aβ protofibrils and low molecular weight oligomers.

2.1. Fibrils

Due to the incompatibility of amyloid fibrils with X-ray crystallography and solution-state NMR, there is no single

DOI: 10.1021/cr500638n
Chem. Rev. 2015, 115, 3518−3563

technique able to readily provide enough structural information to fully specify molecular structure within Aβ fibrils. Our structural knowledge of Aβ amyloid fibrils, therefore, is derived from the integration of complementary information from different experimental techniques. Fibril dimensions (nanometer length scale) have been probed by EM and AFM.[27,66−68] Fibril mass can be quantitatively measured by scanning TEM and, more recently, tilted beam TEM.[69] 2D structure (mostly β-strand) has been probed by FTIR.[70,71] This technique, along with diffraction-based measurements, hydrogen/deuterium exchange, mutagenesis, proteolysis, EPR, and ss-NMR, can provide information on molecular fold and intermolecular packing (β-sheet formation and organization).[25,27,71−79] Fiber diffraction studies established the "cross-β" structure, in which Aβ molecules assemble into β-sheets with β-strands oriented perpendicular to the long axis of the fibril.[72,80−82] The β-sheet structure was further confirmed by the binding of β-sheet-specific dyes such as thioflavin-T and Congo red.[70] It should be noted that Sawaya et al. used X-ray diffraction to measure the detailed cross-β structures of microcrystals of several short peptides forming amyloid fibrils.[83] The data provide atomic details of "steric zippers" created by packing of interdigitated side chains between stacked β-sheets, described in terms of eight possible symmetry classes. The free energies of different steric zipper configurations were also calculated using all-atom molecular dynamics (MD) simulations. Comparisons to experimental results suggest that the observed amyloid-like crystals are thermodynamically stable, although kinetic trapping can be driven by electrostatic side chain interactions.[84]

Among the experimental techniques mentioned here, ss-NMR has provided the most atomic-level detail of Aβ amyloid fibrils. This technique is well suited for amyloid fibrils because it provides information on local structure without requiring long-range orientation order.[85] In 1998, Benzinger used $^{13}C-^{13}C$ dipolar recoupling ss-NMR data on Aβ10−35 fibrils to challenge the then common belief that Aβ amyloid fibrils are composed of antiparallel β-sheets.[86] This preference for antiparallel β-sheets originates from earlier interpretations of FTIR data, the intuition that like-charged side chains are unlikely to be in close proximity, and NMR studies of the Aβ34−42 fibril.[71,87−89] Controversy over the arrangement of β-strands within Aβ amyloid fibrils further motivated the development of improved measurements for nuclear magnetic dipolar interactions[90−92] and more analysis of Aβ fragments.[85,93,94a] It was found that the Aβ1−28 peptide forms in-register parallel β-sheets, in which β-strands are aligned for close proximity between like residues.[95,96] The in-register parallel configuration which maximizes overlap of hydrophobic residues influenced the view that amyloid formation is driven by hydrophobic interactions.[68,85] A recent review on FTIR examines the experimental complications leading to incorrect assignment of antiparallel β-sheets and describes more reliable approaches to data interpretation.[63]

In 2002, Petkova et al. reported a molecular model of an Aβ1−40 fibril based on constraints obtained from ss-NMR and EM.[27] This model refined subsequently with additional NMR constraints[79] reported an unstructured peptide for the first 10 residues with two β-strands (residues 11−24 and 30−40), as shown in Figure 1A. The first 10 residues were assigned as unstructured because isotopic labeling (^{13}C and ^{15}N) yielded NMR signals that were either broad (static disorder) or not observed (dynamic disorder).[27] The β-strands form in-register parallel β-sheets to produce the protofilament (Figure 1B).

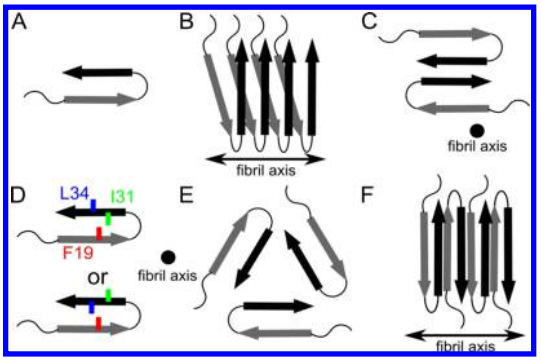

Figure 1. Schematics describing known structural motifs for Aβ1−40 WT and Aβ1−40 D23N fibrils. Arrows, thin lines, and colored symbols represent β-strand regions, non-β-strand regions, and selected residues, respectively. (A) Molecular conformation of Aβ molecules within fibrils, with arrows representing β-strand regions. (B) Organization of Aβ monomers into a protofilament. Each Aβ peptide contributes two β-strands to two stacked in-register parallel β-sheets, with hydrogen-bonding interactions between equivalent β-strands along the fibril axis. (C) Cross-section of the Aβ1−40 fibril model of Petkova et al. composed of two protofilaments.[27,29] (D) Two distinct side chain arrangements experimentally observed for different Aβ1−40 fibrils. (E) Fibril cross-section predicted of the Aβ1−40 model determined by Paravastu et al. and composed of three protofilaments.[67] (F) Antiparallel β-sheet arrangement reported by Qiang et al. for fibrils of the Iowa Aβ1−40 D23N peptide.[29,101]

Protofilaments associate in pairs to form the 2-fold topology for the striated fibrils (Figure 1C). The turn region (residues 25−29) is stabilized by a salt bridge between the charged D23 and K28 side chains. Note that Nussinov et al. also proposed in 2002 the in-register parallel motif on the basis of MD simulations using several topologies.[94b]

The structural model of Petkova does not describe, however, every Aβ1−40 fibril because fibrils are polymorphic. Polymorphism refers to the existence of multiple pathways for self-assembly, producing assemblies that differ in molecular structure. When observed by EM or AFM, distinct fibrils are observed with various width, twist, and cross-section dimensions.[27,66−68] Multiple fibril polymorphs usually coexist within the same samples, although many samples are characterized by a dominant fibril polymorph. Petkova showed that subtle environmental factors such as solution agitation can produce samples with different predominant fibril morphologies (2-fold symmetry under agitation and 3-fold symmetry under quiescent conditions) and that distinct NMR peak positions and line shapes indicate distinct underlying molecular structures.[27,29] Additional factors affecting fibril self-assembly are the pH, the presence of metal ions, and interaction with interfaces.[64,67,97] Furthermore, there is an inheritance of structure when fibrils of one morphology are used to seed the self-assembly of Aβ monomers into new fibrils.[27] Aβ fibril polymorphism was further characterized using cryo-EM by Meinhardt[66] and Paravastu[67] using ss-NMR. An important structural difference between different Aβ fibril polymorphs lies in the orientations of the residues within the β-strands and the presence or absence of the D23−K28 salt bridge (Figure 1D). By taking advantage of observed differences in seeding efficiencies between different fibril polymorphs and using quiescent conditions, Paravastu isolated a new Aβ1−40 fibril with a 3-fold symmetric cross-section (Figure 1E).[67] Bertini reported another Aβ1−40 fibril model with a topology similar to that of Petkova (Figure 1A-C), but with different atomic

DOI: 10.1021/cr500638n
Chem. Rev. 2015, 115, 3518−3563

details.[98] An Aβ1−42 fibril model with a similar configuration was also published by Luhrs, based primarily on hydrogen/deuterium exchange and mutagenesis data, but with different residues in the β-strand and turn regions.[28] While this model differs from structures observed for Aβ1−40, it is not clear how the ranges of possible Aβ1−40 and Aβ1−42 fibril structures could differ. The symmetries of all the experimentally constrained Aβ fibril structural models predict a single molecular conformation. Thus, detection of multiple NMR signals from each labeled site is normally assumed to imply polymorphism within the sample. Contrary to this interpretation, Lopez del Amo et al. recently published an NMR-derived fibril composed of Aβ molecules in two nonequivalent conformations.[99] An asymmetric fibril structure was also proposed by the theoretical work of Wu, but whether such Aβ fibril geometry is correct remains to be validated experimentally.[100]

The growing consensus that Aβ1−40 and Aβ1−42 fibrils are composed of in-register parallel β-sheets has recently been disrupted by recent reports on fibrils formed by the Iowa mutant (D23N) of the Aβ1−40 peptide.[29,101] This peptide forms fibrils composed of antiparallel β-sheets as depicted in Figure 1F. It was suggested that substitution of the positively charged D23 side chain with the uncharged N23 side chain affects the nucleation rate of the parallel β-sheet structure, which is stabilized by the D23−K28 salt bridge.[101] Interestingly, the parallel β-sheet structure remains the thermodynamically preferred structure for the D23N mutant, but antiparallel β-sheet fibrils propagate more slowly in seeding experiments and dissolve at the expense of parallel β-sheet fibrils in mixtures.[29]

Experimental observations of environment-dependent self-assembly led to questions about the biological relevance of structural information from in vitro generated Aβ samples. The use of repeated seeding steps to amplify early-nucleating or fast-growing fibrils within a sample, for example, could result in a kinetically favored structure, which may differ from the most thermodynamically stable structure. The theoretical work of Pellarin based on a mesoscopic model with one internal degree of freedom per peptide supports this notion, suggesting that less thermodynamically favored fibril structures could nucleate more rapidly.[102] In addition, the microenvironment in vivo is likely to differ significantly from environments accessible in vitro and may be affected by conditions promoted by Alzheimer's disease. Paravastu showed that amyloid plaques in the brains of deceased Alzheimer's patients could be isolated at concentrations high enough to seed the self-assembly of synthetic Aβ1−40 monomers, enabling the incorporation of isotopic labels into brain-derived fibril structures.[103] Lu analyzed fibril samples from the brains of two deceased Alzheimer's patients with distinct clinical histories.[29] ss-NMR analysis of brain-seeded fibrils indicates that plaques from each brain are characterized by a single predominant fibril structure, though polymorphism was also observed.[29,103] Dominant structures differed, however, between the two Alzheimer's brains. Lu established a constrained structural model for the brain-derived Aβ1−40 fibril composed of in-register parallel β-sheets.[29] Figure 2 compares the all-atom pictures of the brain-derived Aβ1−40 fibril model and the fibril models of the synthetic Aβ1−40 peptides determined by Paravastu and Petkova. Lu observed NMR signals consistent with an ordered structure for every residue in Aβ1−40 and particularly a structured N-terminal region in contrast to that of the synthetic Aβ1−40 fibrils.[29] How this N-terminal structure will change with the binding of metal ions remains, however, to be determined.

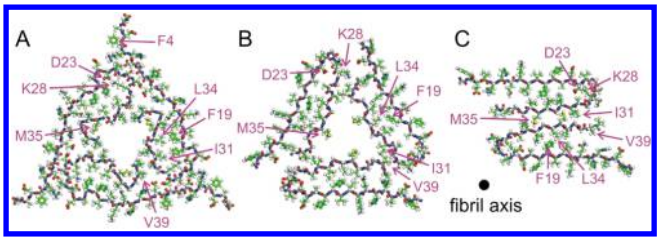

Figure 2. All-atom pictures of cross-sections of brain-derived Aβ1−40 fibrils modeled by Lu et al.[29] (A), compared to cross-sections of models for in vitro generated fibrils reported by Paravastu et al.[67] (B) and Petkova et al.[27] (C). The fibrils in (B) and (C) correspond to the diagrams shown in parts C and E, respectively, of Figure 1.

2.2. Protofibrils and Oligomers

Complexity in Aβ self-assembly was observed with the discovery of multiple soluble metastable Aβ oligomers at early and intermediate aggregation times.[104−108] While systematic classification of soluble Aβ species is difficult without more knowledge of the structure and assembly pathways, soluble Aβ aggregates are generally referred to as protofibrils or oligomers. Protofibrils have elongated aspect ratios and a curvilinear appearance.[106] They are argued to be "on-pathway" intermediates to amyloid fibril formation and are believed to convert to fibrillar structures without first dissociating to monomers.[106,108,109] Protofibrils have been reported to seed the growth of fibrils, have molecular masses near 250 × 10^3 kDa (~60 molecules), consist of β-sheets, and bind thioflavin-T.[110] Oligomers are smaller species, with molecular masses ranging from 9 kDa (Aβ dimers) to hundreds of kilodaltons (~50 Aβ molecules). While oligomers exhibit β-strand secondary structure when probed by FTIR and CD, they do not necessarily bind thioflavin-T or seed fibril formation.[63,111] These observations motivate the interpretation that at least some oligomers are "off-pathway" to fibril formation. Since fibril formation is accelerated by seed- or nucleus-dependent self-assembly, conversion of oligomers into fibrils is prolonged when oligomers are separated from fibrils and protofibrils; this separation is normally accomplished by size exclusion chromatography (SEC).[109] Species isolation and dynamics also increase structural homogeneity, which prevents structure elucidation. Oligomers have been further stabilized by cross-linking or interactions with engineered proteins.[112−114] Several protocols for production and isolation of oligomers have been reported, and the different oligomer products have been named amyloid-derived diffusible ligands, globulomers, amylospheroids, I_β, and annular protofibrils.[105,109,115−119]

Recent studies report structural characterization of protofibrils by ss-NMR. Scheidt stabilized Aβ1−40 protofibrils through interaction with an antibody-derived fusion protein (B10AP) and found ^{13}C NMR chemical shifts which differ from those observed for amyloid fibrils and also indicate shorter β-strand regions.[120,121] The ^{13}C NMR chemical shifts resemble reported values for Iβ oligomers, suggesting that protofibril structure more closely resembles oligomer structure than fibril structure.[121] Although I_β oligomers were reported to be composed of in-register parallel β-sheets, Scheidt et al. proposed an intramolecular antiparallel β-hairpin within Aβ oligomers.[112−114] This β-hairpin model (Figure 3A) predicts hydrogen bonding between β-strands in the same molecule,

DOI: 10.1021/cr500638n
Chem. Rev. 2015, 115, 3518−3563

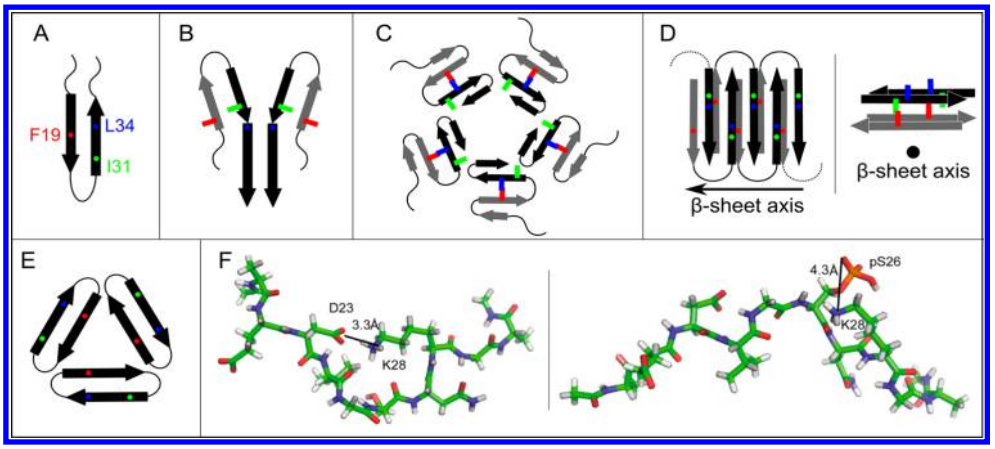

Figure 3. Proposed models for nonfibrillar Aβ aggregates. As in Figure 1, arrows, thin lines, and colored symbols represent β-strand and non-β-strand regions and selected residues, respectively. (A) Antiparallel β-hairpin conformation predicted by Hoyer et al. for the monomer[114] and suggested by Scheidt et al. for protofibrils.[120,121] (B) Dimer structure proposed for preglobulomers by Yu et al.[123] (C) Disk-shaped pentamer model proposed by Ahmed et al.[124] (D) Two different views of the antiparallel β-sheet model for 150 kDa oligomers, reported by Tay et al.[111] (E) X-ray crystallographic structure of the trimer of the designed cyclic Aβ17−36 peptide.[125] (F) Representative structures of highest populations in the MD ensembles of the Aβ21−30 WT peptide with the D23−K28 salt bridge (left) and the Aβ21−30 peptide with pS26 substitution (right).[47]

which does not occur in the fibril structural models (Figure 1). Structural similarity between B10AP-stabilized Aβ1−40 oligomers and protofibrils was supported by intramolecular proximity between E22 and I31 observed for both structures.[120] Although these results do not specify how neighboring Aβ molecules are arranged within protofibrils or oligomers, they suggest that structural rearrangement is required for protofibrils to convert to fibrils. Further evidence for structural reorganization from protofibrils to fibrils was found by Doi using lyophilization to stabilize Aβ1−42 protofibrils and ss-NMR to show that protofibrils are not composed of in-register parallel β-sheets.[122]

The diagrams in Figure 3A−D depict alternative schemes for the intermolecular organization based on experimental data of Aβ1−42 oligomer samples. Hoyer observed that Aβ1−40, which is normally an unstructured monomer in solution, adopts an antiparallel β-hairpin conformation (Figure 3A) upon binding to an antibody-mimicking protein.[114] This result inspired the construction of a double cysteine Aβ mutant (at positions 21 and 30) that was constrained to adopt the β-hairpin conformation. This mutant was shown to form oligomers and protofibrils but not fibrils.[112,113] Yu performed solution NMR on preglobulomers produced through interactions between *N*-Met-Aβ42 (additional M residue on the N-terminus) and sodium dodecyl sulfate (SDS) micelles (0.2% SDS by weight), resulting in the proposed model shown in Figure 3B.[123] This model also predicts intramolecular hydrogen bonds to produce an antiparallel β-hairpin between β-strands spanning residues 17−23 and residues 28−33. In addition, intermolecular parallel β-sheet contacts are predicted for pairs of β-strands formed by residues 34−42. While the preglobulomer molecular mass was measured to be 16 kDa (~4 Aβ molecules), it is not known how the dimer drawn in Figure 3B would assemble into a larger structure. In another study, Ahmed prepared Aβ1−42 pentamers by incubation of monomers at low temperature, and ss-NMR provided the basis for the model of Figure 3C.[124] This model does not include hydrogen bonds between any of the β-strands (no β-sheets). Another ss-NMR study conducted by Tay was based on 150 kDa (~33 Aβ molecules) oligomers produced using a procedure similar to that used for globulomers (removal of SDS from preglobulomer solutions by dialysis).[111] ss-NMR data were consistent with the molecular conformation found in fibrils (Figure 1A), but a significant distinction was reported in terms of intermolecular organization. Unlike fibrils, 150 kDa oligomers are not composed of in-register parallel β-sheets. Instead, Tay proposed the model shown in Figure 3D, with intermolecular antiparallel β-sheets.[111] Consistent with this interpretation, Gu used site-directed spin labeling and EPR on Aβ globulomers to show that their structures are not consistent with in-register parallel β-sheets, but rather antiparallel β-sheet structures.[59] Finally, Nowick et al. designed a macrocycle peptide derived from Aβ17−36 in which residues 17−23 and 30−36 form the β-strands with two δ-linked ornithine β-turns connecting the side chains of D23 with A30 and the side chains of L17 with V36. X-ray structure shows that trimers consist of three highly twisted β-hairpins in a triangular arrangement (Figure 3E), and four trimers form a 12-mer Aβ*56 species with a central cavity, one important species to impair memory.[125]

Despite significant advances, we emphasize that it is not yet clear how Aβ oligomer and protofibril structures can be distinguished. None of the diagrams in Figure 3 correspond to widely accepted models for Aβ protofibril or oligomer structures. In contrast, the fibril structures in Figures 1 and 2 benefitted from much more sample preparation experience and better optimized structural measurements. While the solution-NMR-derived model of Yu is based on many constraints,[123] the high concentration of SDS in the final sample is known to affect Aβ structure. The models in Figure 3A,D are works in progress, in need of many more structural constraints, including complete residue-specific information about secondary structure and experimental constraints on intermolecular packing. In fact, a recent proline mutagenesis study conducted by Haupt reported that oligomers might be distinguished from protofibrils by the structure of the N-terminus.[126] Using fluorescence correlation spectroscopy (FCS) and Förster resonance energy transfer (FRET), Maiti showed that the two hydrophobic regions (residues 10−21 and 30−40) have attained the β-strand conformation in both oligomers and fibrils. However, the conformations of the turn region (residues 22−29) and the N-terminal tail (residues 1−9) are markedly

DOI: 10.1021/cr500638n
Chem. Rev. 2015, 115, 3518−3563

different.[127a] The role of the turn region has also been emphasized by NMR and replica-exchange molecular dynamics (REMD) simulations, which demonstrate that phosphorylation at S26, which interferes with formation of the D23−K28 salt bridge, impairs Aβ1−40 fibrilization while stabilizing its monomer and nonfibrillar aggregates (Figure 3F).[47] Using pulse hydrogen/deuterium exchange MS, the middle region of Aβ1−40 (residues 20−35) was found to be the first to aggregate, followed by residues 36−42 and then the N-terminus (residues 1−19).[24]

It is interesting that these Aβ NMR-derived models from 4 to 33 peptides predict antiparallel β-sheets.[111,120,121,123,124] In some cases, the oligomers take up a β-hairpin structure.[123] This conformation is, however, very different from that in the fibrils. The overall topology looks similar, but the orientation of the hydrogen-bonding network and the side chain contacts are very different. This may be an important factor in the ability of the oligomers to insert into the membrane (because the only large family of membrane proteins with antiparalllel β-sheets consists of porins) and in the formation of the nuclei as described in section 5. Further support for antiparallel β-sheet arrangement of Aβ oligomers (Figure 3A,B,D) comes from FTIR[22] and X-ray crystallography data on a hexamer of a segment of αB crystallin (K11V).[127b] These X-ray diffraction results suggest that it may be possible to study Aβ oligomer structure by crystallography without any chemical modification,[125] and Aβ oligomers could adopt a structure similar to the cylindrical antiparallel β-sheet structure (or cylindrin) of the K11V peptide.[127b] Indeed, these β-barrels were predicted prior to the determination of the K11V peptide structure on several peptides by computer simulations using coarse-grained and all-atom representations in explicit and implicit solvent.[128−132,133a]

Atomistic characterization of the small and large Aβ1−40/1−42 oligomers is very difficult as these oligomers are highly aggregation-prone and degenerate by displaying multiple polymorphic structural variants analogous to strains in prion diseases. In a recent study, Glabe et al. designed 23 monoclonal antibodies against Aβ1−42 and showed that no single antibody is able to recognize the different states of Aβ1−42 in vitro and in AD brain.[133b] What is clear from various experiments is that synthetic Aβ1−40 and Aβ1−42 polymerize through distinct pathways. Photoinduced cross-linking of unmodified protein (PICUP) with a Y10−Y10 side-chain−side-chain bridge followed by SDS−polyacrylamide gel electrophoresis (PAGE), DLS, and SEC has been used to unveil the oligomer size distribution of Aβ oligomers.[134−136] A first study showed that Aβ1−40 exists as monomers, dimers, trimers, and tetramers in rapid equilibrium, while Aβ1−42 preferentially forms pentamer/hexamer units. This difference was linked to the specific roles of I41 and A42: I41 is essential to induce paranucleus formation, while A42 enhances the self-association of these paranuclei.[135] Bowers et al. further used IM-MS to investigate the early oligomers of Aβ1−40 and Aβ1−42.[11] They confirmed that Aβ1−40 dominantly populates monomers, dimers, and tetramers, while Aβ1−42 mostly forms dimers, tetramers, hexamers, and dodecamers, and provided for each species a cross-collision section that can be used to validate the simulations. Moreover, they proposed an assembly mechanism in which the dimer plays a key role, and they identified structural differences in the tetramer that rationalize the formation of higher order oligomers by Aβ1−42, but not by Aβ1−40.[11] However, using the same experiment with mutagenesis, Dadlez showed that Aβ1−40 oligomers consist of at least two families of conformers: compact and extended. The compact form resembles the fibril-like structure, while the extended form resembles the globular form determined by Lu et al., with the C-terminal ends forming intermolecular parallel β-sheets.[137a,b] Note however that other globular structures could fit the cross-collision section. Using fluorescence, Chen and Glabe found that the Aβ alloforms have different conformations and assembly states upon refolding from their unfolded conformations. Aβ1−40 is predominantly an unstable collapsed monomer, while Aβ1−42 samples a stable structured trimer or tetramer at concentrations >12.5 μM.[137c]

Many experimental studies have revealed the importance of the central hydrophobic cluster (CHC; residues L17−A21) and the C-terminus. While these hydrophobic patches form intermolecular β-sheets in fibrils, their role in aggregation is just beginning to become clear. Incubation of Aβ40 fragments with the full-length peptide show enhanced fibrilization rates only for the fragments containing residues L17−F20 or A30−M35.[138] Proline mutations of residues in the 17−20 or 30−35 region in Aβ1−40 and Aβ1−42 are more disruptive to fibrilization than mutations in other regions.[139] Finally, tethered Aβ1−40 demonstrated decreased spin mobility at regions H14−V18, G29−A30, and G38−V40 when investigated with EPR spectroscopy.[140]

Other experimental studies have helped clarify the role of the two additional C-terminal residues in Aβ1−42-specific aggregation. The VPV substitution (G33V, V36P, and G38V), promoting a β-hairpin at the C-terminus, increases the Aβ aggregation rate and higher order oligomers, while the PP substitution (V36-D-Pro, G37-L-Pro), leading to a hairpin-breaking motif, disrupts the Aβ1−42 aggregation kinetics and changes the oligomer size distribution to one more characteristic of Aβ1−40.[141] PICUP results suggest that a turn centered at residues V36 and G37 of Aβ1−42 and its absence in Aβ1−40 are responsible for the characteristic features of Aβ1−42 early oligomers.[136] These findings suggest that the formation of an additional β topology sampled at the C-terminus, driven by hydrophobic side chain interactions, may be responsible for Aβ1−42's unique assembly properties.

The central region, consisting of the hydrophilic residues E22−G29, has also been implicated for its unique properties and effects on Aβ assembly. This region was identified due to its inherent resistance to proteolysis, which is maintained when the Aβ21−30 fragment is isolated. Solution NMR of this fragment reveals that V24−K28 samples two turnlike structures that may be critical in the folding of the monomer,[142] and this was confirmed by computer simulations using various force fields.[143−145] Furthermore, substitution of contiguous pairs of residues in the V24−N27 region with a turn-nucleating D-ProGly motif largely accelerated fibril self-assembly of Aβ1−40.[146] Lastly, charge-altering point mutants of residues E22 and D23 that are implicated in FAD and cerebral amyloid angiopathy also demonstrate increased oligomerization orders and fibrilization rates when introduced into Aβ1−40. Furthermore, the oligomerization propensities of each of these mutants in full-length Aβ are directly correlated to both susceptibility of trypsin proteolysis and instability of the V24−K28 turn for the Aβ21−30 fragment.[147a] This suggests that these FAD mutants may destabilize turnlike structures in the central region, possibly changing the ensemble and allowing the monomer to seed different types of aggregates. This change in turn conformation has been confirmed by MD simulations on the Aβ21−30 peptide with the Arctic, Dutch, and Iowa

DOI: 10.1021/cr500638n
Chem. Rev. 2015, 115, 3518−3563

mutations and two biologically relevant salts ($CaCl_2$ and KCl).[147b]

Recently, various experiments have shed light on the role of the N-terminus in self-assembly. The D7N (Tottori) mutation accelerates the kinetics of transition from random coil states to β-sheet-rich configurations and promotes the early formation of higher order oligomers with more α/β structures that are significantly more toxic than WT Aβ1−40 and Aβ1−42 peptides.[148,149] The H6R mutation, the substitution of K16 by Ala, and the substitution of D1 by Tyr also affect self-assembly and toxicity.[150,151a] A single-molecule AFM experiment shows many dimer configurations stabilized by N-terminal interactions, although there is a difference in the interaction patterns of Aβ1−42 and Aβ1−40 monomers within dimers.[26] Finally, two single mutations at position A2 protect from AD.[54,55]

In summary, in vitro and in AD brain experimental studies indicate polymorphism and inherent diversity of structures present in fibrils and aggregates. Many physical factors can contribute to the formation of strains and in how the β-sheets pack or the strands hydrogen bond to each other: pH, temperature, concentration, supersaturation of the Aβ solution, ionic strength, sample, agitation conditions such as shear forces or sonication, interfaces, and the presence of seeds.[18,29,151b−d] Other data indicate that the structures and polymorphism of Aβ fibrils critically depend on the oligomeric states of the starting materials, the ratio of monomeric to aggregated forms of Aβ1−42 (oligomers and protofibrils), and the probability of secondary nucleation.[16] A recent study investigated how local physical forces interfere with the fibrillation kinetics, the general morphology, and the local structure and dynamics of the fibrils formed from the Aβ1−40 peptide. The well-described hydrophobic contact between F19 and L34 was rationally modified, and the F19G, F19E, F19K, F19W, and F19Y mutants were studied to understand the impact of the change in electrostatic (E and K mutations) and hydrophobic (W and Y mutations) interactions between side chains and larger flexibility of the backbone (G mutation). Local interactions were observed to influence the fibrillation kinetics, dynamics, and structure (the register of the hydrogen bond pattern) of Aβ1−40, but leave the general fibril structure unchanged. These data also indicate the role of the nonlocal F19−L34 contact in the early oligomers.[151e] Overall, a solid fundamental understanding of the principles underlying polymorphism and strain behavior of fibrils remains to be determined.

2.3. Monomers

Although Aβ1−40 and Aβ1−42 monomers are described by disordered conformations, there is experimental evidence suggesting a bias toward β-strand character in the CHC core and the C-terminus and a propensity for turns at specific positions within the Aβ monomers. Solution NMR studies targeting the monomeric state best characterize Aβ with a collapsed coil ensemble and not by a unique structure.[152] Nevertheless, backbone Hα, Cα, and Cβ chemical shift indices suggest β-strand propensities in the CHC, I31−V36, and V39−I41, as well as turn character at D7−E11 and F20−S26 in Aβ1−42.[21] Residues V18−F20 (in Aβ1−40, Aβ1−42, and Aβ1−42-M35ox, i.e., with oxidation of the M35 side chain) and V39−I41 (in Aβ1−42 and Aβ1−42-M35ox) also possess experimental $^3J_{HNHA} > 7.5$ Hz, indicative of a bias toward φ dihedrals characteristic of β-strands in these regions.[153,154] Far-UV CD spectra for Aβ1−40 and Aβ1−42 monomers are also dominated by random coils, but suggest β-strand content.[149,135] Using different preparation methods, CD analysis reported a β-strand content between 12% and 25% and an α-helix content between 3% and 9% at 295 K and pH 7.5 on day 0 (therefore, for a mixture of aggregates), indicative of the dependence of the secondary structure on sample preparation.[20,149] ^{15}N spin NMR relaxation data reveal that Aβ1−42 monomer demonstrates more rigidity at the C-terminus than Aβ1−40, in terms of both side-chain and backbone dynamics,[155,156] suggesting residual secondary structure formation. Although these biases may characterize the Aβ monomeric ensemble in aqueous conditions, other individual structures may be possible. For example, an NMR structure of Aβ1−40 monomer forms a 3−10 helix from H13 to D23 at pH 7.3, even if exchange between the 3−10 helix and other conformations in this region cannot be ruled out.[157a] In contrast to previous NMR studies, this study was conducted at 50 mM NaCl, and it is well established that salt shifts the ensemble from unstructured to more helical conformations.[157a] The structure of Aβ1−40 monomer with a N-terminal cysteine attached to silver nanoparticles has also been interrogated by surface plasmon enhanced Raman spectroscopy (SERS). This shows no change between pH 10.5 and pH 5.5 in the presence of partial α-helical content, indicating the existence of short and transient α-helical conformations for WT Aβ1−40 monomer in physiological conditions.[157b] Finally, a phase-modulated CLEAN chemical exchange experiment with a fast heteronuclear single-quantum coherence (HSQC) detection scheme[158] on Aβ1−40 monomer shows that residues 10−13, 17−22, and 30−36 are partially protected from exchange with solvent, while D23 and the region G25−G29 are susceptible to exchange,[159] consistent with the idea of a solvent-exposed turn in the central region.

3. SIMULATIONS OF Aβ1−40 AND Aβ1−42 MONOMERS IN AQUEOUS SOLUTION

Characterizing the monomeric state of Aβ in atomic detail under physiological conditions can be key to understanding how Aβ assembles into disease-causing oligomers because they represent a base state common to all aggregation pathways.[2] This knowledge could be crucial in developing therapeutics that prevent nontoxic monomers from progressing into toxic species, one of the fundamental strategies in the ongoing effort to treat AD. It is well established that self-assembly is profoundly influenced by very subtle chemical changes, ranging from the two-residue difference between Aβ1−40 and Aβ1−42[135,155] and FAD mutations[21,53] to the single-atom modification caused by M35-ox.[160] The polymorphism of monomeric Aβ under physiological conditions may underlie this relationship. In the absence of unambiguous stable native states, simple chemical modifications could have a profound effect on the type of ensemble sampled by that particular Aβ peptide. This intrinsic disordered property, in addition to the high aggregation propensity, has frustrated experimental efforts to characterize the Aβ1−40/1−42 structures.

The challenges and limitations inherent to the current set of experimental techniques for studying these polymorphic, aggregation-prone Aβ monomers have encouraged many groups to use a wide variety of computational techniques to more thoroughly investigate the conformational properties of these peptides. Over the years, the ability to perform extensive MD simulations has improved. Today, simulations for Aβ extend over multiple microseconds using explicit and implicit solvent models. Additionally, REMD,[161] simulated temper-

DOI: 10.1021/cr500638n
Chem. Rev. 2015, 115, 3518−3563

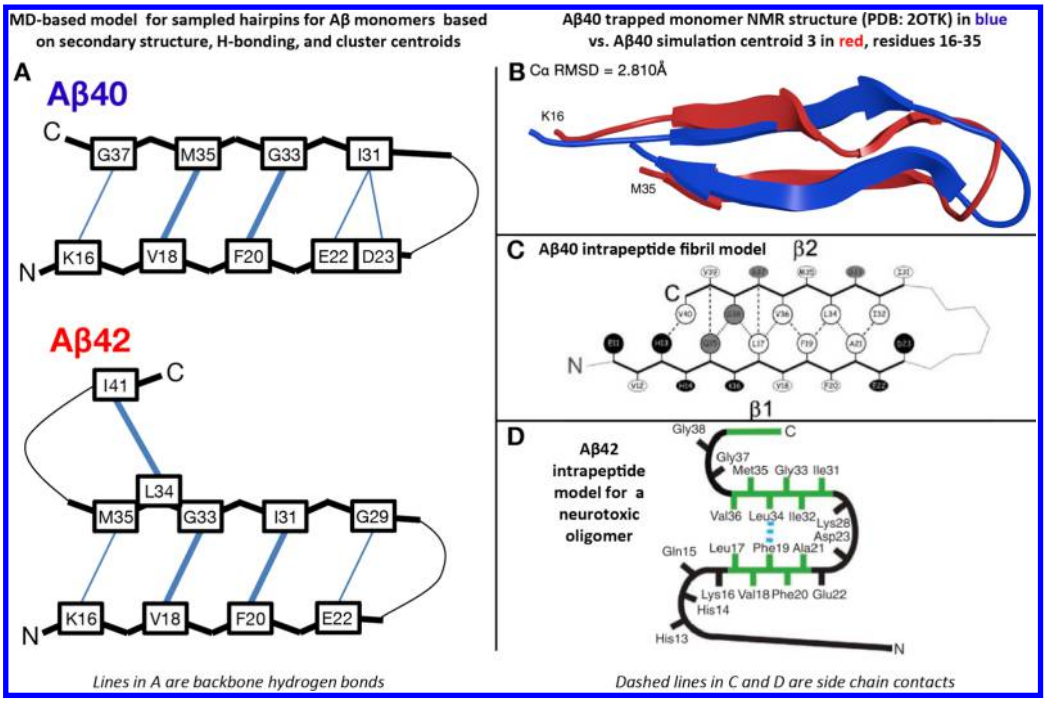

Figure 4. Transient REMD-sampled conformations of Aβ monomers bearing similarity to experimental intrapeptide models of higher order aggregates. (A) β-Hairpin models for Aβ1−42 and Aβ1−40 monomers derived from the simulations of Rosenman et al.,[154] based on the most populated cross-region backbone hydrogen bonds and secondary structure proclivities in the ensemble. Residues that have a high population for both donor to acceptor and acceptor to donor backbone hydrogen bonds are illustrated with a bold line. Sampled conformations matching these models exist as high-ranking centroid structures. (B) Ribbon overlay of residues 16−35 for centroid 3 derived from clustering analysis of the Aβ1−40 simulation[154] and the solution NMR structure of monomeric Aβ1−40 in complex with a phage-selected affibody (PDB entry 2OTK) published by Hoyer et al.[114] (C) Intrapeptide model for Aβ1−40 fibrils based on ss-NMR, as published by Bertini et al.[98] (D) Intrapeptide model for Aβ1−42 "on-pathway" pentamers based on ss-NMR, as published by Ahmed et al.[124]

ing,[162] and metadynamics[163] simulations are used to escape energy minima and enhance sampling. In general, the results obtained in simulations of intrinsically disordered proteins (IDPs) such as Aβ depend strongly on the set of parameters (such as the force field) used to describe the energy of the peptide and its interactions with the aqueous solvent. Widely used force fields for biomolecular simulations are OPLS-AA,[164] AMBER99sb and its variants,[165] and CHARMM22*,[166] while frequently used water models are the three-site models TIP3P[167] and SPC/E[168] and the four-site models TIP4P[167] and TIP4P-Ew.[169] These force fields have been calibrated against model compounds and peptides, and in most instances, the force fields reproduce folded conformations of small globular proteins with root-mean-square deviations (RMSDs) within angstroms of the experimentally determined structures.[170a−d] However, experimental validation of the ensembles produced by these force fields, for either the unfolded states of globular proteins[170e] or IDPs,[170f] remains essentially an unsolved problem. Here, we review some of the more recent simulation studies, which employ state-of-the-art strategies, ranging from all-atom REMD simulations to other approaches, to extensively characterize the equilibrium structures of Aβ1−40 and 1−42 monomers.

All-atom REMD simulations on the microsecond per replica time scale with OPLS-AA/TIP3P conducted by Rosenman et al.[154] revealed that Aβ1−40 sampled β-hairpins between the L17−A21 and I31−V36 regions, while Aβ1−42 sampled a second β-hairpin spanning V39−A42, forming transient β-meander structures. The hairpin model of Aβ1−40 with the backbone of K16 hydrogen bonded to the backbone of G37 is found in both centroids 3 (4.2%) and 4 (3.9%) using a linkage clustering shown in Figure 4A, top. This conformation does not exist for Aβ1−42, as centroid 1 of Aβ1−42 possesses a different CHC to C-terminal hairpin with a backbone H-bond register shifted by two residues. The double hairpin for Aβ1−42 is found in centroid 7 (Figure 4A, bottom). The predicted hairpin for Aβ1−40 is consistent with the NMR structure of Aβ1−40 in complex with a phage-selected affibody[114] as shown in Figure 4B and the intrapeptide model of Aβ1−40 fibrils as published by Bertini et al.[98] shown in Figure 4C. The predicted double hairpin for Aβ1−42 is consistent with the intrapeptide model of Aβ1−42 pentamers as published by Ahmed et al.[124] shown in Figure 4D. Taken together, these REMD-predicted hairpins, by demonstrating a structural similarity to models of higher order aggregates, suggest that they may act as the seeds for Aβ assembly.

Previous characterizations of Aβ through REMD simulations with OPLS-AA/TIP3P and AMBER99sb/TIP4P-Ew also predicted conformations where Aβ was mostly flexible but possessed some structured segments; in particular, β-hairpins populated the C-terminus in Aβ1−42 but not Aβ1−40.[171] A different approach was taken by Ball et al.,[172] who had used 100 ns multiple-reservoir replica exchange (MRRE) simulations with AMBER99sb/TIP4P-Ew to determine that Aβ1−42 was mostly disordered, with significant α character in residues Y10−F19 and E22−N27 and little to no β content. The same group then reported their analysis of multiple trajectories acquired with the same simulation method, this time processing the resulting ensemble using the ENSEMBLE package[173] to select structures that best match experimental chemical shifts, residual

DOI: 10.1021/cr500638n
Chem. Rev. 2015, 115, 3518−3563

dipolar couplings, $^{3}J_{HNHA}$ couplings, and $^{1}H-^{15}N$ NOEs.[174] After refinement with ENSEMBLE, the aforementioned α-content is de-emphasized, and antiparallel β-hairpins between the K16−A21 and G29−V36 regions are promoted in Aβ1−42. Aβ1−40 after ENSEMBLE refinement, in contrast, is characterized by reduced C-terminal β propensity and sampling of a hairpin between the CHC and residues G9−H13.[174] The data suggest that the extra two residues in Aβ1−42 primarily promote hydrophobic clustering that directs the increase in β content in the CHC and G29−V36 region, rather than the direct formation of additional secondary structure, such as the second hairpin discussed above. Furthermore, despite possessing similar overall biases, the ensembles generated by Ball[174] and Rosenman[154] also differ in β content (%) per residue, with the largest residue propensities in the range of 20−30% in the former and 50−60% in the latter. It is worth noting a 100 ns/replica REMD simulation with AMBER99sb/TIP3P also revealed that Aβ1−42 forms contacts between L17−A21 and I31−V36 with a transient turn in the region D23−N26, consistent with a quasi-hairpin-like conformation.[175]

Other approaches beyond atomistic REMD in explicit solvent have also been used to investigate the properties of Aβ. The two alloforms were explored using the Folding@home platform and thousands of MD trajectories with AMBER99sb/TIP3P, each of average length ∼30 ns, for each species.[176,177] Both WT Aβ's are described as mostly disordered ensembles, with some α-helical character from residues 10−20 and almost no β content, in reasonable agreement with the SERS experiment.[157b] Of the β content that exists, β-sheet propensity near the C-terminus is notably less in Aβ1−40 than in Aβ1−42. Granata et al.[178a] investigated the Aβ1−40 ensemble with NMR-guided metadynamics, which uses experimental data as collective variables to drive metadynamics calculations rather than using them purely for simulation validation or as hard structural restraints.[178b] Simulations were carried out with CHARMM22*/TIP3P at 350 K and eight replicas for 310 ns/replica. Each replica was biased by a history-dependent potential acting on a different collective variable, including two variables for the difference between predicted and experimental chemical shifts. The resulting unbiased free energy surface (FES) has many extended and highly disordered states and large radii of gyration.[178a] In terms of structured states, the FES displays structures with long α-helical content similar to the structure predicted by Vivekanadan,[157] structures with short α-helix content similar to the structure predicted by Pande et al.,[176] and structures with various β-hairpins spanning the L17−A21 and I31−V36 regions similar to the structures predicted by Rosenman et al.[178] Further simulations showed the FES does not change at 300 K.

Aβ monomers have also been investigated by REMD[179] with the six-bead CG OPEPv3 model in implicit solvent[180a] and Monte Carlo simulated annealing with the all-atom PROFASI force field.[181a] The OPEPv3 force field has been calibrated against nonamyloid peptides and in most instances predicts folded conformations with 2−3 Å RMSD from the NMR structures,[179,180a−e] although it cannot reproduce vibrational frequencies with high accuracy as all-atom models.[180f,g] OPEP has also been coupled to a greedy algorithm for structure prediction of peptides with 9−52 amino acids.[180h,i] The OPEP-REMD simulation revealed Aβ ensembles that were mostly turn/coil, but possessed substantial β-sheet propensity in the N-terminus.[182] It remains to be determined whether OPEPv5 with better electrostatic interactions leads to a different picture.[183] The PROFASI simulation characterized Aβ1−42 as possessing strong β probability in many of the residues over the peptide.[181b]

All-atom REMD simulation of both alloforms was performed for 110 ns/replica with AMBER99sb/generalized Born (GB).[184a] Each monomer behaves as a unique statistical coil at 298 K with five relatively independent folding units comprising residues 1−5, 10−13, 17−22, 28−37, and 39−42, connected by four turns. The two turns predicted at positions 6−9 and 23−27 are in agreement with NMR, and residues I41 and A42 increase contacts within the C-terminus and between the CHC and the C-terminus, leading to a more structured C-terminus.[184a] Finally, discrete MD (DMD) simulations, where all interparticle interactions are expressed by square-well and steplike potentials, coupled to a four-bead CG model, find that Aβ1−42 displays a turn centered at G37−G38 and a β-hairpin spanning V36−A42 that are absent in Aβ1−40.[184b] DMD simulations also capture two other differences between the alloforms: a highly populated β-strand at A2−F4 in Aβ1−40 but not in Aβ1−42 and a β-hairpin centered at S8−Y10 in Aβ1−42 but not in Aβ1−40.

While the most recent and exhaustive all-atom studies in explicit solvent have started to show some consistent depictions of the properties of the Aβ ensemble, most characterizations of the Aβ1−40 and Aβ1−42 peptides, in our opinion, remain highly divergent. These variations may arise from differences in simulation conditions, extent of sampling, or trajectory analysis. IDPs such as Aβ, or even the unfolded ensembles of well-folded proteins, remain difficult test cases for our current range of computational techniques because they lack nonambiguous energy minima. The types of conformations sampled through simulation may be much more sensitive to simulation conditions than globular proteins, where parameter differences could still lead to similar final results. For the globular villin headpiece, for example, independent MD simulations using different all-atom force fields were able to recapture the experimental folded structure and folding rate of the protein, but the unfolded states and folding mechanism were highly dependent on the force field choice.[185] Meanwhile, in the case of two intrinsically disordered proteins (a 50-residue peptide derived from an FG-nucleoporin and a 20-residue RS repeat peptide), microsecond length REMD simulations with four different all-atom force fields were found to adopt substantially different hydrogen bonds, secondary structure tendencies, and radii of gyration.[185] With this in mind, the force fields that are capable of reversibly folding globular proteins such as AMBER99sb[165a] with *[165b] and/or ILDN[165c] modifications and CHARMM22*[166] in the studies described in refs 170b and 170d may not necessarily be the most suitable for characterizing the metastable states of disordered ensembles.

Given these circumstances, we suggest that multiple simulation studies consistent with experimental data are likely to be much more valuable than a single study with one force field. To sort out ungeneralizable findings, more stringent and sensitive experimental validations are necessary, particularly using better reporters on the tertiary structural biases. Many of the values commonly used for experimental comparison, such as NMR chemical shifts and scalar J-couplings, are good "sanity checks" on sampling, but primarily report on local structure and are highly prone to sequence-specific bias. Full characterization of the structures sampled by intrinsically disordered proteins remains a major challenge. The development of new

DOI: 10.1021/cr500638n
Chem. Rev. 2015, 115, 3518−3563

Table 1. Summary of Aβ Aggregation Simulations from Random States[a]

ref	force field	solvent model	method	time scale	Aβ alloform	oligomer size
195	OPEP 3.2	implicit	HT-REMD	1.25 μs × 26 rep	1−40, 1−42	2
199	CHARMM19	SASA	T-REMD	0.8 μs × 24 rep × 8 sim	1−40	2
202	PROFASI	implicit	MC	2 × 10^{10} steps × 40 sim	1−42	2
204[c]	OPLS-AA	SPC/E	MD	0.05 μs × 1000 sim	1−40, 1−42	2
	OPLS-AA	TIP3P	MD	0.05 μs × 1000 sim	1−40, 1−42	2
207	OPLS-AA	TIP3P	T-REMD	0.2 μs × 64 rep	1−42	2
206	AMBER99sb	TIP4P-Ew	T-REMD	0.05 μs × 52 rep	1−42, 1−43	2
205	AMBER99	TIP3P	MD	0.1 μs	1−42	2
208	OPEP 3.2	implicit	T-REMD	1.2 μs × 22 rep	17−42	3
203[b]	CG	implicit	DMD	6 × 10^7 steps × 8 sim	1−40, 1−42	1−32
200	CHARMM19	SASA	T-REMD	0.8 μs × 24 rep ×8 sim	10−40	4
210[b]	OPLS-AA	GB/SA	T-REMD	0.2 μs × 5 sim	1−42	1−20

[a]In the time scale column, "sim" stands for the number of independent simulations, "rep" stands for the number of replicas for REMD or HT-REMD, and the time is that of one MD trajectory or one replica. [b]Large-scale aggregation simulations resulting in an ensemble of oligomer sizes sampled and analyzed. [c]The all-atom, explicit solvent simulations in ref 204 start from an ensemble of conformations obtained by the CG DMD simulations of ref 203.

experimental techniques to probe the Aβ monomer structures in solution is also needed.

4. SIMULATIONS OF Aβ1−40/1−42 DIMERS AND HIGHER ORDER ASSEMBLIES IN AQUEOUS SOLUTION FROM RANDOM STATES

Soluble Aβ dimers are the smallest toxic species in AD,[10] and isolated from Alzheimer cortex, they directly induce Tau hyperphosphorylation and neuritic degeneration.[186] Trimers and larger aggregates are also toxic. Knowledge of their key structural and dynamical features is of significant interest to design drugs inhibiting their formation and toxicity. The conformational stability of preformed Aβ assemblies of various oligomer sizes, inspired from ss-NMR-derived fibril structures (5-mers and 10-mers of Aβ17−42),[187] fibril polymorphisms of other amyloid sequences (10-mers of Aβ19−42),[188] globulomers (12-mers of Aβ17−42),[189] and the design of triple-sheet motifs (24-mers and 60-mers of Aβ17−42),[190] was assessed by atomistic MD of 50−100 ns, proving only that these states are stable within the simulation times. In what follows, we describe the most recent simulations aimed at understanding the aggregation of Aβ peptides from random states (Table 1). Along with Aβ1−40 and Aβ1−42, we also report the results of three nonpathogenic truncated variants, Aβ9−40, Aβ10−40, and Aβ17−42. We recall the N-terminal, central, and C-terminal regions cover residues 1−16, 22−29, and 30−40/42.

4.1. Dimer Simulations with Simplified Representations

Using the six-bead CG OPEPv3 model with implicit solvent,[61,183,191−194] the structures of Aβ1−40 and Aβ1−42 dimers were determined by HT-REMD simulations starting from randomly chosen conformations.[195] HT-REMD[196] combines standard REMD[179] with a Hamiltonian exchange procedure, where several replicas with reduced nonbonded energies are used at the highest temperature. Both alloforms populate mostly turn/random coil conformations with a β-sheet propensity at the C-terminal region higher than in the monomers. Dimerization is characterized by CHC/CHC, CHC/C-terminal region, and C-terminal region/C-terminal region interpeptide hydrophobic contacts. However, the Aβ1−42 dimer has a higher propensity than the Aβ1−40 dimer to form β-strands at the CHC and in the C-terminal region. The free energy landscape of the Aβ1−42 dimer is also broader and more complex than that of the Aβ1−40 dimer.[195]

United-atom REMD simulations with CHARMM19[197] and a solvent-accessible surface area (SASA) implicit solvent[198] were performed on Aβ1−40 and Aβ10−40 dimers.[199,200] Truncation of the first nine residues leads to minor changes in the structure of the dimer.[200] The conformational ensemble of the Aβ10−40 dimer can be described by three distinct basins differing with respect to the distribution of secondary structure and the amount of inter- and intrapeptide interactions. The interface is largely confined to the region 10−23, which forms the bulk of interpeptide interactions and a few interpeptide hydrogen bonds.[199] Random reshuffling of the amino acids, i.e., sequence permutation, does not impact the Aβ10−40 dimer globule-like states, suggesting that the Aβ10−40 peptides in the dimer behave as ideal chains in a polymer melt, in which amino acids lose their identities.[201] These results run in contrast to MC simulations with the all-atom PROFASI model and implicit solvent,[181a] where the Aβ1−42 dimer is mostly composed of a four-stranded antiparallel β-sheet or two layers with mixed parallel/antiparallel arrangements and three major clearly identified turns at positions 13−16, 23−26, and 35−38.[202]

Finally, extensive DMD simulations coupled to a four-bead CG model found that the Aβ dimer conformations are collapsed and disordered with a small content of β-strands linked by loops and turns.[203] The Aβ1−42 dimer has a higher propensity of β-sheets at the CHC and C-terminal region than the Aβ1−40 dimer. Aβ1−40 dimer formation is mainly driven by intermolecular interactions between the CHC regions, while the C-terminal region plays a significant role for Aβ1−42.[203] Fifty nanosecond MD stability simulations with OPLS-AA/TIP3P or SPC/E starting from the dominant DMD-obtained CG structures confirm the main DMD results[203] and enable a precise analysis of secondary structures, salt bridges, and free energy landscapes.[204] Overall, the free energy landscape of Aβ1−42 is much more complex than that of Aβ1−40.

4.2. All-Atom Dimers in Explicit Solvent

Solvation free energy analysis based on the integral equation theory of liquids and MD trajectories of 100 ns suggests that dimerization occurs through a two-step nucleation-accommodation mechanism: decrease of the monomer solvation free energy followed by structural reorganizations in the dimer, leading to a decrease in the protein internal energy.[205] Fifty

DOI: 10.1021/cr500638n
Chem. Rev. 2015, 115, 3518−3563

Table 2. Secondary Structure Contents of Aβ1−40 and Aβ1−42 Dimers Using Enhanced Sampling Techniques Starting from Randomly Chosen States[a]

	Aβ1−40				Aβ1−42			
ref	helix content (%)	β-strand content (%)	turn content (%)	random coil content (%)	α-helix content (%)	β-strand content (%)	turn content (%)	random coil content (%)
149b[b]	10.5	38.6		50.9				
20[b]	0	12	28	60	11	3	26	60
195	1.3 ± 0.1	12.6 ± 0.1	50.7 ± 0.1	35.4 ± 0.1	4.4 ± 0.1	30.8 ± 0.1	32.4 ± 0.1	32.4 ± 0.1
202					0.9 ± 0.1	42.9 ± 0.7	33.0 ± 0.4	23.2 ± 0.8
203	0.1 ± 0.1	13.6 ± 1.6	40.6 ± 4.1	37.5 ± 5.0	0.0 ± 0.0	15.7 ± 1.9	39.2 ± 3.7	39.0 ± 4.9
204[c]	0.5 ± 0.1	5.5 ± 0.8	43.5 ± 3.6	46.8 ± 4.1	0.9 ± 0.2	6.6 ± 0.8	40.1 ± 3.2	48.0 ± 3.8
207					8.4 ± 0.7	11.9 ± 0.6	51.2 ± 1.0	28.5 ± 0.8

[a]Values from simulations are computed using STRIDE. [b]Circular-dichroism-derived values using different sample preparations. [c]MD values starting from the CG DMD structures of ref 203 and using OPLS-AA and SPC/E. Similar values are obtained using OPLS-AA and TIP3P.

nanoseconds per replica REMD with AMBER99sb/TIP4P-Ew, followed by ab initio energy calculations on selected poses, concluded that the stability of the water molecules solvating around the dimer mainly determines the relative stability for the different conformations of the Aβ1−42 dimer.[206a]

Recently, REMD simulations using OPLS-AA/TIP3P with 250 ns/replica were performed on Aβ1−42.[207] The Aβ1−42 dimer mostly populates coil/turn (80.4%) and then α-helix and β-strand with 11.1% and 8.4%. The latter values do not match exactly, but are consistent with the CD-derived values: an α-helix content varying from 3% to 10.5% and a β-strand content varying between 12% and 38%.[20,149b] The most β-rich signal is at the C-terminal region. Looking at the networks of interchain contacts, the interface of the 1−42 dimer is mainly composed of the C-terminal and CHC regions, as the regions of highest contact probability are C-terminal/C-terminal, CHC/CHC, and CHC/C-terminal. The calculated collision cross-sections of the three most populated dimer states nicely fit to IM-MS values.[11a] Using a general method to characterize oligomer structures,[206b] there is no evidence of well-formed intermolecular parallel and antiparallel β-sheet configurations. Rather, the first 11 N-terminal residues are essentially disordered, and residues 12−17 have a non-negligible probability for α-helix.[207]

4.3. Toward Atomistic Structures for Dimers

As for the monomers, common trends start to emerge from the most recent dimer simulations: (1) the dimerization of Aβ is mainly driven by a hydrophobic collapse through intermolecular contacts involving CHC and the C-terminal region, agreeing with the importance of these regions during aggregation as observed experimentally,[149,124] (2) Aβ1−42 has a larger β-strand propensity than Aβ1−40 at the CHC and C-terminal regions, (3) the free energy landscape of Aβ1−42 is more complex than that of Aβ1−40, (4) all possible salt bridges are highly accessible to the solvent,[207] and (5) both alloforms have many structural differences already at the dimer level that can account for their very different oligomerization pathways and toxicity potencies as observed experimentally.[135,136,11,53] For each alloform the results between the simulations still diverge, and we can identify qualitative differences in the total and per residue propensities of secondary structure (Table 2, Figure 5) and the tertiary/quaternary structures.

4.4. Aggregation of High-Order Assemblies

Simulations of higher order assemblies from random states are very challenging as the number of minima scales exponentially with the number of particles. CG and all-atom models coupled to implicit solvent schemes enable long time scales that are not reachable by all-atom explicit solvent MD.

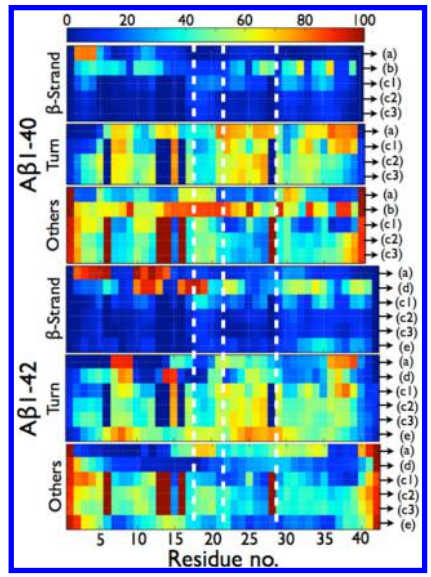

Figure 5. Per residue probabilities of β-strand, turn, and others (coil and α-helix) for the Aβ1−40 and Aβ1−42 dimers as computed by different simulation protocols. As seen in Table 2, the total α-helix content amounts to less than 1.3% in refs 195, 202, 203, and 204, so others represent coil. In ref 195, there is a total of 4.4% α-helix in the dimers of Aβ1−42, and there is a probability of 27% for residues 23−28 to form an α-helix. In ref 204, there is a total of 8.4% α-helix in the dimers of Aβ1−42, and there is a probability of 45% for residues 13−17 to form an α-helix. (a) HT-REMD with the CG OPEP model and implicit solvent.[195] (b) United-atom CHARMM19 REMD with the SASA implicit solvent.[199] (c1) CG DMD with implicit solvent.[203] (c2) All-atom MD with OPLS-AA/SPCE.[204] (c3) All-atom MD with OPLS-AA/TIP3P.[204] (d) All-atom MC with implicit solvent.[181a] (e) All-atom REMD with OPLS-AA/TIP3P.[207] All secondary structure probabilities were computed using STRIDE, except for (b), for which the secondary structures are determined using information on the φ and ψ dihedral angles only, without consideration of the H-bond network. As such, the β-sheet probabilities for (b) must be considered as extended conformations, and no turn probability can be determined. The vertical dotted white lines delimit the four regions: N-terminal (residues 1−16), CHC (residues 17−21), loop region in the fibril (residues 22− 28), and C-terminal (residues 29−40/42).

The structural ensemble of the Aβ17−42 trimer was investigated using REMD and the six-bead CG OPEPv3, with 1.2 μs for each replica.[208] This fragment was selected because it covers the β-strand−loop−β-strand in the Aβ1−42 fibril. At

DOI: 10.1021/cr500638n
Chem. Rev. 2015, 115, 3518−3563

equilibrium and 300 K, the trimer adopts globular conformations with 46% turn, 35% random coil, 8.7% helix, and 7% β-strand. Using an RMSD cutoff of 3 Å, 35% of all sampled conformations can be described by two clusters. The first cluster with a population of 19% displays one chain with a β-hairpin spanning residues F17−L34 and the other two chains with a disordered $\beta-\alpha-\beta$-turn$-\beta$ motif. In this motif, the α-helix spans residues E22−K28, the turn spans G37−G38, and the β-strand signal is rather weak elsewhere. The second cluster (15.4%) is more disordered with an interpeptide antiparallel β-sheet spanning the CHC region and residues I31−I34, an α-helix spanning A21−N26, and turns at positions G37 and G38. The third (13.3%) and fifth (8.2%) clusters are random coil in character, but display intermolecular antiparallel β-sheets between V36−G38 and V39−V41 (cluster 3) or between I31−G33 and G38−V40 (cluster 5). Overall, the preference for a parallel β-sheet is not encoded in the Aβ17−42 trimer. This picture is fully different from the REMD results of the Aβ10−40 tetramer using CHARMM19/SASA, showing rather amorphous states that are structurally similar to the dimers.[200]

A total of five all-atom MD simulations of 200 ns each with OPLS-AA[164] and GB/SA[209] on a 20 Aβ1−42 system at a concentration of 0.8 mM starting from various structures and dispersed peptides[210] reveals that the early aggregation pathways at 300 K are very diverse and are dominated by unstructured oligomers characterized by 82% coil, 7.6% β-strand, and 10% α-helix, consistent with atomistic REMD of the Aβ1−42 dimer in explicit solvent.[207] The conformations are characterized by strong intermolecular interactions involving residues 31−42 and 17−21, and several differences between Aβ1−42 and Aβ1−40 aggregation are observed from the intermolecular contact maps. The oligomer mass distribution, though out of equilibrium within 200 ns, displays a higher population for dimers, tetramers, hexamers, octamers (globular shape), 12-mers, and 18-mers (elongated shape), in agreement with experimental results.[135] A maximum flow transition network analysis unveils a complex aggregation process, although key preferential pathways are found: for instance, the trimer serves as the building block for the hexamer, while the dimer preferentially aggregates into a tetramer and an octamer.[210]

Finally, CG DMD simulations have been used to study the aggregation of 32 peptides of both Aβ alloforms.[184b,203] The simulations reproduce qualitatively the main features of the oligomer size distribution of Aβ1−40 and Aβ1−42 as measured experimentally. Overall, these oligomers, as for the dimer, form rather amorphous aggregates with a low propensity of β-sheet that are stabilized by intermolecular contacts between the CHC and C-terminal regions. The main differences between Aβ1−42 and Aβ1−40 oligomers are the larger β-strand propensity at the C-terminal region and turn propensity at G37−G38 and the larger flexibility and solvent exposure of the N-terminal of Aβ1−42. Interestingly, there is no substantial increase of β-strand content from dimers to hexamers and larger oligomers, with all β contents varying between 14% and 22%. We recall that the β-sheet content amounts to 50% in fibrils. DMD further indicates that Aβ1−40 dimers and hexamers have indistinguishable intramolecular contact maps and tertiary structures, whereas the Aβ1−42 transition from dimers to hexamers is accompanied by a partial loss of intramolecular contacts within the CHC.

In summary, higher resolution experimental data going beyond cross-collision sections (IM-MS), secondary structure content averaged over different oligomer sizes (CD), and hydrodynamic radii (diffusion NMR) as well as standardized simulations will help converge on the most relevant dimer and oligomer structures. While the simulations agree on a few structural aspects, they widely differ on the equilibrium ensemble due to the difficulties associated with correct sampling and force field accuracy. Comparisons between simulations with different force fields are required as well as multiscale approaches that couple cheap potential for fast sampling and more reliable force fields for refinement of selected poses.[204,208] Another possibility is to run CG simulations for a short time and then switch to atomistic simulations for a few picoseconds and so on. It may be at this cost that we will obtain a convergent and reliable free energy landscape of dimers and high-order oligomers.

5. Aβ NUCLEUS IN AQUEOUS SOLUTION

5.1. Nucleation and Protein Aggregation

The nucleation of amyloid fibrils is a process associated with the generation of nanoscale fibrils or protofilaments that have the property of irreversible growth.[114] Unless the nanofibril size exceeds the size N_c of the so-called critical nucleus, the nanofibril is more likely to dissolve rather than grow. Only if the number of monomers becomes larger than N_c can the system grow irreversibly into a macroscale amyloid fibril. From a thermodynamic point of view, the size of the critical nucleus may be defined as a turnover point of the free energy plotted as a function of the number of chains (Figure 6A).[211]

Protein aggregation might occur through three possible pathways. In homogeneous nucleation,[212] new aggregates are generated at a rate that depends on the concentration of monomers alone and is independent of the concentration of existing fibrils. In the fragmentation process, the rate of

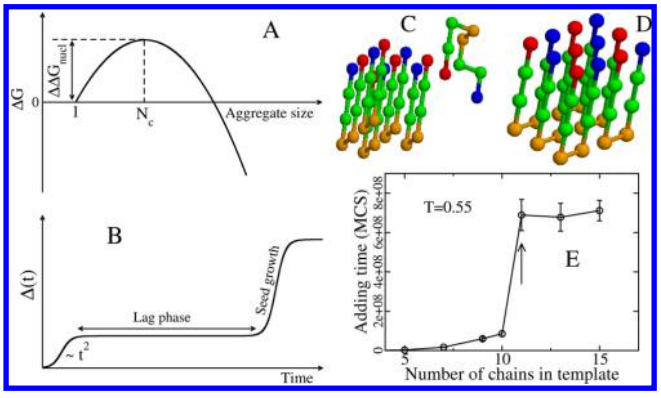

Figure 6. (A) Schematic plot of the free energy of the aggregate, relative to the monomer, as a function of the aggregate size. The critical nucleus size corresponds to the peak of ΔG, while $\Delta\Delta G_{nucl}$ is the barrier to nucleation. (B) Time dependence of the fibril mass, $M(t)$. Within homogeneous nucleation theory, $M(t) \approx t^2$ on short time scales. The plateau corresponds to the lag phase, whose duration is proportional to $\exp(\Delta\Delta G_{nucl}/k_BT)$. (C) A typical initial conformation for the (5 + 1) system in the lattice models with eight-bead sequence +HHPPHH−, where + and − refer to charged residues, while H and P denote hydrophobic and polar residues.[229] (D) Final fibril conformation with the lowest energy. (E) Dependence of the adding time τ_{add} on the number of monomers that belong to the preformed template. Results are averaged over 50 Monte Carlo trajectories. At a concentration of 290 μM, τ_{add} becomes independent of N for $N_{template}$ larger than 11. The arrow refers to N_c = 11.[230]

DOI: 10.1021/cr500638n
Chem. Rev. 2015, 115, 3518−3563

generation of new aggregates depends only on the concentration of existing fibrils.[213] Finally, within the secondary nucleation process, the rate depends on the concentrations of both the monomer and the existing fibrils.[214] The six-bead CG OPEPv3 simulations revealed that the fibril formation of short linear peptides occurs via the homogeneous nucleation mechanism.[215] OPEP has been optimized by discriminating native from non-native structures of proteins and successfully folding peptides to their NMR structures.[179,180a] Using an off-lattice model coupled to enhanced sampling, the rate-limiting step has been suggested prior to nucleation to be associated with a change in the width of the fibrillar aggregate of 3.5.[216] Aβ1−42 aggregation was shown to proceed through the secondary nucleation pathway rather than through a classical mechanism of homogeneous primary nucleation using a combination of kinetic studies and selective radiolabeling experiments.[14]

In homogeneous nucleation, the lag phase (Figure 6B) is weak, and at short times the fibril mass $M(t)$ scales with $C^{N_c+2}t^2$, where C is the monomer concentration. Thus, from the concentration dependence of the slope of log M−log t^2, one can extract the size of the critical nucleus.[217] N_c can also be estimated from the dependence of the lag phase time on the protein concentration, as approximately $C^{-(N_c+1)/2}$.[218]

Using a simple two-state model and Langevin dynamics, the lag phase and the nucleus size N_c have been shown to vary from 4 to 35 linear peptides depending on the energy difference between the amyloid-competent and amyloid-protected minima, and one can generate fibril topologies resembling those observed experimentally, e.g., twist and multifilament composition.[102] Using a lattice model and Monte Carlo (MC) simulations, it was evidenced that the balance between electrostatic and hydrophobic interactions modulates not only the populations of the amyloid-competent monomeric state and the lag phase, but also the topology of the fibrils.[219] Using a more complex on-lattice model and dynamic MC, 10 linear peptides of 7 amino acids with an alternative hydrophobic and hydrophilic pattern remain stable at low temperature. When the short fibrils are subsequently simulated in a grand canonical ensemble, further growth of the structure is observed, indicating that N_c is at least equal to 9.[220] These N_c values are much higher than that derived by atomistic simulations followed by ab initio calculations, where $N_c = 3$ was found to be sufficient to trigger fibril growth of the GNNQQNY peptide.[221] This low N_c value is likely due to the neglect of conformational entropy. Indeed, on the basis of multiscale simulations, De Simone showed that a comprehensive description of the flexibility of all states must also be considered for self-assembly.[222]

By using a mesoscopic model similar to that defined by Caflisch, one can establish a connection between the early nucleation events and the kinetic information available in the later stages of the aggregation process. Using an energy difference between amyloid-competent and non-amyloid-competent states from all-atom simulations and translational and rotational diffusion constants from experiment, the nucleus was estimated as $N_c = 4$ for Aβ1−42 using dynamic MC.[223] This estimate does not agree with the quasi-elastic light scattering (QLS) experiment at an Aβ concentration of 1.16 or 0.47 mM in 0.1 M HCl, where the experimental kinetic data at low pH are reproduced correctly when the number of peptides involved in the critical nucleus of Aβ1−40 is 10.[224] The kinetic data vary, however, with the experimental conditions used, as described below. In contrast, calculating ΔG as a function of the number of monomers with the help of a CG model, Fawzi et al. obtained $N_c = 10$ for Aβ1−40.[225] On the basis of the experimental[226] and theoretical[227,228] observations that the binding of monomers to a preformed fibril obeys the dock−lock mechanism in which a monomer first docks and then undergoes the structural arrangement necessary to lock onto the template, Li et al. proposed that the time for adding a new monomer, τ_{add}, is expected to become independent of the template size when it exceeds N_c.[219,229] By using a lattice model with eight beads for Aβ1−40 (Figure 6C,D), N_c was found to be 11 (Figure 6E). However, the population of the amyloid-competent monomer is found to be on the order of 9% at the folding temperature, a value that is possibly overestimated. Nevertheless, one can show that this approach[230] provides an estimate of N_c consistent with the dependence of the free energy variation on the number of monomers.[211]

By using classical nucleation theory to describe amyloid nucleation, Cabriolu et al. predict the nucleus size and the fibril nucleation rate as a function of the supersaturation of the protein solution. It was found that N_c is 15 for Aβ1−40 at a protein concentration of 120 μM, but variation in the supersaturation of the phase can cause N_c to increase to 50.[231a] This is rather consistent with the experimental estimate of the size of the critical nucleus ($N_c > 29$) using fluorescence correlation spectroscopy at a supersaturation of 100 μM Aβ1−40 solution.[231b] Note that Auer et al. argued that, in some cases, the dependence of the fibril nucleation rate on the concentration of monomer protein is stepwise and not power law.[232] If this were the case also for Aβ1−40 and Aβ1−42, a treatment of the nucleation process based only on CNT would be only approximately correct.

5.2. Nucleus of C-Terminal Aβ Fragments by Atomistic Simulations

Recent advances in sampling techniques allowed studying by an all-atom description the early stages of the aggregation process of the octavaline peptide (Val_8) and the Aβ35−40 peptide.[233,234] Several studies reported the importance of residues 35−40 in triggering the aggregation process of the whole Aβ peptide.[235−237] The microcrystalline structure of this peptide in a amyloid-like configuration reveals antiparallel (AP) β-strands within the sheets and parallel (P) β-sheets.[83a] Aβ35−40 was modeled with AMBER99sb/TIP3P at a concentration of 120 mM and 350 K.[234] At this concentration, the peptide spontaneously forms a compact disordered aggregate, and the "rare event" is the formation of an ordered nucleus. The process was studied by bias-exchange metadynamics,[238] allowing reconstruction of multidimensional free energy landscapes with large barriers and in which a reliable reaction coordinate is unknown.

The free energy landscape of 18 Aβ35−40 peptides displays a funnel with two local minima at its bottom and a third local minimum at a free energy approximately 40 kcal/mol higher (Figure 7).[234] Basin 1 includes structures that are mainly disordered. Basin 2 contains a much larger fraction of antiparallel β-sheets (up to 10−12 β-strands). In this basin the β-strands, although common, are not organized in a stable configuration, and contacts between different layers form only transiently. Basins 1 and 2 are separated by a relatively low barrier that can be crossed on the time scale of a few tens of nanoseconds. Basin 3 includes structures with a high content of antiparallel β-sheets, which are closely packed on top of each

DOI: 10.1021/cr500638n
Chem. Rev. 2015, 115, 3518−3563

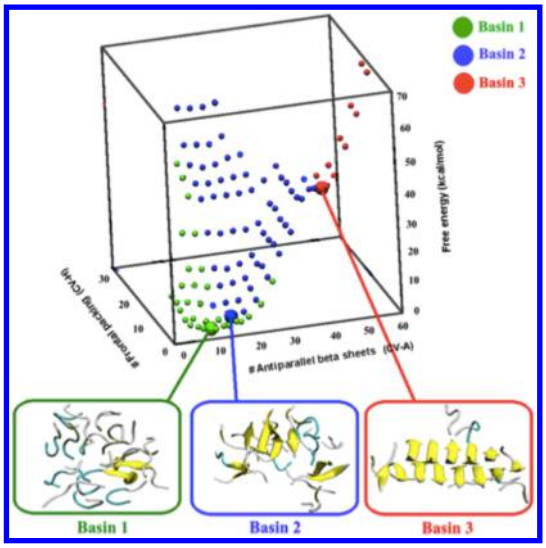

Figure 7. Free energy landscape of 18 Aβ35−40 peptides estimated by atomistic metadynamics simulations with explicit solvent as a function of the number of antiparallel β-sheets and the number of antiparallel frontal packings (different β-sheets facing each other).[178a] Basin 1 includes structures that are mainly disordered, with secondary structure elements formed only transiently. Basin 2 contains a much larger fraction of antiparallel β-sheets (up to 10−12 β-strands). The main characteristic of this basin is that the β-strands, although common, are not organized in a stable nucleus. These structures are only metastable and can convert to the disordered melt in a few tenths of a nanosecond. Basin 3 includes instead structures with a specific interdigitation of the side chains, which are stable at least on the millisecond time scale.

other in a steric zipper. This basin might represent a viable seed for the formation of an amyloid-like ordered aggregate. The structure is similar but not identical to those reported by Sawaya et al.[83a] In particular, the layer of β-sheets (top) is shifted by two residues with respect to the layer (bottom), as compared to the experimental structure. Consequently, intersheet contacts involve different side chains, providing a better screening from the solvent. The barrier associated with the disruption of the structure of basin 3 is 16 kcal/mol at 300 K, indicating that it is remarkably stable, at variance with basin 2, and at variance with the experimental structure, which , if used for constructing a model of an aggregate with less than 30 chains, is stable only for a few nanoseconds. These results led Baftizadeh et al. to hypothesize that the rate-limiting step for the nucleation of Aβ35−40 is not associated with the formation of AP β-sheets, but with the formation of specific interdigitation of the side chains observed in basin 3. Indeed, structures with a content of β-sheets comparable to the one observed in basin 3 will become disordered, while structures arranged in a correct steric zipper are orders of magnitude more stable. This scenario is qualitatively consistent with the dock−lock mechanism.[230]

An unbiased REMD simulation of 16 Aβ37−42 peptides with CHARMM27/TIP3P was performed using 48 replicas, each for 500 ns.[239] Aβ37−42 with opposite charges at the termini is particularly intriguing because it forms amyloid fibrils with AP sheets and P β-strands. Despite frequent β-sheet formation/fragmentation events and 20% free monomers, the population of 4−5 fully P β-strands, consistent with the fibril structure, is 1−2%, while the population of 4−5 fully AP β-strands is 3−8%. The global free energy minimum consists of structures with 2−3 β-sheets, each of 2−3 mixed AP/P β-strands and a variety of sheet-to-sheet pairing angles surrounded by random coil peptides.[239] The aggregates of low-to-medium free energies consist of mixed P/AP β-strands, in agreement with integrative temperature sampling simulations of the same peptide with 16 copies using AMBER99 and GB/SA[240] and CG-REMD of 20 NNQQ and GNNQQNY peptides and other amyloid-forming peptides.[241−245] This free energy picture is also consistent with atomistic metadynamics of 18 Val_8 peptides in explicit solvent,[233] where the maximum free energy involves a transition from P/AP to P orientations when a sufficient number of parallel sheets are formed so that the free energy starts to decrease with fully P β-sheets. The REMD simulation for Aβ37−42 indicates that N_c is >8, but whether N_c is around 12−16 as estimated for the Val_8 peptide[220,233] cannot be determined due to finite size effects.

5.3. Structures of the Nuclei for Aβ1−40 and Aβ1−42 Peptides

Simulating the formation of the critical nucleus of full-length Aβ starting from a disordered aggregate and by describing the system with an atomistic Hamiltonian in explicit water is still not possible with current computational resources. However, the results obtained from the nucleation process of smaller fragments, the MD structural ensemble of the Aβ1−40/42 monomers, and experimental data on small oligomers allow some hypotheses to be drawn on the structure of the nucleus of Aβ1−40/42.

What is clear from various experimental studies is that small Aβ1−40/1−42 oligomers are rich in antiparallel β-sheets.[22,63,111,123,124] A solution NMR structure of Aβ1−40 monomer with a dimer protein is also available,[114] where the CHC and C-terminal form a β-hairpin spanning residues 17−36, with the loop region resistant to proteolysis and the rest of the Aβ residues disordered. This specific structure is also observed in three atomistic simulations of Aβ1−40 monomer using three different force fields[154,174,178] and CG OPEP-REMD of the monomer of Aβ17−36[144] and the trimer of Aβ17−42,[208] albeit with low probabilities. On the basis of these observations, one can speculate that, during aggregation, soluble oligomers may form by stacking β-hairpin-like structures with a loop formed and loose β-strands at positions 30−35 and 17−20. The next step toward the formation of the fibril, once a critical nucleus is formed, would be the crossing of a high-energy barrier associated with a concerted conformational transition in which the β-sheets become parallel and pass from out-of-register to in-register arrangements via chain reptation.[246−250]

This scenario explains why the Aβ peptide with a lactam bridge between residues 23 and 28 does not display any lag phase,[251,252] and the FAD mutations and Pro replacement at positions 21−23 change the time for aggregation.[52,53,253] This scenario is also supported by IM-MS on Aβ1−42, where the first region to aggregate spans residues 20−35, followed by residues 36−42 and then residues 1−19,[56] and the fact that a turn-nucleating D-ProGly motif in the V24−N27 region largely accelerates fibril formation of Aβ1−40.[146] Finally, there is strong theoretical evidence on several amyloid peptides that β-hairpins formed in the monomer provide a perfect seed for further growth of the aggregates and reduce lag phases for fibril formation. This is supported by simulations on Aβ25−35 peptides,[254] prion fragment PrP106−122,[255] β2-microglobulin 20−41 and 83−99 peptides,[256,257] and human islet amyloid polypeptide hIAPP1−37.[258,259] For instance, simulations on

DOI: 10.1021/cr500638n
Chem. Rev. 2015, 115, 3518−3563

Aβ25−35 showed that, although the monomer preferentially forms a β-hairpin, a transition from compact β-hairpin conformations to extended β-strand structures occurs between the dimer and trimer.[254]

An alternative Aβ nucleus is based on the atomistic metadynamics simulations of Val_8,[233] OPEP REMD simulations of GNNQQNY and Aβ16−22,[61] PROFASI MC simulations of Aβ16−22 and Aβ25−35,[260] and enhanced sampling simulations of Aβ37−42 peptides,[239,240] where a mixing of AP/P β-strands dominates in the early low-order oligomers. In this case, the maximum free energy involves a transition from mixed P/AP to fully P orientations, which occurs when a sufficient number of P β-strands is formed so that the free energy starts to decrease to a minimum. Clearly, the transition time varies with the frequency of fragmentation events dependent on the concentration. Aggregation could also start in the C-terminal region or at the CHC. Initiation in the C-terminal region is supported by two IM-MS experiments[56,137b] and the propensity of Aβ35−42 fibrils to display either P or AP β-strands within the sheets.[261a] Initial aggregation at CHC is supported by mutagenesis, where Pro replacement in any residue of region 17−21 leads to the loss of Aβ fibril formation,[253] and replacement of residues F19 and F20 by Leu or Ile does not prevent aggregation, but enhances amyloid formation.[261b]

Lastly, it is possible that fully extended metastable states with a population of 7% as described in the metadynamics of Aβ1−40 monomer[178] and REMD of Aβ1−28 monomer (see section 10) in explicit solvent represent seeds for polymerization. Overall, several nuclei could coexist with populations depending on the experimental conditions, such as T, pH, agitation, etc.

6. INTERACTIONS OF Aβ PEPTIDES WITH MEMBRANES

AD pathology is linked to interactions between various types of assemblies of Aβ peptides (e.g., oligomers, channels, and fibrils) and neural cell membranes, the membrane integrity being directly affected. Several recent experimental and theoretical studies have been aimed at unveiling the details of the specific molecular interactions between Aβ peptides and lipid membranes, providing a wealth of information. Folowing are the key findings and related hypotheses.

(1) Membranes become more permeable to ions in the presence of Aβ peptides. In contrast, monomers or fully developed fibrils have little or no effect on membrane permeability.[262,263] Lipid vesicles may also become more permeable in the presence of attached growing (i.e., not mature) fibrils.[264] Mature fibrils can also affect the structure of membranes to some extent,[265] but the effect is thought to be much less dramatic. Moreover, if the Aβ peptides are modified such that amyloid fibril formation is accelerated and the formation of small soluble oligomers is decreased, both their toxicity and their propensity for binding to lipid membranes are attenuated.[266]

(2) Several different mechanisms that could lead to membrane leakage[267,268] have been proposed and discussed: (i) the simple mechanical "carpeting" by fibrillar peptide aggregates on one leaflet of the membrane surface, which destabilizes the membrane by creating an asymmetric pressure between the leaflets; (ii) the detergent effect—a result of the surfactant-like properties associated with the amphiphilic nature of Aβ, which causes the removal of lipids from the membrane, leading subsequently to thinning or even occurrence of holes in membranes; (iii) the formation of toroid-like Aβ pores and membrane channels. It is well accepted that neuronal death in AD is related to disturbances in Ca^{2+} homeostasis. The formation of Ca^{2+} channels in lipid bilayers was directly observed in experiments where Aβ1−40 peptides were incorporated into planar phosphatidylserine bilayers. A linear current−voltage relationship in symmetrical solutions was recorded, and using AFM, an 8−12 nm doughnut-shaped structure with a 1−2 nm internal pore cavity that protrudes approximately 1 nm above the embedded bilayer surface was revealed.[263] These channels are composed of three, four, five, or six subunits, with the most common structures being those with four or five subunits (Figure 8).[269]

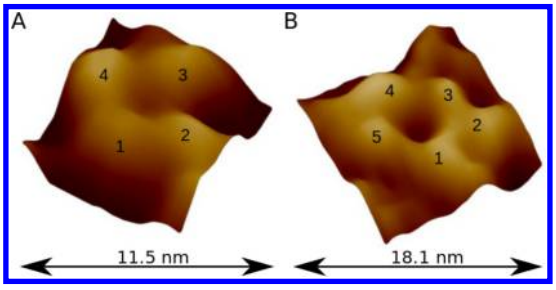

Figure 8. High-resolution AFM images of individual Aβ1−42 channels. They are most often observed as (A) tetrameric or (B) pentameric subunit assemblies. Other types (e.g., hexameric) of porelike Aβ structures were also reported.[269]

(3) Aβ aggregation can be significantly accelerated by the presence of membranes.[270−272] An important factor favoring membrane binding is the presence of electrostatic attractions between negatively charged lipid headgroups and peptides, which even persist in solutions with high ionic strength, where electrostatic interactions are almost fully screened.[270] It has been suggested that electrostatics drives the initial binding of Aβ peptides while preventing a deeper insertion into the membrane.[273] Using two novel mouse models expressing membrane-anchored or nonanchored versions of the human Aβ1−42 peptide, membrane-anchored Aβ accelerates amyloid formation. This strongly suggests that Aβ−membrane interactions play a pivotal role in early onset AD and exacerbate toxicity in mice.[274]

(4) Another factor proposed to favor membrane binding is the propensity of Aβ to form weakly stable α-helical configurations that anchor the peptide to the membrane.[275,276] Several effects have been discussed that might promote the aggregation of membrane-bound peptides.[277,278] Peptides that bind to membranes are oriented and accumulated, and they have a reduced diffusion constant. Furthermore, membranes may induce conformational changes in the binding peptides themselves (i.e., may lower their unfolding activation barriers), and they may even serve as a template for fibril formation.[270]

Many techniques are used to demonstrate the membrane-mediated effect on Aβ aggregation, including imaging methods such as AFM and TEM,[263,279] binding to amyloid-specific dyes, such as thioflavin-T, and techniques monitoring changes in protein size, i.e., gel electrophoresis, SEC, and DLS. AFM is the main technique to demonstrate amyloid pore formation in membranes.[262,267] CD and attenuated total reflection Fourier transform infrared (ATR-FTIR) spectroscopy monitor secondary structure changes upon Aβ−membrane interactions. Electrophysiological techniques allow the study of amyloid-

DOI: 10.1021/cr500638n
Chem. Rev. 2015, 115, 3518−3563

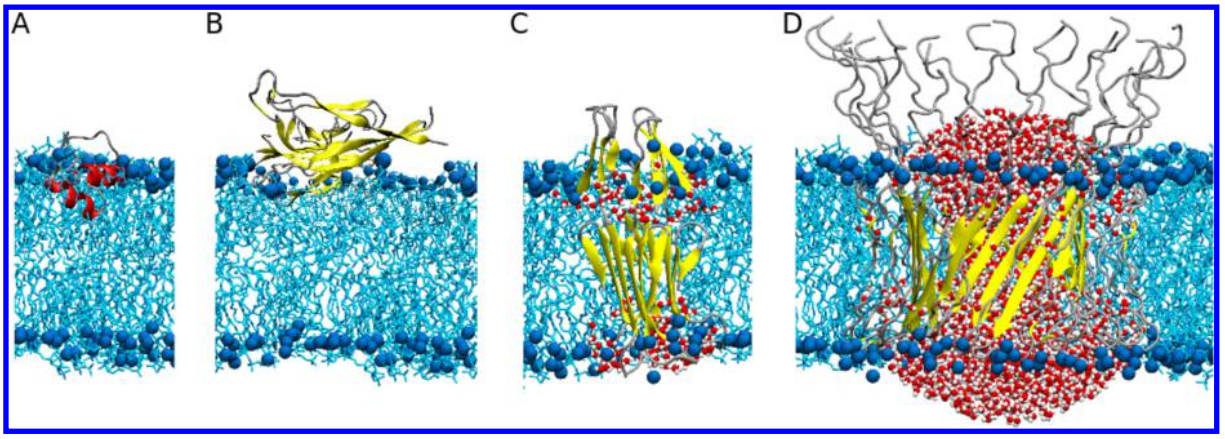

Figure 9. Various models of membrane-bound Aβ studied by MD simulations. (A) Monomeric Aβ1−40 is localized as a helical structure at the interface between membrane and solvent with the C-terminal helix inserting into the membrane.[288] (B) A fibrillar Aβ1−40 oligomer interacting with the membrane on the surface causes both a loss of β-structure and a thinning of the membrane.[273] (C) The membrane-inserted β-sheet tetramer composed of Aβ1−42 allows water to permeate through the membrane[297] and can further assemble into a pore structure.[296] (D) Aβ1−42 barrel structure leading to pore formation in the membrane, which allows water and ion transport across the membrane.[293,294] Note that structures shown here are simulation-based models, as experimental high-resolution structures of membrane-bound Aβ peptides have yet to be resolved. The structural and mechanistic relationships between the simulation models are unknown. Aβ peptides are represented according to their local secondary structure: helices (red), β-sheets (yellow), and turns (silver). The bilayer phosphorus atoms (blue) are shown as van der Waals spheres and the lipid tails as licorice-type structures (cyan). For clarity, only water molecules inside the membrane are shown (van der Waals spheres).

enabled membrane leakage.[263,270] Total internal reflection fluorescence microscopy (TIRFM) enables the visualization of individual Aβ species on membranes and the characterization of their oligomeric states, all at biologically relevant nanomolar concentrations.[58b,280,281]

The numerous recent experimental studies examining Aβ−membrane interactions have led to key, central questions that remain open, such as the following: (i) What is the main pathway for the α-to-β molecular transition accompanying the aggregation of membrane-bound Aβ? Though some studies have suggested an α-helical conformation for the membrane-attached Aβ, there is also evidence that the oligomers that attach the membrane are β-sheet-rich.[281] (ii) What is the primary molecular reason behind the toxicity of aggregated Aβ peptides. (iii) Why are amyloid oligomers the most toxic species?[149b,282] Molecular simulations may help answer these questions in greater detail as they allow the investigation of Aβ−membrane interactions at the atomistic level.

The direct simulation of entire peptide aggregation processes using atomistic models remains a challenge by speed limitations of today's computers.[210] All-atom MD simulations can give insight into the early stages of peptide adsorption and peptide−membrane interactions. Davis and Berkowitz have used REMD simulations and umbrella sampling to study the adsorption of Aβ1−42 on bilayers[283,284] and possible mechanisms of dimerization, focusing in particular on the role of electrostatic interactions.[285] They found that lipid−protein interactions dominate the behavior of Aβ on dipalmitoylphosphatidylcholine (DPPC) bilayers, whereas protein−protein interactions prevail on negatively charged 2-dioleoyl-*sn*-glycero-3-phospho-L-serine (DOPS) bilayers. Independent simulation studies arrived at the conclusion that the adsorption of Aβ on membranes follows a two-step mechanism. First, electrostatic interactions between charged residues and phosphate lipid headgroups drive the initial binding of Aβ to the membrane surface. Once Aβ is anchored to the membrane, hydrophobic interactions involving residues 17−21 and the C-terminal region from residue 30 onward gain in importance, stabilizing membrane-bound Aβ.[272,283,284,286,287] Upon adsorption on the lipid bilayer, the Aβ peptides appear to preferentially adopt a structure involving two helices: a more flexible α-helix in the N-terminal half of Aβ and a second one with a higher conformational stability, involving residues 30−36 (Figure 9A). In addition, binding to the membrane seems to induce the formation of the intrapeptide D23−K28 salt bridge in Aβ. This conformational propensity was determined from all-atom REMD with both implicit[288] and explicit[286] membranes and is in agreement with NMR studies.[275,276] The Aβ peptides are localized at the interface between membrane and water, with the C-terminal helix penetrating into the membrane core, while the polar N-terminal region interacts mainly with the bilayer surface.

Tofoleanu and Buchete probed the molecular interactions between preformed fibrillar Aβ oligomers and lipid bilayers in the presence of explicit water molecules using atomistic MD.[273] They studied the adsorption of models of Aβ1−40 dimer fibrillar oligomers on phosphatidylethanolamine (POPE) lipid membranes (composing about a quarter of all phospholipids in living cells) under different relative orientations between membrane and fibrils. They investigated the relative contributions of different structural elements and interaction factors to the dynamics and stability of Aβ protofilament segments near membranes and simulated the first steps in the mechanism of fibril−membrane interaction. The Aβ1−40 fibril structures used here were constructed on the basis of atomistic constraints from ss-NMR[28,67,79] and refined by MD simulations.[289,290] They identified the electrostatic interactions between Aβ charged side chains and lipid headgroups to be the main force driving conformational transitions, together with hydrogen bonds formed between specific residues in the Aβ protofilaments and the lipid headgroups. These interactions facilitate synergistically the insertion of the hydrophobic C-terminal segment of Aβ peptides through the lipid headgroups, leading both to a loss of the β-sheet-rich fibril structure and to local membrane-thinning effects (Figure 9B).[273] Additional computational studies showed that the chemical composition of

DOI: 10.1021/cr500638n
Chem. Rev. 2015, 115, 3518−3563

Table 3. Summary of Molecular Simulation Studies Focused on Interactions of Aβ Peptides with Lipid Membranes[a]

ref	Aβ system	type of membrane	simulation	key notes
288	Aβ40 monomer	implicit IMM1	all-atom REMD	helical Aβ structure at membrane−water interface
299	Aβ40 monomer	DPPC	all-atom MD	helical Aβ structure in bilayer with tendency to exit the membrane and localize at membrane−water interface
286	Aβ10−40 monomer	DMPC	all-atom REMD	helical Aβ structure at membrane−water interface
283−285	Aβ42 monomer and dimer	DPPC and DOPS	all-atom REMD and umbrella sampling MD	binding of Aβ to membranes, dimerization of membrane-bound Aβ
273, 291, 292	Aβ40 protofilament	POPE and POPC	all-atom MD	interactions between Aβ fibrillar oligomers and membranes influence lipid composition, structural effects
300, 301	Aβ40 monomer	DPPC, POPC, POPS, POPC/POPS, rafts	all-atom MD	stability of membrane-inserted Aβ, effect of insertion depth and membrane composition
302−304	Aβ42 dimer	mixed bilayers with cholesterol and/or GM1-mimicking rafts	all-atom MD	effect of rafts on membrane binding and dimerization of Aβ
296−298	Aβ42 monomer and oligomers	implicit IMM1 POPC, POPG, DPPC	all-atom Monte Carlo and MD	structure prediction for transmembrane Aβ, testing the stability and membrane effects of the resulting β-sheet structures, effect of mutations
293−295	Aβ barrels	DOPC, POPC, POPG	all-atom MD	models for Aβ channel structures, water and ion flux across membranes through Aβ pores, effect of Aβ mutations
311	Aβ40 and Aβ42 monomers	three-bead model for lipids	coarse-grained MD	Aβ adsorption and aggregation on small vesicles

[a]DMPC stands for dimyristoylphosphatidylcholine, POPC for palmitoyloleoylphosphatidylcholine, POPS for 1-palmitoyl-2-oleoyl-*sn*-glycero-3-phosphoserine, and POPG for palmitoyloleoylphosphatidylglycerol.

the lipid headgroups can control in a specific manner both the type and magnitude of interactions between Aβ protofilaments and membranes.[291] These findings suggest a polymorphic structural character of amyloid ion channels embedded in lipid bilayers.[292] Atomistic computational models suggest that putative amyloid channel structures could also be stabilized by interpeptide hydrogen bonds (leading to the formation of long-range-ordered β-strands), though Aβ channels may also present a significant helical content in peptide regions (e.g., the peptide N- and C-termini) that are subject to direct interactions with lipids rather than with neighboring Aβ peptides. Before experimental high-resolution structures of Aβ amyloid channels become available, various models of Aβ porelike structures traversing lipid bilayers were constructed, including helical and β-sheet and combinations of these two secondary structures.[292]

Nussinov et al. developed a model for Aβ channel structures which break into mobile β-sheet subunits and enable toxic ionic flux (Figure 9D).[293−295] The subunits are preferentially tetramers or hexamers, which could serve as building blocks for the transmembrane pores reported from AFM studies (Figure 8).[295] Strodel et al. also proposed Aβ pore models composed of tetramer to hexamer β-sheet subunits, which emerged from a global optimization study of transmembrane Aβ (Figure 9C).[296] Large-scale MD of these β-sheet subunits revealed that the tetramers themselves are sufficient to cause membrane damage, while transmembrane Aβ monomers do not perturb the membrane sufficiently to make them permeable.[297] The membrane-damaging effect of the β-sheet tetramers is further enhanced by Aβ mutations (e.g., the "Arctic" E22G mutation) and may explain the higher toxicity of these mutants compared to wild-type Aβ peptides.[297,298] Also, for helical Aβ peptides in their monomeric states, the membrane-inserted stability was tested for several pure and mixed model membranes.[297,299−301] Different insertion depths were considered, with K28, V24, D23, or K16 located at the membrane−water interface. The most stable transmembrane α-helix was observed for Aβ peptides positioned at residue D23 at the interface of a DPPC membrane,[297] while unsaturated lipids or smaller insertion depths cause a loss of α-helix, in some cases in favor of β-strands. The first stages of Aβ self-assembly inside mixed bilayers were recently tested by MD, revealing the formation of a β-sheet between two peptides in the presence of cholesterol[302] or ganglioside GM1.[303,304a,b] In the absence of GM1, no β-sheet formation is observed as GM1 mediates the initial interactions between Aβ peptides leading to oligomerization. These computational findings are in agreement with the observation that lipid rafts (i.e., cholesterol- and sphingolipid-enriched highly ordered membrane microdomains) are potential modulators of Aβ production, aggregation, and toxicity.[305] Finally, one MD simulation with umbrella sampling has recently focused on the effect of attached Aβ1−42 monomers on the free energy of membrane pores modeled with DPPC lipids. They found that the attached Aβ1−42 monomers reduce the free energy of membrane pores by 2 kcal/mol, increase the lifetime of pores, and enlarge the pore density.[306] Most of the simulations studying membrane interactions with Aβ are summarized in Table 3.

For studying the membrane-mediated aggregation of Aβ peptides on a larger time scale, one must resort to coarse-grained simulations. A number of models have been proposed.[307−311] One may distinguish between specific models, where amyloids are represented by a specific sequence,[308a] and phenomenological models, which are designed to reproduce the aggregation process in general.[309] One of the latter, the two-state mesoscopic model for proteins,[310] has been combined with a simple solvent-free three-bead model for lipids by Friedman et al. to study peptide adsorption and aggregation on small vesicles and peptide-induced membrane damage.[311] In agreement with the experimental picture, this Langevin dynamics study found that vesicle leakage occurs primarily due to transient defects during filament growth; mature fibrils did not damage the vesicles. Studying the fibril degradation in the presence of vesicles, the simulation showed that it results in protofibrillar intermediates whose structure differs from those formed upon aggregation or upon disaggregation without lipid vesicles.[311]

All these results suggest that, in spite of the high complexity of the systems including lipid membranes, computational

DOI: 10.1021/cr500638n
Chem. Rev. 2015, 115, 3518−3563

studies are becoming increasingly more feasible due both to accelerated hardware and to methodological developments and may guide new experiments that could test more efficiently the assembly and structural features of membrane-formed amyloid channels. Future simulations should be able to unravel how membranes can facilitate the aggregation of Aβ peptides and modulate the formation of oligomers, fibrils, and channels, while novel experiments are still needed to provide high-resolution structures of membrane-bound Aβ aggregates.

7. INTERACTIONS OF Aβ PEPTIDES WITH METAL IONS

7.1. Relevance of the Interaction of Metal Ions (Cu, Zn, and Fe) with Aβ

The accumulation of zinc, copper, and iron ions in amyloid plaques, a hallmark of AD, is well documented.[312] Interestingly, human plaques showed higher metal content than plaques in AD model mice.[313] Raman studies further suggested that Zn(II) and Cu(II) are bound directly to Aβ, the main constituent of amyloid plaques. Amyloid plaques are also enriched in iron, mainly present as particles containing Fe(III) supposed to originate from ferritin. Whether ionic, mononuclear iron is bound to Aβ is not clear.[314]

Although there is clear evidence for Zn and Cu interactions with Aβ in amyloid plaques, it is not known at which time point or which aggregation state these metal ions bind to Aβ in vivo. However, it seems that under normal physiological conditions Zn(II) and Cu(I/II) do not bind to monomeric Aβ, and the hypothesis is that only upon metal and/or Aβ deregulation can the formation of metal−Aβ complexes occur.[315] This is in agreement with the finding that amyloid plaques are formed around synapses in which high concentrations of Zn and Cu are released in the synaptic cleft. These released metal ions are a peculiar pool. Their ligands are not known, but these metals are readily accessible for chelation by ligands with moderate affinity. This is in contrast to classical metalloproteins, where metal ions are strongly bound and often buried in the proteins. This suggests that these synaptic metal pools are kinetically labile and moderately thermodynamically stable.[316]

Numerous other studies, from in vitro to in vivo, report evidence of a connection among metal metabolism, Aβ metabolism, and AD. This includes, for instance, reports on a Cu pool in the blood as an AD marker, the mutual regulating effects of APP and metal ions, the association of a single-nucleotide polymorphism of the Cu transporter ATPase (ATP7B) with sporadic AD, and the decrease of amyloid plaque load in AD mice after disruption of the Zn transporter ZnT-3.[317,318]

Taken together, these data suggest that metal ions such as Zn and Cu can bind to Aβ under AD conditions and could have two important impacts directly linked to AD: modulation of the aggregation behavior and, for Cu, catalysis of toxic reactive oxygen species (ROS) production.

7.2. Structure of the Cu-, Zn-, and Fe-Binding Sites of Aβ

The metal-binding sites of Cu(I/II), Zn(II), and Fe(II) within the Aβ sequence have been studied during the past two decades. Complexes of Fe(III) with Aβ at neutral pH are not stable enough to inhibit precipitation of Fe(III) as iron oxide.[314] This suggests that the interaction of Fe(III) with Aβ is only relevant in a ternary complex with another biomolecule or with particles containing Fe(III). There is a general agreement that the main binding sites for Cu(I/II), Zn(II), and Fe(II) are located in the first 16 amino acids of the peptide, at least for the monomeric form.[314] The truncated Aβ1−16 peptide containing the metal-binding domain, which is more soluble and hence more appropriate for studies in solution and does not form amyloids, is often used instead of the full-length peptide. Indeed, several spectroscopic studies showed that the metal binding of Aβ1−16 is very similar to that of the full-length Aβ1−40/42. However, as small changes can have a large impact on aggregation, further experimental and theoretical studies well connected to experiments are needed to elucidate the detailed structures of truncated and full-length Aβ.

The current knowledge on the metal-binding sites of the most relevant metal ions is summarized in Figure 10.[314,319−322] They have been identified for the soluble, monomeric complexes, but might be different in the aggregated Aβ. A general feature for all these metal-binding complexes is that

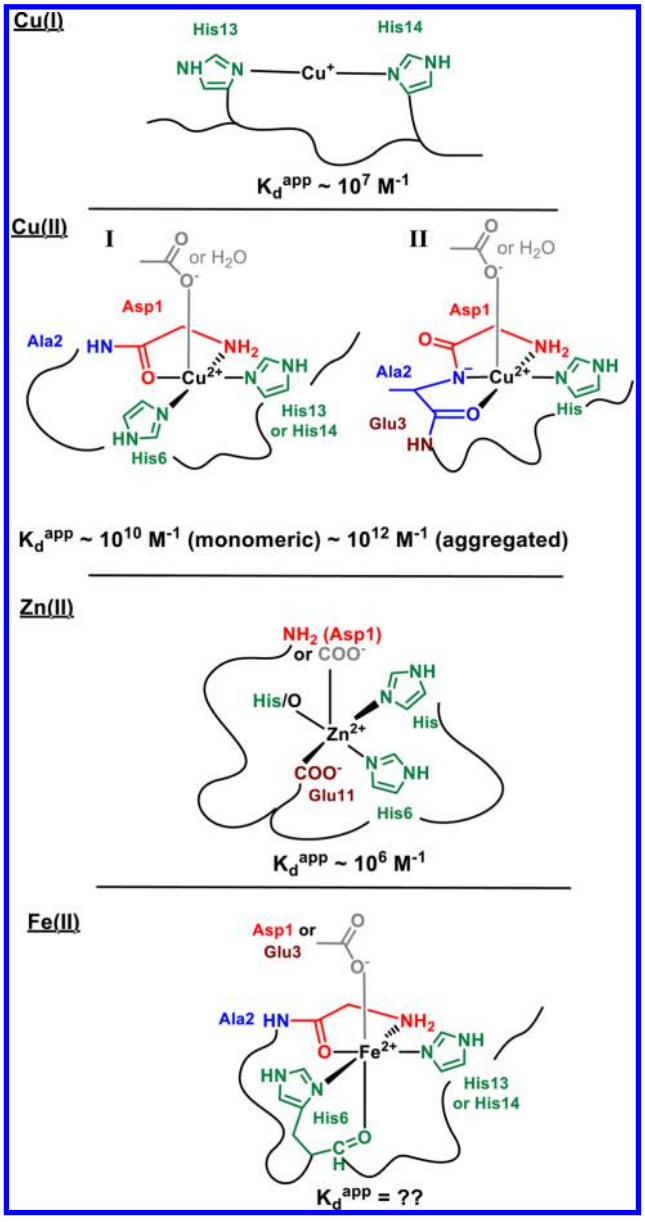

Figure 10. Models of the coordination sphere of different monomeric metal−Aβ complexes. K_d^{app} stands for apparent dissociation constant (i.e., dissociation constant at pH 7.4 in 0.1 M salt and in the absence of buffer).

DOI: 10.1021/cr500638n
Chem. Rev. 2015, 115, 3518−3563

they are very flexible and dynamic. Monomeric Aβ remains an intrinsically disordered peptide upon metal binding, as fast ligand exchange reactions and equilibrium between different binding sites exist, leading to a polymorphism in the coordination environment.

There is consensus about the Cu(I)-binding site within Aβ at pH 6−8, which consists of a linear site with two His residues as ligands. The main site is with H13 and H14 as ligands (Figure 10, top), but this site is in fast exchange (less than seconds) with linear Cu(I) bound to H6 and H13/H14.[314] Cu(II)−Aβ around neutral pH exists with two different types of coordination spheres, called components I and II (Figure 10), which are in fast equilibrium (less than seconds). Moreover, in each of these two components, further exchange between the same type of ligand occurs (e.g., between H13 and H14). Recent MD simulations confirmed this polymorphism of Cu(II)−Aβ.[323,324] There was a long debate about the coordination sphere of component I, but a consensus has been reached following the application of site-specific isotope labeling and advanced EPR and other experimental and theoretical methods.[314,319,322] Regarding component II, there are still different models proposed, but most results support the structure shown in Figure 10. Drew described however an alternative structure.[319]

Mutations of amino acids in Aβ (such as A2V, H6R, D7N), even when they concern residues not directly involved in metal binding, can have a large impact on the coordination site via second-sphere interactions.[322] This is exemplified by the comparison of Cu(II) binding to human murine Aβ, in which the mutation responsible for a dramatic change of the major coordination is R5G and leads to the following major coordination sphere: D1 (via NH_2 and O═C) and H6 (imidazole N and amide N). The impact of mutants outside the metal-binding domain remains to be established.[325]

Less is known about the binding sites in aggregated Aβ (oligomers, amyloids, etc.). Most studies suggest the same type of residues coordinating Cu(II) for the soluble Aβ, but these might come from two different Aβ molecules. A very recent study based on advanced EPR methods of fibrillar Cu(II)−Aβ1−40 confirmed the same equatorial coordination sphere of component I as in monomeric Cu(II)−Aβ1−16.[326] The results propose that the Cu(II) sites along the fibrils alternate between the two subcomponents Ia (D1, H6, H13) and Ib (D1, H6, H14). This would be in contrast to the soluble form, in which a fast (less than seconds) equilibrium between subcomponents Ia and Ib exists. Cu(II) binding to amyloid Aβ1−40 fibrils was also studied by ss-NMR coupled to MD.[327] In general, the results agreed with the EPR measurements, because H13 and H14 resonances were broadened upon addition of Cu(II) (H6 and D1 were not addressed). Other residues were also affected, in particular the C-terminal COO^- and Glu side chains. This might be explained by axial binding to Cu(II), as it was also suggested for COO^- groups in monomeric Cu(II)−Aβ1−16.[328]

In contrast to Cu, the coordination spheres of Zn(II) and Fe(II) have been less investigated. Current favored models are given in Figure 10. The models show the main ligands involved, but due to their flexibility, a polymorphism in the coordination can be expected.[329] Indeed, recent MD simulations on Zn(II)−Aβ reported that the COO^- from either D1 or E7 can bind, but in two different conformations and with a higher population for E7. The binding of either D1 or E7 had an impact on the preferred partner (i.e., D22 or E23) of the salt bridge with K28.[330] Due to the insolubility of Fe(III) even in the presence of Aβ, no well-defined species for structural studies has so far been obtained.[320,331]

The apparent binding constants of metal ions to Aβ have been determined by several methods (Figure 10 and refs 331 and 332). After some discussions in the literature, an apparent dissociation constant K_d^{app} (pH 7.4 in the absence of buffer) of Cu(II) from monomeric Aβ on the order of 10^{-10} M is now relatively consensual.[332] Interestingly, the affinity for aggregated Aβ is about 2 orders of magnitude higher.[333] A consensual value for K_d^{app} for Zn of around 1−10 μM is reported, with an up to 10-fold higher affinity for aggregated Aβ.[321] No values are reported for Fe(II/III). The binding affinity of Cu(I) to Aβ is still under debate, with values for K_d^{app} from 10^{-7} to 10^{-10} M.[334,335] In general, the affinities obtained for Cu(I/II)− and Zn(II)−Aβ are several magnitudes below the affinities of Cu− and Zn−proteins with a defined 3D structure. This is in line with the entropic penalty of metal binding to a disordered peptide. Moreover, this suggests that metals might only be able to bind Aβ at the Zn- and Cu-rich synapses and under Alzheimer conditions where metal deregulation occurs.

7.3. Role of Metal Ions in the Aggregation of Aβ

The effects of metal ions on Aβ aggregation, i.e., in terms of kinetics, thermodynamics, and structures formed and their populations, are not clear and are condition-dependent.[320,326,336a] There are two effects on which there is a wide agreement in the literature: (i) metal ions (mainly Cu(II) and Zn(II) are studied) modulate the aggregation and (ii) the effects are metal-specific; e.g., Cu(II) affects Aβ differently from Zn(II). We recently did a survey of the literature about the effects of Cu(II) and Zn(II) on the aggregation of Aβ.[320,325] Several tendencies could be identified: (i) Zn(II) and Cu(II) at high micromolar concentrations and/or in large superstoichiometric ratios compared to Aβ promote amorphous-type aggregates (precipitation) over the ordered formation of fibrillar amyloids. (ii) Metal ions affect the kinetics of Aβ aggregation, with the most significant impact on the nucleation phase. (iii) Cu(II) and Zn(II) affect the population and/or the type of aggregation intermediates formed.

At least two parameters might be important in the influence of Zn(II) and Cu(II) binding on Aβ aggregation: changes in the 3D structure(s) and in the overall charge of the Aβ complexes. At neutral pH Aβ has an overall charge of about −3: divalent metal ion binding hence yields a more neutral charge (about −2 with Cu(I/II)−Aβ and −1 to −2 with Zn(II)−Aβ at pH 7.4: note that one has to consider not only the charge of the metal ion, but also the replacement of protons by metal binding), and a faster aggregation is expected. The fact that the aggregation behavior is metal-dependent shows clearly that the structural changes upon metal binding (which are also metal specific; see Figure 10) play an important role as well.

In a more general way, metal ions can promote amorphous aggregates and amyloid-type aggregates in a condition-dependent way. It seems that the system proneness to aggregation is crucial to determine which type of aggregates are formed (amorphous vs amyloid). If conditions are such that aggregation of Aβ is already fast (as with high concentrations of Aβ and Aβ1−42, pH close to pI, etc.), Cu(II) or Zn(II) binding (in particular at high concentrations or ratios) accelerates aggregation and favors amorphous aggregates. Aggregation is too fast, however, to properly align the Aβ peptides into an ordered β-sheet structure as in amyloids. For a

DOI: 10.1021/cr500638n
Chem. Rev. 2015, 115, 3518−3563

system with a low propensity to aggregate (as with higher pH, low concentrations of Aβ and Aβ1−40, etc.), metal ions (in particular at lower concentrations or ratios) favor formation of amyloid-type aggregates. Using MD simulations, Miller et al. showed that Zn ions promote Aβ aggregation via a population shift of polymorphic states.[336b]

It is not well-known how much the structure of amyloid fibrils differs from metal-free Aβ peptides to metal−Aβ peptides for Cu(II,I) and Fe(II,III). For Cu(II), addition of this metal to preformed amyloid fibrils of Aβ does not change the peptide structure, as monitored by ss-NMR.[327] The conformation of the Zn(II)-attached fibrils has also been investigated by ss-NMR.[336c] The data show the absence of the D23−K28 salt bridge, but the presence of the F19−L34 contact. Also, Zn(II) tends to accelerate the precipitation of the oligomers without changing the overall solubility of the peptide, which may help explain why Zn(II) at low concentrations lowers Aβ toxicity.[336d]

7.4. Cu−Aβ as a Catalyst for the Production of Reactive Oxygen Species

A large body of evidence suggests that oxidative stress is implicated in AD, but it is not clear if it is a primary cause or a consequence.[337] The production of ROS is a major contributor to oxidative stress, and indeed, AD-affected tissue shows signs of enhanced ROS production, in particular around the amyloid plaques. Cu is well-known to be able to catalyze the production of ROS, and hence, it is possible that the complex Cu−Aβ is implicated in the production of ROS in AD.[331]

Indeed, in vitro experiments reported that Cu−Aβ is able to catalyze the production of H_2O_2 and HO$^\bullet$ in the presence of a biologically relevant reducing agent (such as ascorbate) and dioxygen (Figure 11, top). There is an ongoing discussion of whether Aβ is an antioxidant or prooxidant. Aβ is considered as an antioxidant on the basis of the fact that Cu in buffer catalyzes ROS production more efficiently than Cu−Aβ. However, "free" Cu concentrations are extremely low in biology as Cu

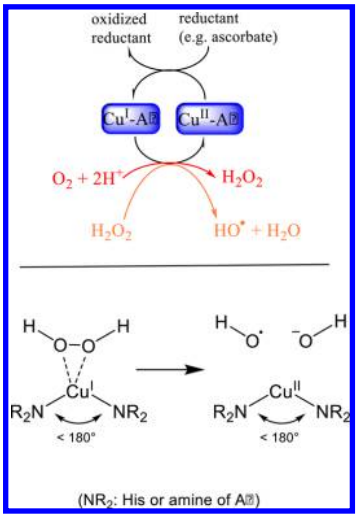

Figure 11. Catalytic role of Cu−Aβ in the production of reactive oxygen species. Top: Cu−Aβ is able to catalyze the production of H_2O_2 and HO$^\bullet$ in the presence of a reducing agent and dioxygen. Bottom: catalytic active state capable of catalyzing the Fenton-type reaction. Active are only the conformations with a diagonal ligation by the peptide remote from an angle of 180° and in which the H_2O_2 binds to Cu(I) side-on.

metabolism is tightly controlled. Hence, an antioxidant activity of Aβ compared to "free" copper might be only relevant under particular conditions where free Cu reaches higher concentrations. It does not seem evident that this ever occurs, when taking into account the presence of high concentrations of potential ligands (such as glutathione, histidine, cysteine, etc.).

Therefore, in the framework of an imbalance of Cu, it seems more relevant to compare the efficiency of Cu−Aβ with that of the Cu pool from which Aβ obtains Cu in AD instead of free Cu. However, the identity of this Cu pool is not known. To address this, the ROS efficiency of Cu−Aβ was compared with that of several biologically relevant Cu−peptide or Cu−protein complexes. Generally, Cu−Aβ was quite active, and hence, one can conclude that Cu−Aβ has the potential to contribute to oxidative stress in AD. This is supported by the finding that oligomeric Cu−Aβ aggregates have a higher ROS production activity than monomeric Cu−Aβ, in line with the higher toxicity of oligomeric Aβ.[331]

Electrochemistry of Cu−Aβ suggested that the reduction and oxidation do not occur directly between the two ground states (most populated), shown in Figure 10.[314] The reorganization energy is too important, as can be seen from the very different structures of Cu(I)− and Cu(II)−Aβ. Instead, a low-populated, (0.1%) intermediate state exists in equilibrium with the ground states, but only this intermediate state undergoes a rapid redox reaction. Thus, this state can be considered as a kind of transient entatic state. This suggests that this low-populated, intermediate state is responsible for all the redox activity, and hence, such a type of state might also be responsible for the reactivity with dioxygen and a biological reducing agent to produce ROS. Recent advances were made in the understanding of this intermediate, "hot" state.[338] The ligands of this intermediate state were assessed, and H13, H14, and D1 were identified. Interestingly, H6 is not involved. This shows that the intermediate redox-competent state is different from the two ground states.

Further computational studies using MD (Car−Parrinello) and DFT suggested that the highly reactive Cu(I)−Aβ state consists of N−Cu(I)−N coordination with an angle far from 180° and high water crowding at the open side (Figure 11, bottom).[339] This allows side-on entrance of H_2O_2 and its cleavage to form a hydroxyl radical. Interestingly, a reactive Cu(I)−Aβ state was more easily originated when starting with a dimer model (Cu(II)−Aβ_2) compared to a monomer (Cu(II)−Aβ), likely due to structural constraints of the peptide. This is in line with the higher ROS production reactivity of Cu(II)−Aβ oligomers.

7.5. Metal-Based Therapeutics

As discussed above, AD involves a mismetabolism of Cu and Zn. This mismetabolism is rather an imbalance than a general overload or lack. The imbalance tends toward an extracellular increase and an intracellular decrease of Zn and Cu. Moreover, the extracellular Cu(II) is prone to catalyze ROS.[340] On this basis, therapeutical strategies have been developed to use compounds that bind the misplaced Zn and/or Cu pool and diminish the Cu prooxidant activity (i.e., redox silence it so that it does not catalyze ROS production).[312,341] This can be achieved by moderate affinity ligands. Such drugs should have the following properties: (i) they should be nontoxic, (ii) they should cross the blood−brain barrier, (iii) they should have the right affinity, higher than that of Aβ but lower than that of

DOI: 10.1021/cr500638n
Chem. Rev. 2015, 115, 3518−3563

essential metalloproteins, and (iv) the Cu−ligand complex should not itself produce ROS.[342]

Moreover, it seems also more advantageous not only to bind the misplaced pool and redox silence it, but to transport it back into the cell.[343] Thus, a fifth property can be added: (v) the metals should be relocated, from extracellular to intracellular. The free ligand as well as its metal complex should be able to cross the membrane. A driving force is needed to release the metal intracellularly. In the case of Cu with two chemical ligands, gtsm (glyoxal−bis(*N*(4)-methylthiosemicarbazone) and PBT2 (hydroxyquinoline), the driving force is the reduction of Cu(II) to Cu(I) and subsequent decomplexation.[343] These properties are characteristic of ionophores or chaperones. Several compounds have been synthesized along these lines and tested in vitro or in AD models as inhibitors of Aβ aggregation or toxicity (for some examples, see Figure 12). The compound PBT2 went to a phase IIa clinical trial and showed improvements in two executive function component tests in a battery of neuropsychological tests.[312,315] These effects have been attributed to the ability of PBT2 to facilitate intracellular copper uptake (point v).

8. Aβ INTERACTIONS WITH PROTEIN RECEPTORS

Understanding the interactions that Aβ establishes with various cellular components is a key challenge to unveil the molecular mechanisms at the onset of AD. Aberrant interactions with membrane-associated proteins and receptors can mediate the neurotoxic effects of Aβ1−42 oligomers, such as in the case of the highly specific binding to the cellular prion protein (PrP^C).[34,35,345] This controversial interplay has been associated with impaired activity of NMDA receptors,[345,346] which mediate critical functions in the central nervous system, in conjunction with copper binding from both Aβ oligomers and prion protein. Other proposed receptors for toxic Aβ assemblies include mGluR5,[347] EphB2,[348] and GM1,[349] for which the first simulations of GM1 complexes with Aβ1−42 in lipid membranes have been reported.[304,305]

In contrast, other proteins are functionally employed as a primary biological defense against the effects of Aβ aggregation. In this context, both intracellular and extracellular chaperones are able to bind and stabilize misfolded oligomer species in such a way as to prevent further fibrilization or dissociation. In particular, clusterin, highlighted in genome-wide association studies, is thought to play a role as an extracellular chaperone.[350,351] Furthermore, serum albumin, the most abundant protein in blood plasma and cerebrospinal fluid (CSF), inhibits Aβ fiber formation.[352]

In addition to PrP, Aβ can bind to other amyloid peptides, in particular serum amyloid P (SAP),[353] islet amyloid polypeptide (IAPP; ref 354), and transthyretin.[355] Both SAP and PrP have been found within plaques of AD patients.[356,357] Finally, we should not forget Aβ1−42 interactions with other forms of Aβ, for example, Aβ1−40, that may be crucial to the misassembly process.[358,359]

8.1. Aβ−Prion Protein

The membrane-anchored PrP^C has been identified as a cell surface receptor of Aβ. Specifically, a screen of more than 200 000 proteins, using an unbiased cDNA expression library, has identified PrP^C as a principle candidate to bind to Aβ.[34] This study also showed that interaction between PrP^C and Aβ1−42 oligomers leads to the inhibition of long-term potentiation (LTP) in the hippocampal slices from normal mice expressing PrP^C. Crucially, it was shown using a mouse model of AD with a knockout PrP that AD pathology was dependent on the expression of PrP^C,[34] while PrP knockout mice can develop Aβ plaques but do not exhibit neurotoxicity.[360]

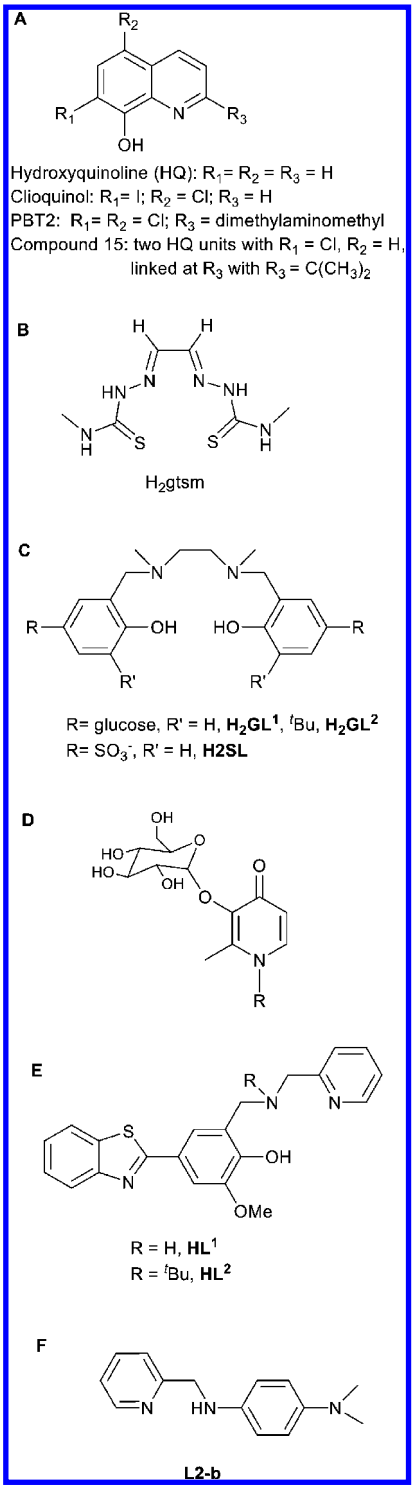

Figure 12. A selection of ligands studied in the context of metal mismetabolism in AD. **A** and **B** have ionophoric properties, a dimeric form (compound **15**) is derived from clioquinol, where the covalent attachment of two hydroxyquinolines increases Cu(II) affinity and selectivity, compounds **C** are water-soluble Cu(II) chelators, **C** and **D** are brain-penetrating Cu(II) ligands, and **E** and **F** are bifunctional Cu(II) chelators with an Aβ-targeting unit (for more details, see refs 342 and 344).

DOI: 10.1021/cr500638n
Chem. Rev. 2015, 115, 3518−3563

A nanomolar affinity between Aβ oligomers and PrP^C has consistently been reported.[34,361−364] This interaction is generally accepted; what remains contested is the influence of PrP^C on Aβ toxicity in vivo.[363−366] The conflicting observations might be explained by the multifactorial nature of AD; some of its pathology could be independent of PrP^C, while other aspects of Aβ toxicity could be PrP^C-dependent. The conflicting observations might simply reflect differences in the AD mouse model used or in some instances the Aβ preparations used. There are however a growing number of reports in animal models and hippocampal primary culture showing PrP^C-dependent Aβ toxic effects, which impair synaptic plasticity and cause special memory defects and axon degeneration.[34,345,360,367−372] Furthermore, ex vivo AD brain extracts indicate the colocalization of Aβ and PrP in amyloid plaques.[357,373,374]

Numerous lines of inquiry have consistently highlighted the natively unstructured N-terminal domain of PrP^C as the recognition site for Aβ. For example, the α-helical folded domain of PrP^C spanning residues 113−231 has no influence on Aβ fiber growth, while the N-terminal half of PrP^C spanning residues 23−126 inhibits amyloid fiber formation in favor of non-ThT-binding Aβ oligomers.[35] These PrP^C-trapped Aβ oligomers bind the oligomer-specific A11 antibody, and SEC indicates they are 12 and 24 Aβ monomers in size. More recently, larger protofibril structures of Aβ have also been identified in the presence of PrP^C.[372] Solution NMR indicates that the interaction between Aβ and PrP^C is conformation-dependent. Aβ monomer has little affinity for PrP^C, and it is not until Aβ forms oligomers that it interacts with PrP^C. It is also clear that PrP profoundly inhibits fiber formation by trapping Aβ in an oligomer form and is capable of disassembling mature fibrils.[35] The ability to trap and concentrate Aβ into toxic oligomers suggests a mechanism by which PrP^C might confer Aβ neurotoxicity in AD.

The structural bases of this interaction are currently unknown. A major limiting factor in this context is the inability of current techniques of structural investigation to characterize Aβ oligomers, which is largely due to the transient and heterogeneous nature of these aggregates. Several models of Aβ oligomers have been proposed on the basis of direct and indirect experimental evidence. These range from highly structured assemblies (mainly composed of a β-sheet scaffold) to poorly ordered oligomers, yet a consensus is still elusive on the size of the most toxic assemblies, showing a dynamic distribution of assemblies ranging from 2 to 14 monomers. An additional barrier in the study of the interaction between Aβ oligomers and PrP^C is associated with the unstructured nature of the N-terminal domain of PrP^C (residues 23−126), which poses significant challenges of studying intrinsically disordered proteins.[375,376] It was proposed that the N-terminus of PrP^C is the locus of the interaction with poorly structured, highly toxic Aβ oligomers.[362] This interaction was recently studied using computational approaches based on extensive MD simulations of dodecameric Aβ assemblies featuring short antiparallel β-hairpins at the C-terminus of the protein monomers.[377] The resulting oligomer models were used to infer the interaction with the unstructured N-terminal tail of residues 23−127 by using PrP^C models from an experimental NMR ensemble (PDB code 1QLX) and by performing mutant deletions according to ref 362. While this study could only rely on a massive use of modeling and simulations, it evidenced a conceptual model for the interaction between PrP^C and toxic Aβ oligomers that can be useful for seeding new experiments.

While the function and misfunction roles of the disordered N-terminal domain of PrP^C remain largely elusive, a large number of studies have dissected the misfolding pathways of the C-terminal PrP^C domain in the mechanisms leading to PrP^{Sc}, the scrapie fibrillar form of the protein that is associated with the prion disorders. The large number of NMR structures of the C-terminus domain provides an important starting point to sample misfolding pathways using computational[378−380] or experimental[381,382] approaches. One of the most accredited scenarios, which accounts for the role of a number of pathological mutations, is the misfolding of the native interface between two subdomains of PrP^C, the first spanning strands S1 and S2 and helix H1 and the second spanning helices H2 and H3.[383−385] This pathway, corroborated by a series of experimental evidence, possibly can interplay also in the mechanisms of interaction with Aβ oligomers by the exposure of hydrophobic surfaces that are natively hidden in the interior of the folded part of the protein.

It has been proposed that Aβ has an effect on CNS function mediated by NMDA receptor activity, including strong inhibition of long-term potentiation and enhancement of long-term depression.[346] Interestingly, it has been shown that PrP^C limits excessive NMDA receptor activity that might otherwise promote neuronal damage.[386] Significantly, PrP^C only affects the NMDA receptor in a copper-loaded state.[345] A mechanism for the PrP^C-dependent Aβ toxicity has been proposed which indicates Aβ disrupts copper homeostasis at the synapse, which is required for normal PrP^C-dependent inhibition of excessive NMDA receptor activity.[345] Aβ released at the synapse, with a picomolar affinity for Cu^{2+},[387] may disrupt Cu^{2+} binding to PrP^C and so, in part, mediate neuronal and synaptic injury.[345] The mechanism by which PrP mediates Aβ toxicity and NMDA activity[346] may also involve the Fyn receptor.[369] Several lines of evidence have been reported on the direct binding between Aβ and NMDA receptors both in vitro and in vivo[388−391] as well as on the activation of NMDA receptors by Aβ oligomers.[392] Furthermore, Aβ promotes endocytosis of NMDA receptors and so reduces the surface of NMDA receptors.[346]

The structural details of the Aβ−PrP interaction are clearly of interest and yet to be fully elucidated. Indeed, if the PrP−Aβ interaction is responsible, at least in part, for Aβ toxicity, then identifying a molecule that blocks this interaction represents a novel pharmaceutical target.[367]

8.2. Aβ−Clusterin

Genome-wide association studies have highlighted a link between the development of AD and an ATP-independent chaperone, clusterin.[393] Clusterin belongs to a family of extracellular protein-folding chaperones, including α2-macroglobulin, haptoglobin, and αS1- and β-casein, which have been shown in vitro to stabilize proteins and prevent their aggregation under conditions that normally lead to the formation of amyloids.[350,351,394−396] Clusterin is able to intervene in amorphous aggregation of a broad range of proteins in such a way as to redirect the aggregation process in the assembly process of soluble high-molecular-weight aggregates.[395,397] It has been shown by single-molecule fluorescence that clusterin interacts with small Aβ oligomers ranging from dimers to 50-mers in such a way as to form long-lived, stable complexes.[351] In this way clusterin can interplay

DOI: 10.1021/cr500638n
Chem. Rev. 2015, 115, 3518−3563

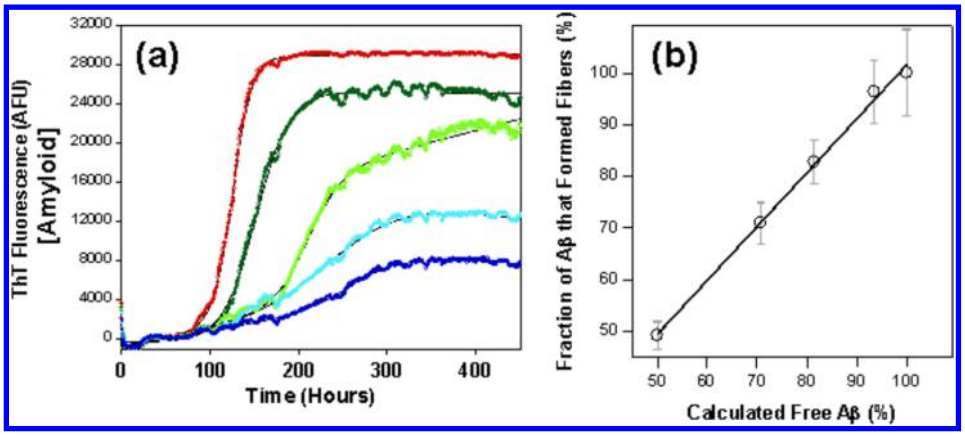

Figure 13. Physiological micromolar concentrations of albumin inhibit fiber formation. (a) Kinetics of Aβ fiber formation in the presence of no albumin (red) and 1 μM (dark green), 3 μM (green), 5 μM (light blue), and 10 μM (dark blue) albumin. (b) Competitive effects of albumin on total Aβ fibrils generated with a strong direct correlation between the fraction of fibers generated and the calculated fraction of Aβ free to form fibers (not bound to increasing concentrations of albumin), based upon a K_d of 5 mM. Adapted with permission from ref 352. Copyright 2012 American Society for Biochemistry and Molecular Biology.

with both aggregation and disaggregation processes of Aβ, sequestering small oligomers, which have been shown to be the most toxic forms of Aβ, thereby mitigating the toxic effects of Aβ aggregation. This Alzheimer's disease mechanism is corroborated by the recent discovery of colocalization of clusterin with extracellular amyloid deposits containing Aβ.[350] It has indeed been suggested that clusterin may interplay in a novel extracellular proteostasis system, in which a series of extracellular chaperones bind to misfolded proteins in vivo to keep them soluble and to inhibit the formation of toxic aggregates to facilitate their bulk uptake and degradation via receptor-mediated endocytosis.[398] The Aβ–clusterin interactions remain to be studied by computer means.

8.3. Aβ–Albumin

An extracellular binding partner identified for Aβ is human serum albumin (HSA). This interaction was first described when Aβ was isolated from blood plasma, with 90–95% of Aβ within blood plasma directly bound to albumin.[399,400] It is suggested that this interaction might explain why, unlike systemic amyloid-related diseases, although Aβ is found at a similar concentration in blood plasma and CSF (0.1–0.5 nM),[401,402] Aβ plaque deposits are typically only observed in the brain and not peripheral tissue.

Albumin is the most abundant protein found in blood plasma with a concentration of ca. 640 μM. Concentrations of albumin in the CSF are much lower (3 μM).[403] Although markedly less concentrated than in blood, this still constitutes the most abundant protein in the CSF. The affinity of monomeric Aβ for HSA has been determined, and a dissociation constant (K_d) of 5–10 μM, for both Aβ1–40 and Aβ1–42, has been consistently reported.[400,404,405] Despite the relatively weak micromolar affinity (K_d = 5–10 μM) of Aβ for albumin, a concentration in the CSF of 3 μM suggests the capacity of albumin to bind approximately half of Aβ in the brain CSF. Furthermore, this will be quite sensitive to changes in HSA concentrations. It is generally presumed that Aβ will bind to the hydrophobic pockets within albumin, which are often occupied by fatty acids, although this is not confirmed. There are reports to indicate HSA binds monomeric[400,404] or oligomeric[406,407] Aβ.

Recently, it has been shown in vitro that physiological micromolar levels of albumin found in the CSF do indeed inhibit Aβ amyloid fiber formation, significantly increasing the time before fiber nucleation occurs and decreasing the total amount of fibrils produced,[352] as shown in Figure 13. Furthermore, it was shown that the amount of amyloid fibers generated directly correlates to the proportion of Aβ not competitively bound to HSA.[352] Indeed, it is likely nearly half of Aβ in the CSF will be bound to HSA and inhibited from forming fibers. This suggests a role for HSA in regulating Aβ fibril growth in the brain interstitium, and computer simulations should soon be able to provide insights into the Aβ–HSA energy landscape as reported for HSA interacting with other molecules.[408] Thus, levels of albumin in CSF should represent a risk factor and therapeutic target in AD. It is therefore perhaps surprising that the correlation between albumin levels in CSF and risk of developing AD pathology is yet to be conclusively identified. This might suggest that typically Aβ has already formed fibers within intracellular vesicles before release into the synapse. Alternatively, Alzheimer's is a multifactorial disease, and albumin might just be one of many risk factors associated with the disease. Small variations in albumin levels in middle age may not be easily recognized, masked by a multitude of other factors that protect against or exacerbate AD pathology.

In summary, we have characterized Aβ protein interactions into three broad themes: First are cell surface interactions, for which we have focused on the prion protein (PrP^C) and its connection with NMDA receptor activity. In addition, we have looked at protective defenses against the effects of protein misfolding and aggregation in vivo, in particular by the extracellular chaperone clusterin and also human serum albumin. Finally, the interaction with other amyloidogenic proteins suggests possible interconnections between different protein misfolding diseases. For Aβ–Tau interactions, the reader can find recent data in refs 186 and408b. Overall, Aβ may exert its toxicity on neurons via more than one mechanism. Furthermore, different forms of Aβ, monomeric, oligomeric, and fibrillar, can present different recognition sites to different binding partners. There is still much to be understood about the molecular interactions of Aβ, both intra- and extracellular and at the synaptic cleft, as it is these interactions that may constitute new pharmaceutical targets.

DOI: 10.1021/cr500638n
Chem. Rev. 2015, 115, 3518–3563

9. INTERACTIONS OF Aβ WITH INHIBITORS

The failures of recent phase III clinical trials on two Aβ-targeting monoclonal antibodies, bapineuzumab and solanezumab, in the summer of 2012 indicate that the timing of the intervention of AD needs to be reconsidered.[42,409] In light of these reports, are we back to 2008 when news in *Nature* reported that the major conundrum in the field is whether we are just treating people too late? The good news is that three studies were launched in 2014 on asymptomatic individuals identified as being at increased risk of developing AD on the basis of genetic predisposition or amyloid levels.[42]

First, several protein-like drugs are briefly discussed. A homodimeric protein of 58 residues, $Z_{Aβ3}$, was found to bind to Aβ1−40 monomer and inhibit the fibrilization process. The structure of the $Z_{Aβ3}$−Aβ1−40 complex by solution NMR revealed that Aβ1−40 is locked into a β-hairpin conformation spanning residues 17−36, with the rest of the amino acids disordered, and the edges of Aβ1−40 β-sheets were capped by the two β-strands of $Z_{Aβ3}$, thus blocking the β-sheet extension of Aβ1−40.[114] Similarly, reelin, an extracellular matrix protein, was reported to stabilize the Aβ1−42 oligomers, leading to reduced toxicity and delayed fibrillization.[410]

A series of *N*-methylated peptides or D-amino acid peptides were also found capable of inhibiting Aβ amyloid formation, targeting either Aβ residues 32−37[411] or Aβ residues 16−21 (SEN304; ref 412). For instance, SEN304 was found to bind to the Aβ1−42 monomer and oligomers and to promote the formation of nontoxic aggregates. With a concentration as low as 100 nM, SEN304 was able to almost completely remove the inhibition of LTP by 1 μM Aβ1−42 in a hippocampal slice.[412] Recently, two inhibitors with alternating D- and L-amino acids of lengths 21 and 23 designed by MD simulations to form an α-sheet having all its peptide groups orientated in the same direction were found to reduce Aβ1−42 aggregation and toxicity at a molar ratio of at least 10:1.[413]

Small molecules as potential drug candidates against AD have been investigated intensively in recent years. Though differing in size, geometry, and chemical properties, the compounds in general exhibit inhibitory effects by three modes. First, the compounds can bind to fibrils and reduce toxicity by limiting fibril fragmentation. In a recent study, several compounds, including BAF31 shown in Figure 14, were found to reduce Aβ1−42 cytotoxicity against mammalian cells by up to 90%.[9b] The compounds were identified through virtual screening of 18 000 purchasable molecules and ranked according to their calculated binding energies to fibrillar Aβ16−21 segments. What is interesting in this study is that the compound binding increases the fiber stability to limit fragmentation, rather than reducing fiber formation, and the compounds do not bind to oligomers.

Second, the compounds can accelerate the formation of fibrils and reduce the lifetime of toxic oligomers. An example is an orcein-related polyphenol, O4 (Figure 14). The molecule was found to bind directly to oligomers and promote the conversion into larger amyloid fibrils, with O4 interacting with hydrophobic residues of Aβ1−42.[414]

In the third mode, the small molecules interact with oligomers and prevent fibrillization. The resulting complexes are believed to be off-pathway and nontoxic. Several polyphenols were reported to rescue AD in this way. ε-Viniferin glucoside (EVG for short; Figure 14) is one of the polyphenols that inhibits fibril formation in Aβ25−35, Aβ1−40, and Aβ1−42 and protects against PC12 cell death induced by these peptides.[415] Electrospray ionization mass spectrometry showed a noncovalent complex between one Aβ1−40 peptide and two EVG molecules.[415] Solution NMR and molecular modeling were used to characterize the interaction between the compounds, using 1 mM Aβ40 and 2 mM EVG in DMSO.[416] EVG induces the formation of turns in the 10−12 and 28−30 regions of Aβ. Chemical shift perturbations and short-range intramolecular nuclear Overhauser effects (NOEs) confirmed that EVG predominantly interacts with clefts formed by Y10, V12, Q15, and F19 or by K28, G29, A30, and I31, although no intermolecular NOEs were observed.[416]

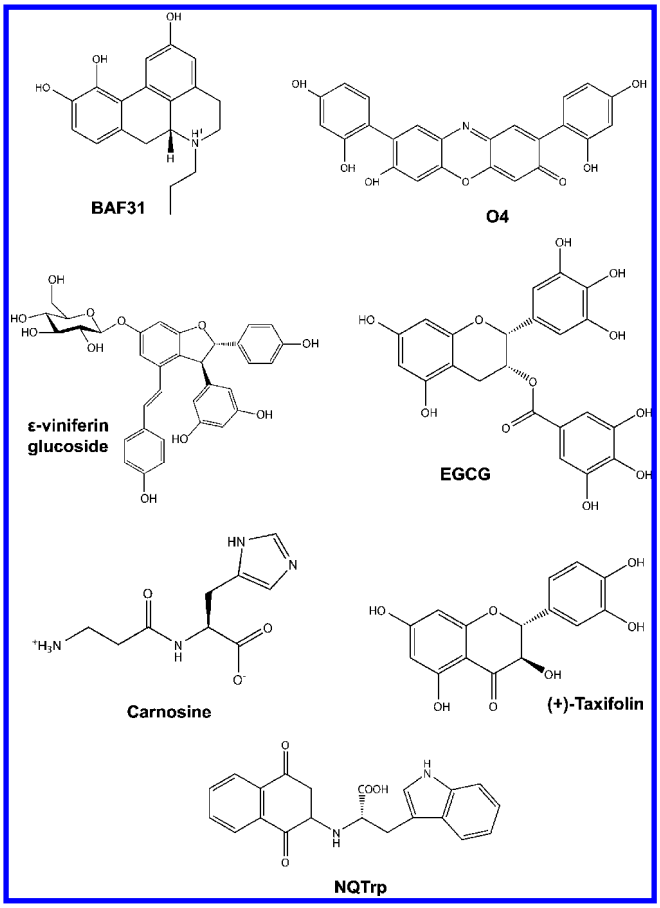

Figure 14. Chemical structures of small compound inhibitors of Aβ aggregation and toxicity.

The epigallocatechin gallate (EGCG; Figure 14) is another polyphenol showing effects similar to those of EVG. EGCG is currently undergoing a phase 2−3 clinical test against early stages of Alzheimer's disease (NCT00951834), which is expected to be completed in June 2015. EGCG was shown to redirect the Aβ aggregation pathway and generate off-pathway nontoxic oligomers which are incapable of amyloid fibrillogenesis.[417] EGCG can also remodel mature Aβ fibrils into nontoxic oligomers,[418] suggesting its therapeutic potential for treatment of AD patients. Thermodynamic analysis using isothermal titration calorimetry for EGCG and Aβ fragments/full-length peptides by Wang et al. reported that EGCG mainly interacts with Aβ residues 1−16 through hydrogen bonding and residues 17−42 through hydrophobic interactions.[419,420] Higher resolution structures of the Aβ−EGCG complex are also available. Solution-state NMR measurements performed by Lopez del Amo et al. showed that the EGCG-induced Aβ1−40

DOI: 10.1021/cr500638n
Chem. Rev. 2015, 115, 3518−3563

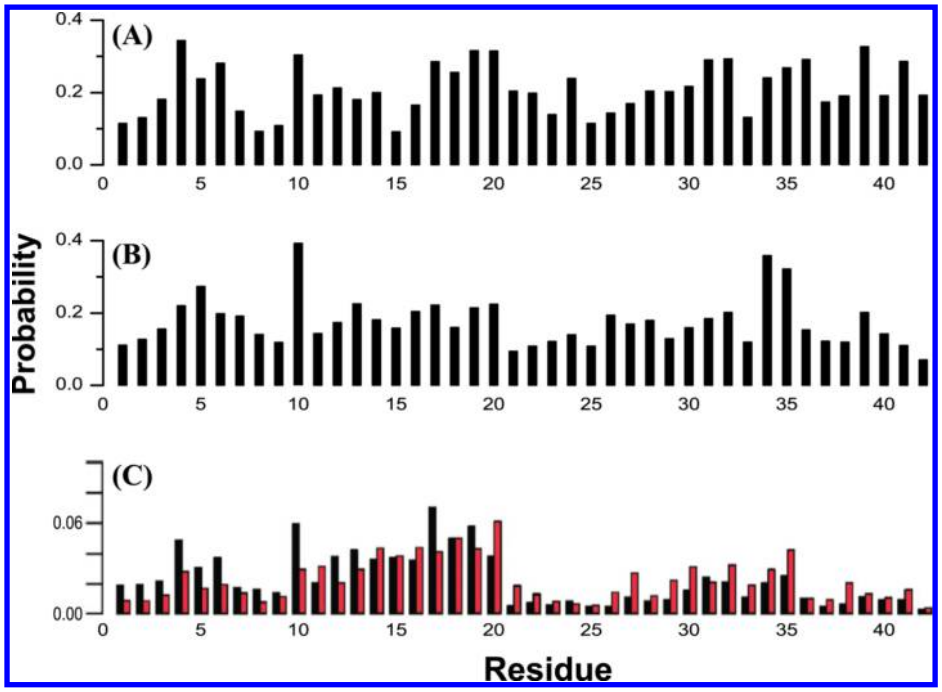

Figure 15. Contact probabilities of each Aβ1−42 amino acid with compounds. (A) Between EGCG and Aβ1−42 dimer from atomistic REMD simulation.[207] (B) Between NQTrp and Aβ1−42 dimer from atomistic REMD simulation.[432] (C) Between 10 small organic molecular fragments (e.g., dimethyl ketone, furan, and pyrazole) and Aβ1−42 monomer from REMD and FTMap.[175] Nonbonded (black bars) and hydrogen-bonding (red bars) interactions are shown separately.

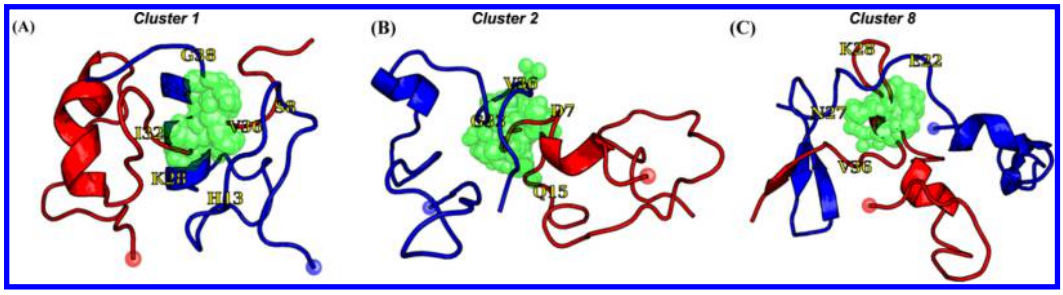

Figure 16. Representative structures of Aβ1−42 dimer−NQTrp from atomistic REMD simulations: (A) cluster 1, (B) cluster 2, and (C) cluster 8. Chains A and B are colored red and blue, respectively. The red and blue spheres represent the Cα atoms of Asp1. The center of mass of NQTrp is shown as green spheres, and we show NQTrp if it forms a contact of <4 Å with any heavy atom of Aβ1−42. Residues colored yellow assist in the reading.

oligomers adopt a well-defined structure, rather than disordered, in which residues 22−39 maintain a β-sheet conformation and residues 1−20 are unstructured.[421] Atomistic REMD simulations for the Aβ1−42 dimer with 10 EGCGs found that the equilibrium structures of the Aβ42 dimer in the presence of EGCG were characterized by the existence of 5% free Aβ42 monomers. Upon EGCG binding, the intermolecular contacts between the CHC and residues 29−42 were also greatly impacted.[207] The simulations also revealed EGCG was most likely to interact with F4, R5, H6, Y10, L17−F20, I31−I32, L34−V36, V39, and I41 (Figure 15A).

Apart from the polyphenols discussed above, non-polyphenol molecules were also found to inhibit Aβ fibrillization through binding to oligomers. Carnosine (β-alanyl-L-histidine; Figure 14), a naturally occurring dipeptide, was found to bind Aβ and inhibit fibril formation. With MD simulations and NMR experiments, again without any detection of intermolecular NOEs, carnosine was found to form transient salt bridges with charged residues in Aβ (R5, K16, and K28) and hydrophobic contacts with the CHC and flanking regions.[422] Arai et al. also designed a nonpeptidic inhibitor targeting CHC under the assumption that intermolecular side-chain and main-chain interactions must be optimal and minimal, respectively.[423]

Recently, the autoxidation of polyphenols, (+)-taxifolin,[424] and EGCG[425] into quinone derivatives was reported to be essential. The experiments revealed the potential of quinone derivatives as Aβ aggregation inhibitors. Indeed, the quinones and quinone derivatives were found to inhibit amyloid aggregation several years ago.[426−428] In 2010, Scherzer-Attali et al. observed that a quinone derivative, NQTrp (1,4-naphthoquinon-2-yl-L-tryptophan; Figure 14), was able to inhibit fibril formation by Aβ1−42 and completely recover the phenotype in a transgenic AD *Drosophila* model.[429] An extensive REMD simulation using the coarse-grained OPEP force field, followed by all-atom docking calculations, picked the NQTrp molecule as the best ligand of Aβ17−42 trimeric structures among five small-molecule drugs, including three polyphenols.[208] The NMR study with the presence of a 0.25 molar ratio of NQTrp to Aβ12−28 monomer found that the structures of NQTrp-bound Aβ12−28 were characterized by

DOI: 10.1021/cr500638n
Chem. Rev. 2015, 115, 3518−3563

two turns formed by residues 18−20 and 22−26, although no intermolecular NOEs were observed.[429] While several simulations focusing on the binding of NQTrp to Aβ fragments were performed,[430,431] an all-atom REMD simulation of the Aβ1−42 dimer with the presence of two NQTrp molecules in explicit solvent provided a different binding picture.[432] The structure representing the first most populated cluster shown in Figure 16A is characterized by two helices spanning the CHC or part of the CT (residues 30−35) region in each chain. The second cluster in Figure 16B is essentially a random coil with two short helices spanning residues 3−6 in one chain and residues 24−28 in the other chain. A structure with three β-strands is found in cluster 8 (Figure 16C), where a β-hairpin formed by residues 32−34 and 37−40 of one chain packed against a third strand formed by residues 39−41 of the other chain. Overall, 555 clusters were identified, and the residues with high probabilities to interact with NQTrp are F4−D7, Y10, H13−H14, K16−L17, F19−F20, S26, K28, I31−I32, L34−M35, and V39 (Figure 15B).[432]

Complexes of EGCG or NQTrp with Aβ both involve several hydrophobic residues, including Y10, L17, F19−F20, I31−I32, L34, and V39, though, overall, the sites with the highest interaction probability are clearly different (Figure 15A,B). R5, K16, K28, and the CHC region are found in the binding sites of both NQTrp and carnosine. The proclivity of Aβ1−42 monomer to form pockets able to bind small molecules was investigated by Zhu et al. with a 100 ns REMD simulation with AMBER99sb/TIP3P.[175] The 35 most populated Aβ1−42 monomer centroids were subjected to fragment-based calculations and the most populated binding pockets identified using FTMap[433] and FRED.[434,435] The CHC residues were found to have the highest propensity to bind small molecular fragments, but F4, Y10, and M35 were also involved in many of the hotspots (Figure 15C).[175] In contrast, the central region (particularly 22−26) had a much lower tendency to form binding hot spots. This reduced probability agrees with the reduced experimental $^{1}H-^{15}N$ HSQC chemical shift perturbation of central region residues when certain small compounds are titrated into the Aβ monomer sample.[435,436]

Obtaining high-resolution structures of Aβ monomer−inhibitor complexes from NMR with intermolecular NOEs remains a challenge. The strategy adopted in REMD simulations of Aβ−EGCG and Aβ−NQTrp complexes suggests a general first-order approach to screen Aβ−inhibitor interactions, but this remains a very difficult task because current inhibitors interacting with the Aβ monomer, dimer, and trimer show many binding sites with small occupancies and contact surfaces.[207,432,437] Apart from simulations, the cost-effective virtual screening favors the discovery of novel inhibitors with high-quality receptor structures. Recently, a ligand-based drug design provided an approach different from virtual screening to the discovery of novel inhibitors.[438] The method used a known inhibitor, a substituted Aβ1−42 peptide termed [Nle^{35},D-Pro^{37}]Aβ1−42. The structure of residues 35−40 from the inhibitor was stripped of side-chain atoms except D-Pro and used as a query to screen for small molecules with similar spatial geometry and recapitulated hydrogen-bonding interactions. A compound was found to inhibit Aβ1−42 aggregation with an IC_{50} of 13 μM. The approach is of great interest as it provides a good demonstration for both theoretical and experimental work of how to cooperate and the great benefits.

10. TRUNCATED VARIANTS OF Aβ AND PATHOGENIC AND PROTECTIVE Aβ MUTATIONS

Familial forms of Alzheimer's disease represent only a small fraction of all AD cases and show an autosomal dominant pattern of inheritance, which often results in early onset symptoms (in general between 40 and 65 years old). FAD mutations occur on the presenilin PSEN1 and PSEN2 genes as well as on the APP gene from which Aβ is processed.[439] We will therefore focus on APP mutations and particularly within Aβ spanning residues 672−714 for the 42 amino acid sequence.

10.1. Experimental Findings

Over 30 mutations in the APP gene are known today, 25 of which are pathogenic and autosomal dominant with an early onset disease phenotype and 2 of which are reported to be protective mutations against AD.[440] To better understand the pathogenic and/or protective effects of AD mutations, it is important to genetically screen significantly large groups of AD and non-AD patients to obtain very good single-nucleotide polymorphism (SNP) statistics.

Four types of FAD genetic aberrations have been observed to happen within the APP gene: complete gene duplications, single-point missense substitutions, and deletion or insertion of a nucleotide. Gene duplications cause an overexpression of APP, which inevitably implies an overproduction of Aβ[441] and all the consequential toxicity known to accompany it. Some mutations occur near the APP-to-Aβ β- and γ-cleavage sites, which generally results in an overproduction of Aβ[442,443] or shifts the relative amounts of Aβ1−40 and Aβ1−42 toward a higher production of the more toxic Aβ1−42.

Many pathogenic FAD mutations increase Aβ propensity to aggregate in vitro.[442,443] In particular, the mutations located in and near the CHC, the Flemish (A21G), Dutch (E22Q), Italian (E22K), Arctic (E22G), and Iowa (D23N) mutations, are also known to increase the toxicity mediated by Aβ. Because of their close proximity to the α-cleavage site (K16−L17), some of these mutations have been reported to also decrease the production of nonamyloid products and increase Aβ levels while making the mutant Aβ resistant to the Aβ-degrading enzyme neprilysin.[444] Teplow et al. characterized the role of various residues and reported that Aβ1−40 is mostly sensitive to mutations at positions 22 and 23 such as E22G and D23N, while Aβ1−42 is most affected by A21G.[150] It has been shown that A21G decreases fibril elongation and promotes protofibril and toxic oligomer formation, while E22G is observed to increase the rate of protofibril formation. The effects of the FAD A21G and E22G mutations have also been studied using IM-MS, showing that the early oligomer distributions differ for each mutant and the Aβ alloform.[53] Another pathogenic FAD mutation is the Osaka E22Δ mutation, which consists of a deletion of residue 22. E22Δ is known to induce a cholesterol-mediated toxicity as the mutation modulates levels of intracellular and extracellular Aβ, the secretion of which normally regulates cholesterol efflux.[445] The de novo D23Y mutant and proline substitutions in the CHC have also been shown to affect self-assembly and toxicity.[139,446]

Experiments have also highlighted the importance of the N-terminal residues 1−16,[50,53−55,444,447] whose role has been underestimated in the past owing to their highly disordered structure in synthetic Aβ fibrils. These include the pathogenic FAD H6R (English), D7H (Taiwanese), and D7N (Tottori) mutations. In particular, D7N accelerates the kinetics of transition to β-sheet-rich configurations and promotes the

DOI: 10.1021/cr500638n
Chem. Rev. 2015, 115, 3518−3563

Table 4. Computational Studies on the Variants[a]

Ref.	Mutations	Aβ alloforms	Oligomer size	Force field & solvent model	Method	Timescale	Theoretical findings upon mutation
473	A2V	1-28	1	CHARMM22* TIP3P	T-REMD	9.8 μs	- population of β-hairpins increased 4-fold - intrinsic disorder decreased 2-fold - Free-energy landscape very different from WT
465	H6R	1-40, 1-42	1, 2	OPLS-AA TIP4P	MD	3.7 μs	- rate of fibril formation increased - in Aβ1-42: increase in β-structure at C-terminal (monomer and dimer) + increased stability of 23-28 salt-bridge in monomer - in Aβ1-40: increase due to enhanced turn in region 25-29 and decrease in α-helix propensity in regions 10-13, 26-29 and 30-34 (monomer)
466	D7H	1-40, 1-42	1	OPLS-AA GB/SA	T-REMD	24 μs	- 2-fold decrease in overall β-propensity + decrease in salt-bridge 23-28 formation in both monomers.
464	D7N	1-40, 1-42	1, 2	OPLS-AA TIP3P	MD	7.4 μs	- monomer changes its fold and its salt-bridges network - dimer changes its secondary structure, salt-bridges and topology - increase in the aggregation rate
462	A21G	1-40, 1-42	2	GROMOS96 GB/SA	MD	60 ns	- mutation destabilizes β-sheets and slows down aggregation for Aβ1-40 but not Aβ1-42 - mutation increases the flexibility of the CHC in Aβ1-40 & Aβ1-42 - mutation affects intra- and inter-molecular salt-bridges involving Glu22, Asp23 and Lys28
177	E22K, E22Q E22G, D23N	1-42	1	AMBERFF99SB TIP3P	MD	>1000 μs	- all monomers are rather disordered - elimination of electrostatic interactions of E22K and E22Q increases α-helices in region 20-23 - all mutants decrease α-helix propensity in the C-terminal region 33-36 but same β-propensity.
460	E22Δ	1-40, 1-42	1	AMBERFF99SB Implicit GB/SA	T-REMD	2.4 μs	- higher α-helix propensity (both Aβ1-40 & Aβ1-42) - turn structure in region 21-30 less abundant in both Aβ1-40 & Aβ1-42 - disappearance of key intramolecular interactions between N-terminal, CHC and C-terminal - Aβ1-40-mut is more prone to aggregation that Aβ1-42-mut - 30% decrease in Lys16 salt-bridges but strengthening of Lys28 salt-bridges
178	E22K	1-42	1	AMBERFF99SB TIP3P	MD	>700 μs	- E22K increases α-helix propensity in region 20-24
184b	E22G	1-40, 1-42	1	CG Implicit	DMD	$60*10^7$ steps	- E22G destabilizes contacts within the region 21-30 for Aβ1-40 & Aβ1-42 - major N-terminal structural change that prevents formation of β-hairpin at A2-F4 (Aβ1-40) - higher β-propensity in N-terminal: induces a toxic β-hairpin at R5-H13 (Aβ1-40)
463	D23N	15-40	2	AMBERFF99SB TIP4P-Ew	Minimization ab-initio FMO	n. a.	- disappearance of salt-bridge between Asp23 and Lys28 in parallel β-sheet conformation = loss of stability for parallel β-sheet conformer
202	F20E E22G E22G I31E	1-42	2	PROFASI Implicit	MC	$80*10^{10}$ steps	- all mutations affect the aggregation propensity - main structural variations in region 20-30
474	Pyroglu-tamate variants	3-40, 3-42, 11-40, 11-42	32	CG Implicit	DMD	$3.2*10^9$ steps	- truncated variants form larger oligomers - Aβ3-40/42 has a more flexible & solvent exposed N-terminal region - Aβ11-40/42 sees its N-terminal be less accessible to the solvent which might explain why it is less toxic than full-length Aβ

[a]The abbreviation "na" stands for not applicable.

early formation of higher order oligomers with more α/β structures that are significantly more toxic compared to WT Aβ1−40 and Aβ1−42.[149a] An IM-MS study also showed that the FAD D7N mutation leads to early oligomer distributions that differ from that of Aβ1−40 to Aβ1−42.[53] The double substitution D1E/A2V also affects Aβ1−40 fibrillogenesis and predominantly forms neurotoxic aggregates.[448] Finally, a novel FAD mutation, K16N, found in one family was shown to increase Aβ production as it is a poorer substrate for α-secretase. The mutant K16N Aβ is itself not harmful, but becomes toxic when mixed in an equimolar ratio with WT Aβ, inhibiting WT Aβ1−42 fibril formation and producing more Aβ oligomers.[444]

In many cases, key side chain interactions are reported to be at the origin of Aβ toxicity. On the basis of the Aβ1−42 fibril model,[29] the K16N mutation is reported to add a hydrogen bond between the side chains of K16 and N16 in heterotetramers, therefore increasing the stability of the aggregates.[444] The importance of the lysine residues in Aβ has been further highlighted by Sinha et al., who rationally designed K16A and K28A mutants.[151a] K16 is known to be important for driving fibrillogenesis, while K28 is thought to stabilize a loop driving Aβ folding. What they found is that each mutation by alanine has profound effects on Aβ assembly and dramatically reduces Aβ toxicity, suggesting the design of inhibitors targeting K16 and K28. Another example is provided by the FAD D23N mutation, which, by preventing the formation of a salt bridge with K28, also modifies toxicity. Finally, the English mutation, by adding one charged residue, and the Taiwanese and Tottori mutations, by deleting one charged residue, are also likely to change the network and populations of all salt bridges.

Surprisingly, there are no toxic FAD mutations reported in the C-terminal region (residues 30−42), though a high percentage of Aβ with a Met-sulfoxide at position 35 is present in the AD brain,[449] yet the de novo Aβ G33A and GI33 variants have been shown to promote the aggregation process in vitro by increasing the population of large oligomers (16−20-mers) at the expense of small oligomers (2−4-mers). However, how they affect the structures of the early-formed Aβ1−42 oligomers is an open question.[450] On the basis of in vitro and in vivo experiments, Aβ1−42 oligomers with substitution of G33 by alanine and isoleucine are much less toxic than the WT Aβ1−42, suggesting that G33 may represent the critical residue linking toxicity and oligomerization, therefore adding complexity to the origin of toxicity.[450] Enhanced aggregation propensity of Aβ1−40 was also confirmed in the double de novo mutants G33V/V40A and I31L/M35L,[451] and in a more extensive study, Hecht et al. demonstrated that particular nonpolar side chains in the C-terminal half of Aβ1−42 are not required for aggregation and amyloidogenesis.[452]

Besides Aβ1−40 and Aβ1−42, the truncated Aβ4−42 and Aβ5−42,[46] Aβ1−26, Aβ1−30, and Aβ1−39 peptides are found in amyloid plaques.[40] The Aβ1−43 peptide, extended by a single threonine at the C-terminus relative to Aβ1−42, has a stronger neural toxicity and higher aggregation capacity than Aβ1−42[453] and increases the rate of extent of protofibril aggregation and confers slow C-terminal motions in the monomeric and protofibril-bound forms of Aβ1−43.[454] In addition, many post-translational modifications of Aβ peptides are also observed in amyloid plaques. Among the modifications, proteolytic removal of D1 and A2 and the subsequent cyclizing of E3 and E11 to a pyroglumate (Aβ3(pE) and Aβ11(pE)) are particularly interesting.[47−49] Aβ(pE) is more cytotoxic and aggregates more rapidly than conventional Aβ. Only 5% Aβ3(pE)-42 mixed with 95% WT Aβ1−42 is enough to significantly enhance the cytotoxicity in vivo through the formation of hybrid Aβ3(pE)-42/Aβ1−42 oligomers. In light of these observations, it was postulated that Aβ3(pE) might trigger AD by propagating through a template-folding prion-

DOI: 10.1021/cr500638n
Chem. Rev. 2015, 115, 3518−3563

like mechanism with Aβ1−42. This truncated variant is also known to be acting in a Tau-dependent manner and to be particularly resistant to degradation.[50]

The most intriguing and interesting mutations are undoubtedly the AD-protective ones, but they have not been extensively studied experimentally and theoretically. Two protective mutations at position 2 of Aβ (position 673 in APP) have been reported. A rare genetic mutation observed in a single Italian kindred, A2V, causes an early onset of AD when it is only inherited from both parents, while heterozygous carriers of A2V are unaffected. A2V enhances Aβ1−40 aggregation kinetics by a factor of 4, but the mixture of the Aβ1−40 WT and A2V peptides protects against AD.[54] Using multiple low-resolutions methods, an equimolar solution of Aβ1−42 WT and A2V produces smaller aggregates with much slower kinetics than Aβ1−42 WT, suggesting instability of the mixed aggregates.[455]

The A2T mutation, on the other hand, is always a protective mutation, independently of its homozygous or heterozygous form. It was reported in 79% of a non-AD control group with better cognitive test results compared to those of an AD group by using a large-scale DNA screening of Icelanders.[55] Thus far, this mutation has not been observed in non-Nordic populations.[456,457] This mutation reduces Aβ production by 40%, at variance with A2V in its homozygous state, which enhances Aβ production.[54] Importantly, ThT fluorescence essays reveal that the mutations, while having little effect on Aβ1−42 peptide aggregation, drastically modify the properties of the Aβ1−40 pool, with A2V accelerating and A2T delaying aggregation of the peptides. In agreement with the results of ref 455 on the mixed A2V/WT aggregates, A2T forms smaller aggregates than the WT peptides.[458] This finding on the kinetics and oligomer sizes should however be confirmed by Nile red binding and static light scattering experiments, respectively. Whether more unstable oligomers render them more available for degradation is sufficient to explain in vitro experiments showing that A2T attenuates the APP-mediated intracellular cell death[459] remains to be determined. Taken together, the physical properties of the Aβ1−40/42 A2V/A2T and Aβ3(pE)-42 peptides raise many questions and open new drug-design perspectives.

10.2. What We Have Learned from Mutational Computational Studies

Most of the simulations studying the effects of mutations are summarized in Table 4. For each mutant, we give its polymeric state, the method used, and the main findings. Many simulations of the Arctic E22G mutation have been performed and highlight its destabilizing effect on the region 20−30[184b,202] and its increased β-strand effect on the N-terminal.[184b] The other mutations at position 22 also have significant effects on the CHC structure and flexibility and either induce more[176,177,460] or less[176] α-helix structure, although all mutants remain essentially disordered. Lin et al., on the basis of thousands of MD trajectories simulated with AMBER99sb/TIP3P, have therefore postulated that there might exist a link between α-helix propensity and aggregation kinetics.[177] As a result, an increased helix−helix interaction between dimers may result in altered kinetics of oligomerization.

Other mutations in the region 20−23 have been shown experimentally to modulate the rate of aggregation.[442,443] This effect is observed in several computational studies showing an increased aggregation propensity for E22Q[461] and a reduced aggregation propensity for F20E dimers.[202] In some cases, the CHC residues may also become solvent exposed and then serve as docking sites for Aβ deposition onto the fibril (E22Q).[461] MD simulations on A21G report a decrease in β-strand propensity for the Aβ1−40 and Aβ1−42 dimers upon substitution,[462] and this was confirmed by an IM-MS experiment.[53] The simulations also reveal that the per residue β probability varies from that of Aβ1−40 and Aβ1−42 dimers upon A21G substitution. The D3N mutant in both alloforms was also studied by all-atom MC simulations and OPEP CG REMD simulations, both in implicit solvent, and showed that, by perturbing the side-chain H-bond network, the peptide remains compact[202] or displays a rather independent N-terminus.[195] In particular, the latter simulation showed that the D23N mutation causes nonlocal perturbations of the WT conformational ensemble by increasing the β-sheet propensity at the C-terminal region. This result is in agreement with the ss-NMR structure of a highly synaptic Aβ1−40 toxic oligomer with a stable N-terminal β-strand.[126] Finally, the dimers of Aβ15−40 WT and D23N were studied using a selected number of parallel and antiparallel molecular-mechanics-generated conformations that were refined by ab initio FMO (fragment molecular orbital) calculations. It is found that, in water, the parallel conformation is more stable than the antiparallel one, due to the larger hydration energy for the parallel conformation for both the WT and the D23N Aβ15−40 dimers.[463]

Simulations of the FAD D7N and H6R variants also proposed different mechanisms for the increased Aβ aggregation.[464−466] For instance, all-atom MD simulations showed that D7N enhances the aggregation rate by decreasing the turn propensity at residues 8−9, by perturbing salt bridge half-lives, and by reducing the bending free energy of the loop region.[464] Simulations on H6R, in contrast, show the rate of fibril formation of Aβ1−42 increases due to increased β-structure at the C-terminal in both the monomer and dimer and enhanced stability of salt bridge Asp23−Lys28 in the monomer, while the enhancement of the turn at residues 25−29 and reduction of the coil in regions 10−13, 26−19, and 30−34 would play the key role for Aβ1−40.[465] The results of the FAD D7H simulations[466] are discussed in Table 4.

De novo mutations were also investigated, such as the mutation D23Y, whose effect on the hexamer of Aβ1−40 was reported to favor the locking of Aβ monomer onto fibrils, thus promoting fibril growth. Simulations found that the interactions with the aromatic ring of Y23 are more fibril-compatible than those with the negatively charged D23.[467] The de novo G33A and G33I mutations were also explored on the monomer and dimer of Aβ29−42, and the REMD simulations showed a significant reduction of the β-hairpin population upon both mutations and a destabilization of the dimer due to an increase in hydrophobicity.[468]

Atomistic MD simulations of monomeric Aβ1−40 Met-ox found that M35 oxidation decreases the β-strand content of the C-terminal (residues 29−40), with a specific effect on the secondary structure of residues 33−35, thus potentially impeding aggregation. Furthermore, there is an important interplay between oxidation state and solution conditions, with pH and salt concentration augmenting the effects of oxidation.[469] REMD simulations of Aβ1−43 dimers followed by ab initio calculations revealed a ring-shaped conformation, in which T43 is hydrogen bonded to R5, which is absent in Aβ1−42 dimers.[470] Simulations of Aβ1−39 monomer and dimer with CHARMM/SASA revealed a very high percentage of α-helices,

DOI: 10.1021/cr500638n
Chem. Rev. 2015, 115, 3518−3563

which is likely due to the very high bias for α-helix of this force field.[471,472]

Finally, the A2V variant and the Aβ3(pE)-42 peptides have started to be studied by computer simulations. First, Nguyen et al. have found via all-atom REMD simulations that the A2V mutant of Aβ1−28 is much less intrinsically disordered than the WT peptide, increases the propensity to form β-hairpins, and enhances the α-helix in the region 17−24. Both peptides display a non-negligible population (7%) of extended metastable conformations, differing however in their atomic details, that represent ideal seeds for polymerization. More importantly, the two conformational ensembles are totally different, suggesting unstable dimers.[473] This result is in agreement with the increase in β-propensity of pure A2V aggregates by light scattering and provides a first answer for the reduced aggregation kinetics of the mixture of WT and A2V peptides.[54] Atomistic REMD simulations of WT−WT, WT−A2V, and WT−A2T Aβ1−40 dimers are in progress.

A DMD-CG simulation in aqueous solution of 32 AβpE3 and AβpE11 peptides lacking pyroglumate at positions 3 and 11 reported that truncation of the N-terminal residues in Aβ3−40, Aβ3−42, Aβ11−40, and Aβ11−42 shifts the oligomer size distribution toward larger oligomers as observed experimentally.[474] Moreover, the fact that the N-terminal of the AβpE3−40/42 and Aβ11−42 variants is more flexible than the Aβ1−40/42 WT peptides could be related to their increased toxicities relative to those of the WT peptides. The activity of Aβ3(pE)-42 pores has been studied using a planar bilayer recording and their architectures provided by all-atom MD simulations showing that the N-terminal β-strands tend to reside in the hydrophobic lipid core, in contrast to those of WT Aβ1−42 peptides.[475] Using multiple experimental essays and MD simulations, Lee et al. compared the adsorbed and membrane-inserted oligomeric species of AβpE3−42 and Aβ1−42 peptides. They found lower concentrations and larger dimensions for both species of membrane-associated AβpE3−42 oligomers. The larger dimensions are attributed to the faster self-assembly kinetics of AβpE3−42. Membrane-inserted AβpE3−42 oligomers were also found to modify the mechanical properties of the membrane.[476]

11. CONCLUSIONS

We have reviewed what experiments and computer simulations can tell us about the amyloid β protein and its link to Alzheimer's disease. Our knowledge of the structures of synthetic Aβ1−40/1−42 fibrils, protofibrils, and large oligomers has markedly increased in recent years, and it is clear that polymorphism is present from the monomer to fibrils. We know that fibrils with different molecular structures can result from environment-dependent self-assembly and kinetic rather than thermodynamic control. We also know that metastable states can be alleviated by using appropriate seeds or under shear flow and the structural models of the Aβ1−40 fibrils that build up take on different structures in the brain of diseased Alzheimer's patients with different AD symptoms. This high degree of polymorphism, which arises from many physical factors and persists in vitro and in brain tissues, is correlated to different phenotypes and is rather bad news for drug design because one drug may be efficient for one patient but not for another.

Structural and dynamical characterization of the smallest oligomers, the most toxic species, and the monomers has been moving at a lower pace due to their transient character and intrinsic disorders, but with the help of new experimental methods and efficient sampling methods using multiple force fields and representations, our knowledge of these species in aqueous solution, in proximity to or in the membranes, with and without ion metals should significantly increase, although polymorphism of the aggregates and high sensitivity of external conditions will not facilitate the reproducibility of the experimental readouts and the convergence of the simulations. One particular advantage of computer simulations, however, is that calculations can be repeated using different pH conditions and model membranes and the effects of site-specific mutations can be investigated.

Characterizations of the primary nucleus/nuclei and the population of the amyloid-competent monomeric state[477] prior to the lag phase remain difficult both experimentally and theoretically due to the sensitivity of the experimental conditions and the amino acid sequence. One amino acid substitution is sufficient to change the free energy landscape as evidenced from the kinetics and the oligomer size distribution of FAD Aβ variants and the recent isotope-edited and ss-NMR findings that Aβ16−22 with E22Q displays by unexpected antiparallel β-strand orientation intermediates that later transition completely into parallel β-strands, suggesting a new nucleation mechanism in a progressive assembly pathway.[478]

Understanding the interactions that the Aβ1−40/42, Aβ1−40/42 A2V and A2T variants, and Aβ3(pE)-42 peptides in both monomeric and oligomeric forms establish with metal ions and various cellular components is a top challenge to unveil the molecular mechanisms at the onset of AD. Again, both biochemical and biophysical experiments along with simulations have just started to give a more precise picture, but important efforts toward this direction should be pursued.

How the structures of Aβ may relate to the mechanism of toxicity is still unknown since toxicity comes from all oligomers to the fibrils. One source of toxicity comes from membrane channel formation, and the cylindrin conformation has been suggested to be toxic, but other antiparallel β-sheet conformations are also considered toxic. In addition, a single amino acid change is able either to reduce (A2T, A2V) or to increase (FAD, K16A) toxicity. Another source of toxicity comes from metal ions and the interactions with the cellular partners, but our understanding is still limited. To this end, we are currently investigating the polymerization and depolymerization processes of Aβ WT, A2V, and A2T assembly in the absence and presence of PrP as well as the toxicity of the assemblies.

Despite extensive studies, drug after drug aimed at targeting Aβ has failed to slow the progression of AD in clinical trials. If it is true that we are treating people too late, there are however two other hurdles for drug improvement. First, while many groups are working on developing drugs that bind to Aβ fibrils (therefore reducing the fragmentation process) or bind to Aβ oligomers to slow or accelerate fibrillation, and in all cases reduce Aβ cytotoxicity, how any interact with Aβ1−42 and Aβ3(pE)-42 oligomers is unknown at an atomic resolution, yet obtaining high-resolution structures of the Aβ oligomer/drug complexes is a prerequisite to optimizing the kinetic and thermodynamic binding properties of promising compounds (and thus their specificity), prior to cell viability essays, animal models for AD, and clinical trials. The second hurdle is that repeated identification of the same types of molecules as promising hits against different proteins is polluting the chemical literature. For instance, quinones are redox cyclers,

DOI: 10.1021/cr500638n
Chem. Rev. 2015, 115, 3518−3563

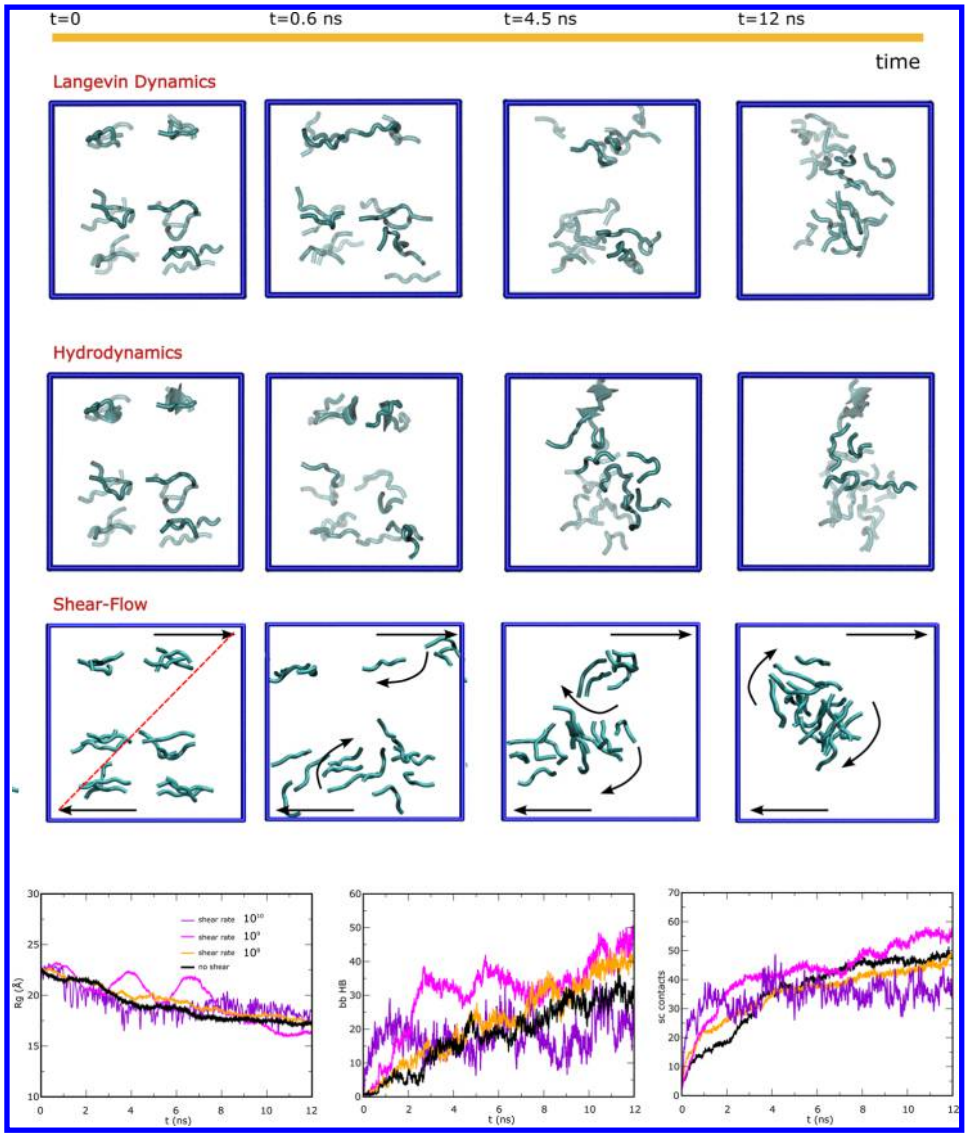

Figure 17. Aβ16−22 aggregation simulations under several conditions. (Top panels) Pictorial representation of monomer aggregation for several simulation schemes: (i) Langevin dynamics, (ii) Langevin dynamics with hydrodynamic interactions (HIs), and (iii) Langevin dynamics with HIs and longitudinal shear, shear rate $\Delta v/\Delta z = 10^8$ s^{-1}. The time evolutions show the effect of HIs on the aggregation kinetics. When shear flow is activated, also the details of the aggregation change: i.e., first two separate aggregates form, and their relative motion in the shear flow (translation and rotation) guides their further encounter and fusion. (Bottom panels) Time evolution of key parameters describing the aggregation process in shear flow for different values of the shear rate $\Delta v/\Delta z$ (0, 10^8, 10^9, and 10^{10} s^{-1}): the gyration radius R_g (left panel), the number of interpeptide hydrogen bonds formed between backbone NH and O groups (middle panel), and the number of interpeptide side-chain contacts (right panel). The system is composed of 18 peptides placed in a cubic box of L = 65 Å, and the shear gradient is generated along the z direction.

metal complexers, and covalent modifiers.[479] It has also been found that curcumin from turmeric, EGCG from green tea, and resveratrol from grapes, which reduce Aβ aggregation in vitro, also alter lipid bilayer properties and the function of diverse membrane proteins.[480] Therefore, the effect of one drug might not be what we expect, and in this context, we recently showed using expressed and then produced Aβ1−28, Aβ1−40, and Aβ1−42 peptides with multiple assays and different readouts that the NQTrp inhibitor exerts its inhibitory effect via mechanisms other than direct interactions with Aβ peptides (O. Berthoumieu et al., unpublished results).

Along with the next steps already described at the end of each section, some challenges should be considered.

The first challenge is that the population of dimers, trimers, and dodecamers (Aβ*56) in brain tissues vary with aging, indicating that the species to be targeted at early or late onset AD are not the same. By using 75 cognitively intact individuals, ranging from young children to the elderly, and 58 impaired subjects with mild cognitive impairment or probable Alzheimer's disease, it was found that Aβ*56 may play a pathogenic role very early in the pathogenesis of AD.[481]

The second challenge is that experiments have reported drastic acceleration of fibril formation for the Aβ1−40 peptide in shear flow.[482−484] The origin of such a kinetic speed-up is still debated. In addition, while atomistic simulations in explicit solvent of the full aggregation of the Aβ1−40/42 peptides and causing or protecting variants are still out of reach, coarse-grained simulations in implicit solvent require the treatment of hydrodynamics effects.[61,485] In Figure 17 we report preliminary results of the early steps of the aggregation of 18 Aβ16−22 peptides blocked by acetyl and amine under shear flow as obtained from simulations using the CG model OPEP with

DOI: 10.1021/cr500638n
Chem. Rev. 2015, 115, 3518−3563

hydrodynamic interactions (S. Melchionna, P. Derreumaux, and F. Sterpone, unpublished results). For the sake of exemplarity, the simulations were performed at rather high concentration (109 mM) and in the absence of shear rates or in the presence of high shear rates (10^8, 10^9, and 10^{10} s^{-1}). With hydrodynamic effects, the early steps of aggregation are already very different from those of Langevin dynamics as seen from the size of the oligomers. With high shear rates, we observe formation of a unique elongated aggregate within 10 ns. For this highly concentrated system the presence of the laminar shear flow does not seem to affect the overall kinetics of the collapse, but however does influence the way the aggregation proceeds. Namely, by increasing the rate, an oscillatory behavior in the aggregation process emerges (see the left panel reporting the time evolution of the system's gyration radius). The highest shear rate also breaks down the hydrogen bonds and side-chain contacts in the aggregates; thus, a nonmonotonic behavior as a function of the hydrodynamic perturbation is expected for similar aggregation processes of proteins. We are currently investigating the dynamics over a much longer time scale.

A third challenge is to have a direct observation of Aβ protein self-assembly in live cells as a result of crowding effects. Using noninvasive fluorescence lifetime recordings and super-resolution fluorescence, the formation of Aβ1−40 and Aβ1−42 aggregates in live cells was dissected. Both peptides are retained in lysosomes, where their accumulation leads to aggregation, but the kinetics of Aβ1−42 aggregation are considerably faster than those of Aβ1−40 and, unlike those of Aβ1−40, show no detectable lag phase. Compact amyloid aggregates were observed for both alloforms.[486] While these experiments represent one step ahead toward understanding aggregation in the cells, higher spatial resolution methods and how the cellular environment affects the dynamics of Aβ1−40/42 and their variants are major concerns. To this end, in-cell NMR of Aβ protein is an ideal tool for gaining information at the atomic level, but several obstacles remain.[487,488]

It is also a challenge to determine the impact of PrP and HSA on Aβ oligomerization. We are addressing both aspects experimentally by polymerization and depolymerization kinetic experiments and theoretically by performing exascale simulations. In this respect, we have recently shown that it is possible to get the dynamics of 18 000 HSA proteins comprising 80 million particles with hydrodynamic interactions consistent with the experimental translational and rotational diffusion constants as a function of the density of the system.[61]

Finally, pathogenic events involve an imbalance between the production and the clearance of the Aβ peptide. It is important to understand in atomic detail how the Aβ is cleaved by γ-secretase and how this process is affected by A2V and A2T mutations. Clearly, the recent release of the 3D structure of the human γ-secretase complex at 4.5 A[489] combined with simulations going beyond the Aβ1−55 dimer[490] should help clarify this issue.

While many inhibitors have been designed to target a specific region of Aβ, it would be interesting to study in cells the cumulative effect of inhibitors designed to recognize different regions of Aβ. It would also be of great interest to combine different drugs targeting Aβ processing and rendering Aβ aggregates very unstable and more prone to degradation. Today, we are just seeing the tip of the iceberg in understanding phenotype-related toxicity and aggregation propensity of WT Aβ and its familial disease and protective variants, but continuous and synergetic efforts between in vitro and in vivo studies (including basic verifications such as purity and reproducibility of the results using various readouts or transgenic animals with different sexes and times of AD incubation) and theoretical studies (using multiple approaches) should get us closer to finding a cure for AD.

AUTHOR INFORMATION

Corresponding Author

*Phone: 33 1 58 41 51 72. E-mail: philippe.derreumaux@ibpc.fr.

Notes

The authors declare no competing financial interest.

Biographies

Jessica Nasica-Labouze is a Postdoctoral Fellow on the Talents FVG Outgoing Mobility Fellowship (Consorzio per l'AREA di Ricerca di Trieste) and is involved in a collaborative project between UPR9080 CNRS, Paris, and SISSA, Italy. She got her Ph.D. in biophysics at the Universite de Montreal (Canada), where she worked on characterizing the self-assembly mechanism of amyloid peptides and then did a postdoctoral study at SISSA, investigating the dynamics of chromatin via coarse-grained simulations. Her current research interests focus mainly on the effects of protective and pathogenic mutations on the folding and interactions of the amyloid β protein, involved in Alzheimer's disease, via a wide spectrum of computational methods.

Phuong H. Nguyen is a CR1 permanent researcher at CNRS. He earned a Ph.D. in condensed matter theory at the Physics Department of Bielefeld University, Germany. His postdoctoral study in the Chemistry Department of Frankfurt University, Germany, focused on nonequilibrium molecular dynamics simulations aimed at understanding energy flows and photoinduced conformational dynamics in biomolecules. His current research focuses on the development and application of efficient, physically rigorous theoretical methods for

DOI: 10.1021/cr500638n
Chem. Rev. 2015, 115, 3518−3563

studying equilibrium and nonequilibrium structure, dynamics, and thermodynamics of single and amyloid proteins at the all-atom and coarse-grained levels.

Fabio Sterpone is currently a researcher at the CNRS, France. He graduated from the University of Paris UPMC (biophysics) and then occupied several postdoctoral positions; he dealt with quantum classical simulations of materials and the effect of solvent on biomolecular structure and dynamics. Presently, he is mainly interested in the study of protein stability and aggregation in extreme environments by applying and developing multiscale simulation methodologies.

Olivia Berthoumieu is a postdoctoral researcher in the Coordination Chemistry Department of CNRS in Toulouse, France. She graduated from Oxford University, where she received a Ph.D. in biochemistry. Her research interests include (a) membrane proteins as tools for bionanotechnological applications, (b) ligand−receptor interactions and high-resolution imaging using atomic force microscopy, and (c) metal ion interactions with the amyloid β peptide and inhibition of Aβ aggregation.

Nicolae-Viorel (Vio) Buchete is Lecturer of Theoretical & Computational Nano-Bio Physics in the School of Physics and Principal Investigator in the Complex & Adaptive Systems Laboratory, a research institute at the University College Dublin (UCD), Ireland. He received his Ph.D. from Boston University, and he held a postdoctoral research fellowship at the National Institutes of Health in Bethesda, MD. Ongoing research projects in his group at UCD are concerned with statistical mechanics and conformational dynamics of biomolecular systems, protein folding, amyloid aggregation, structural aspects of systems biology and bioinformatics, and multiscale modeling of biomolecules and complex fluids.

Sébastien Côté is currently a Ph.D. student under the supervision of Professor Normand Mousseau in the Department of Physics at the Université de Montréal in Montréal, Canada. He received his Honours B.Sc. in physics at McGill University, Montréal, in 2009. His research interests are nonamyloid/amyloid protein folding/oligomerization, peptide−membrane interactions, and the development of new coarse-grained methodologies.

DOI: 10.1021/cr500638n
Chem. Rev. 2015, 115, 3518−3563

Alfonso De Simone is Lecturer and Group Leader in the Department of Life Sciences of the Imperial College London. He obtained the Ph.D. in 2007 in structural biology at the University of Padova. He was then a postdoctoral research associate at the University of Cambridge in the laboratory of Chris Dobson, working on new combinations of biomolecular NMR and molecular simulations to characterize the structure and dynamics of transient protein states along biochemical processes, including protein aggregation into amyloids, enzymatic reactions, and biomaterial assembly. In 2011 he established his group at Imperial College London, where he is working on the definition of advanced methods at the interface of solution/solid-state NMR and molecular simulations. Current research topics span intrinsically disordered proteins, membrane proteins, biotechnologically relevant enzymes, and biomaterials.

Andrew J. Doig is Professor of Biochemistry at the University of Manchester. He earned his Ph.D. at the University of Cambridge, United Kingdom, and id his postdoctoral training in the Department of Biochemistry at Stanford University, California. His research interests are (a) drug discovery for Alzheimer's disease, (b) bioinformatics studies on drug target proteins, genes in mouse development, amyloidoses, and protein vibrational spectroscopy, and (c) the effects of β-amyloid on the proteome, metabolome, and cytoskeleton.

Peter Faller is Professor in Chemistry at the University of Toulouse Paul Sabatier (F) and Group Leader in the Laboratoire de Chimie de Coordination du CNRS. He was born in St. Gallen, Switzerland. He trained to be a teacher for elementary school (Kreuzlingen, Switzerland). He then studied at the University of Zürich, Switzerland, earning a Ph.D. in (bio)chemistry on metallothioneins. He did his postdoctoral study on photosystem II. Ongoing research projects of his group are on the interactions of amyloidogenic peptides with metal ions, inhibitors, and markers.

Angel Garcia is Professor of Physics at Rensselaer Polytechnic Institute. He obtained a Ph.D. in theoretical physics from Cornell University. His main research interest is the understanding of the physicochemical principles that determine protein folding, stability, and dynamics and the application of these principles to build computer models that describe these processes. A main effort in his laboratory has been the characterization of the ensemble of conformations adopted by the Aβ peptides in the monomeric state. He uses state-of-the-art enhanced sampling methods and parallel computers to perform atomistic simulations of various forms of the Aβ peptides in explicit solvent and over multiple microsecond time scales. These simulations are carefully validated against J-couplings, RDC, and other data.

Alessandro Laio is Associate Professor in the Physics Department of SISSA. He obtained a Ph.D. in solid-state physics at SISSA. Then he moved for a postdoctoral study to ETH, Switzerland, where he worked first on a QM/MM approach to molecular biochemistry and then on the development of techniques for computer simulations of rare events. His current research interests are (a) the development of techniques aimed at computing the free energy by atomistic simulations, (b) protein folding, protein aggregation, and protein–protein interaction, and (c) structural bioiformatics and algorithm development for data mining.

DOI: 10.1021/cr500638n
Chem. Rev. 2015, 115, 3518–3563

Suan Li Mai is Professor of Physics at the Institute of Physics, Polish Academy of Sciences. He earned his Ph.D. at the Kishinev State University, Moldova, and habilitation degree at the Institute of Physics, Polish Academy of Sciences. His research interests are (a) development of coarse-grained models for studying protein folding and misfolding, (b) protein unfolding under an external mechanical force, (c) mechanisms of protein and peptide aggregation, and (d) computer-aided drug design for Alzheimer's disease, influenza A virus, and breast cancer.

Simone Melchionna is a researcher at the Institute for Chemico-Physical Processes of the Consiglio Nazionale delle Ricerche. He has a Ph.D. in chemistry from the University of Rome—La Sapienza. During his Ph.D. study, he developed techniques for studying the molecular dynamics of biological systems, such as constrained mechanics, enhanced sampling, and isothermal–isobaric dynamical approaches. Then he moved for three years to Cambridge, where he worked on confined fluids and water via density functional theory and other theoretical approaches. Subsequently, he worked on lattice Boltzmann and multiscale simulation numerical methods, with applications to DNA translocation. His research focuses on high-performance computing applied to proteins and other biological systems.

Normand Mousseau is Professor of Physics and Canada Research Chair in Computational Physics of Complex Materials at the Université de Montréal. He obtained his Ph.D. from Michigan State University and pursued postdoctoral studies at Oxford University, United Kingdom, and the Université de Montréal. His research interests focus on the kinetics of complex systems on the atomic scale studied with the help of various computational methods often developed in his group. Over the past few years, in biophysics, he has been working on the first steps of amyloid aggregation as well as protein flexibility. He is currently working on the development of new coarse-grained potentials in addition to pursuing a number of avenues for accelerated sampling techniques.

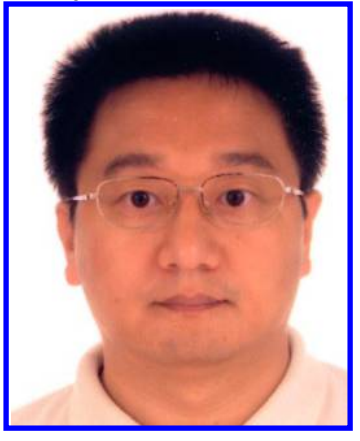

Yuguang Mu is Associate Professor in the School of Biological Sciences of Nanyang Technological University in Singapore. He earned his Ph.D. at Shandong University, China, and did his postdoctoral training at the Alexander von Humboldt Foundation in Germany. His research interests are (a) MD simulation and data analysis method development, (b) peptide and protein folding and unfolding, aimed at the folding and misfolding mechanism which could lead to an amyloid fibril, and (c) DNA dynamics and DNA–protein and DNA–counterion interactions.

DOI: 10.1021/cr500638n
Chem. Rev. 2015, 115, 3518–3563

Anant Paravastu is Associate Professor of Chemical and Biomedical Engineering at Florida State University. He received his Ph.D. in chemical engineering at the University of California, Berkeley, and his postdoctoral training at the National Institutes of Health. His primary research interests are in solid-state NMR structural analysis of peptide assembles, including Aβ oligomers and designer peptide nanofibers with applications in regenerative medicine.

Samuela Pasquali is Associate Professor in the Biology/Biochemistry Department of the University of Paris Diderot, where she teaches math and bioinformatics to biology students. She earned a Ph.D. in statistical physics in 2005 at New York University, having worked on theoretical modeling of RNA folding and polymer folding under confinement. She then moved to Paris at ESPCI for a 3-year postdoctoral study on numerical approaches to compute Casimir forces, both classical (van der Waals) and quantum. In 2008 she was hired as Associate Professor at Paris Diderot, and since then, she has devoted her research to the problem of RNA folding, for which she developed an efficient coarse-grained model and an improvement of the coarse-grained protein model for amyloid and nonamyloid proteins.

David J. Rosenman earned his B.S. with Honors in biology from the California Institute of Technology in 2009. He became a Ph.D. student in the Biology Department at Rensselaer Polytechnic Institute in 2010, under the mentorship of Dr. Angel Garcia and Dr. Chunyu Wang. His research focuses on the combined use of molecular dynamics and nuclear magnetic resonance techniques to characterize the conformational ensembles of the amyloid β peptides implicated in Alzheimer's disease.

Birgit Strodel is Head of the Multiscale Modeling Group at the Jülich Research Centre and is Assistant Professor at the Institute of Theoretical and Computational Chemistry at the Heinrich Heine University Düsseldorf. Her main research interests are in the thermodynamics and kinetics of protein aggregation and protein–protein interactions. A large part of the simulations performed in her laboratory focus on the aggregation of amyloidogenic peptides, aiming to understand the molecular basis of Alzheimer's disease.

Bogdan Tarus is a postdoctoral researcher in the Laboratory of Theoretical Biochemistry, Institut de Biologie Physico-Chimique (IBPC). He received a Ph.D. in physical chemistry at Boston

DOI: 10.1021/cr500638n
Chem. Rev. 2015, 115, 3518–3563

University, Massachusetts. Then he moved for a postdoctoral study to Heidelberg University, Germany, where he continued to work on amyloid protein aggregation. Moving to INRA, France, he worked on designing small chemical compounds that interact with proteins of biological interest. His work at IBPC involves studying amyloid protein aggregation and developing chemical compounds to inhibit the aggregation. His current research interests are protein dynamics and aggregation using computational methods at atomistic and coarse-grained resolution, drug design, protein−drug interaction, and inhibition of protein aggregation.

John Viles has an active research program studying protein misfolding associated with amyloid formation in neurodegenerative diseases. Biophysical approaches include NMR, CD, IR, EPR, and transmission electron microscopy. His main research areas include copper and zinc in Alzheimer's disease, the structure and misfolding of the prion protein in transmissible spongiform encephalopathy's "mad-cow" disease, and amyloid β and its protein binding partners. He received his Ph.D. from the University of London in 1994 and continued his research with Prof. P. J. Sadler (Fellow of the Royal Society, FRS) studying metalloproteins using NMR. In 1997 he took up a postdoctoral position with Prof. P. Wright at the Scripps Research Institute, California. In collaboration with the Nobel Laureate Prof. S. Prusiner, he has published a number of significant papers on the structure of the prion protein. He returned to the United Kingdom in 2000 to take up a lectureship position at Queen Mary and is currently Associate Professor (Reader) in Biochemistry at the Queen Mary University of London.

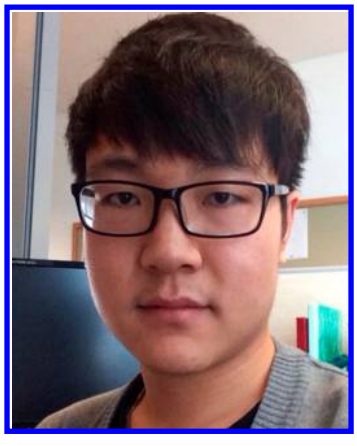

Tong Zhang is a Ph.D. student under the supervision of Prof. Derreumaux and Associate Professor Yuguang Mu in the School of Biological Sciences at the Nanyang Technological University (NTU), Singapore. He received his B.Sc. in biology at NTU in 2010. His research interests are the use of computer-aided approaches to understand the folding and aggregation of Alzheimer's Aβ and Aβ−small-molecule interactions.

Chunyu Wang is Associate Professor of Biology at Rensselaer Polytechnic Institute. He obtained his Ph.D. in biochemistry from Cornell University and M.D. from Peking Union Medical College. He mainly uses solution NMR technique to study the structure, dynamics, and interactions of amyloid β peptide in combination with molecular dynamics simulation. His other interests include intein-mediated protein splicing and related phenomena, such as hedgehog autoprocessing.

Philippe Derreumaux has been Director of UPR9080 since 2007 and is a senior member of the Institut Universitaire de France (IUF). He obtained his HDR in physics at Pierre and Marie Curie University. He worked with Gerard Vergoten, Warner Peticolas, Martin Karplus, and Tamar Schlick from 1983 to 1994. Presently, he is interested in the development of enhanced conformational techniques and coarse-grained protein (OPEP) and RNA (Hire-RNA) models. The theoretical advances are used to understand the aggregation process of amyloid proteins, and notably the Aβ protein, in aqueous solution and comprehend the equilibrium conformation ensemble and dynamics of Aβ in a crowded environment with the prion protein and serum albumin or in a real cell environment.

ACKNOWLEDGMENTS

J.N.-L. acknowledges funding from the European Social Fund (ESF), Operational Programme 2007−2013, Objective 2, Axis 5, TALENTS FVG Programme—Activity 2—Outgoing-Scheme—FP code: 1418521006, managed by AREA Science Park. P.H.N., B.T., and P.D. thank DARI (Grant x2014077198) for computer resources. F.S. and S.M. acknowledge funding from the European Research Council (ERC) under the European Community's Seventh Framework Programme (FP7/2007−2013), Grant Agreement No. 258748. Simulations

DOI: 10.1021/cr500638n
Chem. Rev. 2015, 115, 3518−3563

with shear forces used high-performance computing (HPC) resources from GENCI (CINES and TGCC, Grants 2012 c2012086818 and 2013 x201376818). O.B. and P.F. thank their collaborators and in particular Drs. Christelle Hureau, Emmanuel Gras, Fabrice Collin, and Giovanni La Penna for helpful discussions. N.-V.B. and B.S. thank Ratnesh Lal and Ruth Nussinov for providing the AFM images shown in Figure 8 and John E. Straub and Ruth Nussinov for providing the structure files of the membrane-bound Aβ models illustrated in Figure 9. S.L.M. thanks Narodowe Centrum Nauki in Poland (Grant 2011/01/B/NZ1/01622). Y.M. acknowledges Tier 1 Grant RG 23/11 from the Nanyang Technological University, Singapore. Finally, P.D. acknowledges the support of the University of Paris Diderot, ANR SIMI7 GRAL 12-BS07-0017, ANR LABEX Grant "DYNAMO" (ANR-11-LABX-0011), the 6th European PRCD (Immunoprion, Grant FP6-Food023144), the Institut Universitaire de France (IUF), the French/Singapore Merlion Ph.D. program (Grant 5.08.10), the Pierre de Gilles de Gennes Foundation and its international Ph.D. grant program, Fudan University in China, CNRS—Polish Academy of Sciences (Grant 168836), and the CNRS Institute of Chemistry (INC).

REFERENCES

(1) Alzheimer's Association Home Page. http://www.alz.org/ (accessed Mar 17, 2015).
(2) Hardy, J.; Selkoe, D. J. *Science* **2002**, *297*, 353−356.
(3) Hernández-Rodríguez, M.; Correa-Basurto, J.; Martínez-Ramos, F.; Padilla-Martínez, I. I.; Benítez-Cardoza, C. G.; Mera-Jiménez, E.; Rosales-Hernández, M. C. *J. Alzheimer's Dis.* **2014**, *41*, 1073−1085.
(4) Selkoe, D. J. *Physiol. Rev.* **2001**, *81*, 741−766.
(5) Tan, C. C.; Yu, J. T.; Wang, H. F.; Tan, M. S.; Meng, X. F.; Wang, C.; Jiang, T.; Zhu, X. C.; Tan, L. *J. Alzheimer's Dis.* **2014**, *41*, 615−631.
(6) Valverde, E.; Sureda, F. X.; Vázquez, S. *Bioorg. Med. Chem.* **2014**, *22*, 2678−2683.
(7) Yan, R.; Vasser, R. *Lancet Neurol.* **2014**, *13*, 319−329.
(8) Wischik, C. M.; Harrington, C. R.; Storey, J. M. *Biochem. Pharmacol.* **2014**, *88*, 529−539.
(9) (a) Doig, A. J.; Derreumaux, P. *Curr. Opin Struct. Biol.* **2015**, *30C*, 50−56. (b) Jiang, L.; Liu, C.; Leibly, D.; Landau, M.; Zhao, M.; Hughes, M. P.; Eisenberg, D. S. *Elife* **2013**, *2*, e00857.
(10) Shankar, G. M.; Li, S.; Mehta, T. H.; Garcia-Munoz, A.; Shepardson, N. E.; Smith, I.; Brett, F. M.; Farrell, M. A.; Rowan, M. J.; Lemere, C. A.; Regan, C. M.; Walsh, D. M.; Sabatini, B. L.; Selkoe, D. J. *Nat. Med.* **2008**, *14*, 837−842.
(11) (a) Bernstein, S. L.; Dupuis, N. F.; Lazo, N. D.; Wyttenbach, T.; Condron, N. N.; Bitan, G.; Teplow, D. B.; Shea, J. E.; Ruotolo, B. T.; Robinson, C. V.; Bowers, M. T. *Nat. Chem.* **2009**, *1*, 326−331. (b) Sherman, M. A.; Lesné, S. E. *Methods Mol. Biol.* **2011**, *670*, 45−56.
(12) Jan, A.; Adolfsson, O.; Allaman, I.; Buccarello, A. L.; Magistretti, P. J.; Pfeifer, A.; Muhs, A.; Lashuel, H. A. *J. Biol. Chem.* **2011**, *286*, 8585−8596.
(13) Knowles, T. P.; Waudby, C. A.; Devlin, G. L.; Cohen, S. I.; Aguzzi, A.; Vendruscolo, M.; Terentjev, E. M.; Welland, M. E.; Dobson, C. M. *Science* **2009**, *326*, 1533−1537.
(14) Cohen, S. I.; Linse, S.; Luheshi, L. M.; Hellstrand, E.; White, D. A.; Rajah, L.; Otzen, D. E.; Vendruscolo, M.; Dobson, C. M.; Knowles, T. P. *Proc. Natl. Acad. Sci. U.S.A.* **2013**, *110*, 9758−9763.
(15) Schmit, J. D.; Gosh, K.; Dill, K. *Biophys. J.* **2011**, *100*, 450−458.
(16) Jeong, J. S.; Ansaloni, A.; Mezzenga, R.; Lashuel, H. A.; Dietler, G. *J. Mol. Biol.* **2013**, *425*, 1765−1781.
(17) Qiang, W.; Kelley, K.; Tycko, R. *J. Am. Chem. Soc.* **2013**, *135*, 6860−6871.
(18) Tycko, R.; Wickner, R. B. *Acc. Chem. Res.* **2013**, *46*, 1487−1496.
(19) Meisl, G.; Yang, X.; Hellstrand, E.; Frohm, B.; Kirkegaard, J. B.; Cohen, S. I.; Dobson, C. M.; Linse, S.; Knowles, T. P. *Proc. Natl. Acad. Sci. U.S.A.* **2014**, *111*, 9384−9389. (b) Assarsson, A.; Hellstrand, E.; Cabaleiro-Lago, C.; Linse, S. *ACS Chem. Neurosci.* **2014**, *4*, 266−274.
(20) Kirkitadze, M. D.; Condron, M. M.; Teplow, D. B. *J. Mol. Biol.* **2001**, *312*, 1103−1119.
(21) Hou, L.; Shao, H.; Zhang, Y.; Li, H.; Menon, N. K.; Neuhaus, E. B.; Brewer, J. M.; Byeon, I.-J. L.; Ray, D. G.; Vitek, M. P.; Iwashita, T.; Makula, R. A.; Przybyla, A. B.; Zagorski, M. G. *J. Am. Chem. Soc.* **2004**, *126*, 1992−2005.
(22) Sarroukh, R.; Cerf, E.; Derclaye, S.; Dufrêne, Y. F.; Goormaghtigh, E.; Ruysschaert, J. M.; Raussens, V. *Cell. Mol. Life Sci.* **2011**, *68*, 1429−1438.
(23) Bertini, I.; Gallo, G.; Korsak, M.; Luchinat, C.; Mao, J.; Ravera, E. *ChemBioChem* **2013**, *14*, 1891−1897.
(24) Kim, B. H.; Lyubchenko, Y. L. *Nanomedicine* **2014**, *4*, 871−878.
(25) García, S.; Cuscó, C.; Brissos, R. F.; Torrents, E.; Caubet, A.; Gamez, P. *J. Inorg. Biochem.* **2012**, *116*, 26−36.
(26) Lv, Z.; Roychaudhuri, R.; Condron, M. M.; Teplow, D. B.; Lyubchenko, Y. L. *Sci. Rep.* **2013**, *3*, 2880−2888.
(27) Petkova, A. T.; Leapman, R. D.; Guo, Z. H.; Yau, W. M.; Mattson, M. P.; Tycko, R. *Science* **2005**, *307*, 262−265.
(28) Petkova, A. T.; Ishii, Y.; Balbach, J. J.; Antzutkinm, O. N.; Leapman, R. D.; Delaglio, F.; Tycko, R. *Proc. Natl. Acad. Sci. U.S.A.* **2002**, *99*, 16742−16747.
(29) Luhrs, T.; Ritter, C.; Adrian, M.; Riek-Loher, D.; Bohrmann, B.; Doeli, H.; Schubert, D.; Riek, R. *Proc. Natl. Acad. Sci. U.S.A.* **2005**, *102*, 17342−17347.
(30) Lu, J. X.; Qiang, W.; Yau, W. M.; Schwieters, C. D.; Meredith, S. C.; Tycko, R. *Cell* **2013**, *154*, 1257−1268.
(31) Gunderson, W.; Hernández-Guzmán, J.; Karr, J.; Sun, L.; Szalai, V.; Warncke, K. *J. Am. Chem. Soc.* **2012**, *134*, 18330−18337.
(32) Eury, H.; Bijani, C.; Faller, P.; Hureau, C. *Angew. Chem., Int. Ed.* **2011**, *50*, 901−905.
(33) Stanyon, H. F.; Viles, J. H. *J. Biol. Chem.* **2012**, *287*, 28163−28168.
(34) Laurén, J.; Gimbel, D. A.; Nygaard, H. B.; Gilbert, J. W.; Strittmatter, S. M. *Nature* **2009**, *457*, 1128−1132.
(35) Younan, N. D.; Sarell, C. J.; Davies, P.; Brown, D. R.; Viles, J. H. *FASEB J.* **2013**, *27*, 1847−1858.
(36) (a) Zou, K.; Gong, J. S.; Yanagisawa, K.; Michikawa, M. *J. Neurosci.* **2002**, *22*, 4833−4841. (b) State of Aggregation (editorial). *Nat. Neurosci.* **2011**, *14*, 399, DOI: 10.1038/nn0411-399.
(37) Götz, J.; Matamales, M.; Götz, N. N.; Ittner, L. M.; Eckert, A. *Front. Physiol.* **2012**, *3*, 320 DOI: 10.3389/fphys.2012.00320.
(38) Kim, T.; Vidal, G. S.; Djurisic, M.; William, C. M.; Birnbaum, M. E.; Garcia, K. C.; Hyman, B. T.; Shatz, C. J. *Science* **2013**, *341*, 1399−1404.
(39) Zempel, H.; Luedtke, J.; Kumar, Y.; Biernat, J.; Dawson, H.; Mandelkow, E.; Mandelkow, E. M. *EMBO J.* **2013**, *32*, 2920−2937.
(40) Um, J. W.; Kaufman, A. C.; Kostylev, M.; Heiss, J. K.; Stagi, M.; Takahashi, H.; Kerrisk, M. E.; Vortmeyer, A.; Wisniewski, T.; Koleske, A. J.; Gunther, E. C.; Nygaard, H. B.; Strittmatter, S. M. *Neuron* **2013**, *79*, 887−902.
(41) Kanekiyo, T.; Xu, B.; Bu, G. *Neuron* **2014**, *81*, 740−754.
(42) Aisen, P. S.; Vellas, B.; Hampel, H. *Nat. Rev. Drug Discovery* **2013**, *4*, 324 DOI: 10.1038/nrd3842-c1.
(43) Abbott, A. *Nature* **2008**, *458*, 161−164.
(44) Nguyen, P.; Derreumaux, P. *Acc. Chem. Res.* **2014**, *47*, 603−611.
(45) Moore, B. D.; Chakrabarty, P.; Levites, Y.; Kukar, T. L.; Baine, A. M.; Moroni, T.; Ladd, T. B.; Das, P.; Dickson, D. W.; Golde, T. E. *Alzheimer's Res. Ther.* **2012**, *4*, 18 DOI: 10.1186/alzrt121.
(46) Rembach, A.; Faux, N. G.; Watt, A. D.; Pertile, K. K.; Rumble, R. L.; Trounson, B. O.; Fowler, C. J.; Roberts, B. R.; Perez, K. A.; Li, Q. X.; Laws, S. M.; Taddei, K.; Rainey-Smith, S.; Robertson, J. S.; Vandijck, M.; Vanderstichele, H.; Barnham, K. J.; Ellis, K. A.; Szoeke, C.; Macaulay, L.; Rowe, C. C.; Villemagne, V. L.; Ames, D.; Martins, R. N.; Bush, A. I.; Masters, C. L.; AIBL Research Group. Changes in Plasma Amyloid Beta in a Longitudinal Study of Aging and Alzheimer's Disease. *Alzheimer's Dementia* **2014**, *10*, 53−61.

DOI: 10.1021/cr500638n
Chem. Rev. 2015, 115, 3518−3563

(47) Rezaei-Ghaleh, N.; Amininasab, M.; Giller, K.; Kumar, S.; Stündl, A.; Schneider, A.; Becker, S.; Walter, J.; Zweckstetter, M. *J. Am. Chem. Soc.* **2014**, *136*, 4913−4919.
(48) Atwood, C. S.; Perry, G.; Zeng, H.; Kato, Y.; Jones, W. D.; Ling, K. Q.; Huang, X.; Moir, R. D.; Wang, D.; Sayre, L. M.; Smith, M. A.; Chen, S. G.; Bush, A. I. *Biochemistry* **2004**, *43*, 560−568.
(49) Masters, C. L.; Selkoe, D. J. *Cold Spring Harbor Perspect. Med.* **2012**, *2*, a006262.
(50) Nussbaum, J. M.; Schilling, S.; Cynis, H.; Silva, A.; Swanson, E.; Wangsanut, T.; Tayler, K.; Wiltgen, B.; Hatami, A.; Rönicke, R.; Reymann, K.; Hutter-Paier, B.; Alexandru, A.; Jagla, W.; Graubner, S.; Glabe, C. G.; Demuth, H. U.; Bloom, G. S. *Nature* **2012**, *485*, 651−655.
(51) Deng, B.; Lian, Y.; Wang, X.; Zeng, F.; Jiao, B.; Wang, Y. R.; Liang, C. R.; Liu, Y. H.; Bu, X. L.; Yao, X. Q.; Zhu, C.; Shen, L.; Zhou, H. D.; Zhang, T.; Wang, Y. J. *Neurotoxic. Res.* **2014**, *26*, 211−215.
(52) Tomiyama, T.; Nagata, T.; Shimada, H.; Teraoka, R.; Fukushima, A.; Kanemitsu, H.; Takuma, H.; Kuwano, R.; Imagawa, M.; Ataka, S.; Wada, Y.; Yoshioka, E.; Nishizaki, T.; Watanabe, Y.; Mori, H. *Ann. Neurol.* **2008**, *63*, 377−387.
(53) Gessel, M. M.; Bernstein, S.; Kemper, M.; Teplow, D. B.; Bowers, M. T. *ACS Chem. Neurosci.* **2012**, *3*, 909−918.
(54) Di Fede, G.; Catania, M.; Morbin, M.; Rossi, G.; Suardi, S.; Mazzoleni, G.; Merlin, M.; Giovagnoli, A. R.; Prioni, S.; Erbetta, A.; Falcone, C.; Gobbi, M.; Colombo, L.; Bastone, A.; Beeg, M.; Manzoni, C.; Francescucci, B.; Spagnoli, A.; Cantù, L.; Del Favero, E.; Levy, E.; Salmona, M.; Tagliavini, F. *Science* **2009**, *323*, 1473−1477.
(55) Jonsson, T.; Atwal, J. K.; Steinberg, S.; Snaedal, J.; Jonsson, P. V.; Bjornsson, S.; Stefansson, H.; Sulem, P.; Gudbjartsson, D.; Maloney, J.; Hoyte, K.; Gustafson, A.; Liu, Y.; Lu, Y.; Bhangale, T.; Graham, R. R.; Huttenlocher, J.; Bjornsdottir, G.; Andreassen, O. A.; Jönsson, E. G.; Palotie, A.; Behrens, T. W.; Magnusson, O. T.; Kong, A.; Thorsteinsdottir, U.; Watts, R. J.; Stefansson, K. *Nature* **2012**, *488*, 96−99.
(56) Zhang, Y.; Rempel, D. L.; Zhang, J.; Sharma, A. K.; Mirica, L. M.; Gross, M. L. *Proc. Natl. Acad. Sci. U.S.A.* **2013**, *110*, 14604−14609.
(57) Santi, S.; Musi, V.; Descrovi, E.; Paeder, V.; Di Francesco, J.; Hvozdara, L.; van der Wal, P.; Lashuel, H. A.; Pastore, A.; Neier, R.; Herzig, H. P. *ChemPhysChem* **2013**, *14*, 3476−3482.
(58) Johnson, R. D.; Schauerte, J. A.; Chang, C. C.; Wisser, K. C.; Althaus, J. C.; Carruthers, C. J.; Sutton, M. A.; Steel, D. G.; Gafni, A. *Biophys. J.* **2013**, *104*, 894−903. (b) Narayan, P.; Ganzinger, K. A.; McColl, J.; Weimann, L.; Meehan, S.; Qamar, S.; Carver, J. A.; Wilson, M. R.; St George-Hyslop, P.; Dobson, C. M.; Klenerman, D. *J. Am. Chem. Soc.* **2013**, *135*, 1491−1498.
(59) Gu, L.; Liu, C.; Guo, Z. *J. Biol. Chem.* **2013**, *288*, 18673−18683.
(60) Drew, S. C.; Noble, C. J.; Masters, C. L.; Hanson, G. R.; Barnham, K. J. *J. Am. Chem. Soc.* **2009**, *131*, 1195−1207.
(61) Sterpone, F.; Melchionna, S.; Tuffery, P.; Pasquali, S.; Mousseau, N.; Cragnolini, T.; Chebaro, Y.; St-Pierre, J.; Kalimeri, M.; Barducci, A.; Laurin, Y.; Tek, A.; Baaden, M.; Nguyen, P. H.; Derreumaux, P. *Chem. Soc. Rev.* **2014**, *43*, 4871−4893.
(62) Tycko, R. *Annu. Rev. Phys. Chem.* **2011**, *62*, 279−299.
(63) Sarroukh, R.; Goormaghtigh, E.; Ruysschaert, J.; Raussens, V. *Biochim. Biophys. Acta, Biomembr.* **2013**, *1828*, 2328−2338.
(64) Miller, Y.; Ma, B.; Nussinov, R. *Chem. Rev.* **2010**, *110*, 4820−4838.
(65) Faendrich, M.; Schmidt, M.; Grigorieff, N. *Trends Biochem. Sci.* **2011**, *36*, 338−345.
(66) Meinhardt, J.; Sachse, C.; Hortschansky, P.; Grigorieff, N.; Faendrich, M. *J. Mol. Biol.* **2009**, *386*, 869−877.
(67) Paravastu, A. K.; Petkova, A. T.; Tycko, R. *Biophys. J.* **2006**, *90*, 4618−4629.
(68) Paravastu, A. K.; Leapman, R. D.; Yau, W. M.; Tycko, R. *Proc. Natl. Acad. Sci. U.S.A.* **2008**, *105*, 18349−18354.
(69) Chen, B.; Thurber, K. R.; Shewmaker, F.; Wickner, R. B.; Tycko, R. *Proc. Natl. Acad. Sci. U.S.A.* **2009**, *106*, 14339−14344.
(70) Nilsson, M. R. *Methods* **2004**, *34*, 151−160.
(71) Fraser, P.; Nguyen, J.; Surewicz, W.; Kirschner, D. *Biophys. J.* **1991**, *60*, 1190−1201.
(72) Sunde, M.; Serpell, L. C.; Bartlam, M.; Fraser, P. E.; Pepys, M. B.; Blake, C. C. F. *J. Mol. Biol.* **1997**, *273*, 729−739.
(73) Eanes, E. D.; Glenner, G. G. *J. Histochem. Cytochem.* **1968**, *16*, 673−677.
(74) Serpell, L. C.; Fraser, P. E.; Sunde, M. *Methods Enzymol.* **1999**, *309*, 526−536.
(75) Morris, K. L.; Serpell, L. C. X-ray Fibre Diffraction Studies of Amyloid Fibrils. *Amyloid Proteins: Methods and Protocols*, 2nd ed.; Methods in Molecular Biology, Vol. *849*; Springer: New York, 2012; pp 121−135.
(76) Kisilevsky, R. *J. Struct. Biol.* **2000**, *130*, 99−108.
(77) Kheterpal, I.; Williams, A.; Murphy, C.; Bledsoe, B.; Wetzel, R. *Biochemistry* **2001**, *40*, 11757−11767.
(78) Torok, M.; Milton, S.; Kayed, R.; Wu, P.; McIntire, T.; Glabe, C. G.; Langen, R. *J. Biol. Chem.* **2002**, *277*, 40810−40815.
(79) Petkova, A. T.; Yau, W. M.; Tycko, R. *Biochemistry* **2006**, *45*, 498−512.
(80) Makin, O. S.; Sikorski, P.; Serpell, L. C. *Curr. Opin. Chem. Biol.* **2006**, *10*, 417−422.
(81) Jahn, T. R.; Makin, O. S.; Morris, K. L.; Marshall, K. E.; Tian, P.; Sikorski, P.; Serpell, L. C. *J. Mol. Biol.* **2010**, *395*, 717−727.
(82) Sipe, J. D.; Cohen, A. S. *J. Struct. Biol.* **2000**, *130*, 88−98.
(83) (a) Sawaya, M. R.; Sambashivan, S.; Nelson, R.; Ivanova, M. I.; Sievers, S. A.; Apostol, M. I.; Thompson, M. J.; Balbirnie, M.; Wiltzius, J. J. W.; McFarlane, H. T.; Madsen, A. O.; Riekel, C.; Eisenberg, D. *Nature* **2007**, *447*, 453−457. (b) Eisenberg, D.; Jucker, M. *Cell* **2012**, *148*, 1188−1203.
(84) Park, J.; Kahng, B.; Hwang, W. *PLoS Comput. Biol.* **2009**, *5*, e1000492.
(85) Tycko, R. *Annu. Rev. Phys. Chem.* **2001**, *52*, 575−606.
(86) Benzinger, T. L. S.; Gregory, D. M.; Burkoth, T. S.; Miller-Auer, H.; Lynn, D. G.; Botto, R. E.; Meredith, S. C. *Proc. Natl. Acad. Sci. U.S.A.* **1998**, *95*, 13407−13412.
(87) Lansbury, P. T.; Costa, P. R.; Griffiths, J. M.; Simon, E. J.; Auger, M.; Halverson, K. J.; Kocisko, D. A.; Hendsch, Z. S.; Ashburn, T. T.; Spencer, R. G. S.; Tidor, B.; Griffin, R. G. *Nat. Struct. Biol.* **1995**, *2*, 990−998.
(88) Lazo, N. D.; Downing, D. T. *Biochemistry* **1998**, *37*, 1731−1735.
(89) Fabian, H.; Nauman, D.; Otvos, L.; Schultz, C.; Backmann, J. *J. Mol. Struct.* **1995**, *348*, 5−8.
(90) Halverson, K.; Fraser, P. E.; Kirschner, D. A.; Lansbury, P. T., Jr. *Biochemistry* **1990**, *29*, 2639−2644.
(91) Ishii, Y. *J. Chem. Phys.* **2001**, *114*, 8473−8483.
(92) Ishii, Y.; Balbach, J. J.; Tycko, R. *Chem. Phys.* **2001**, *266*, 231−236.
(93) Tycko, R. *J. Chem. Phys.* **2007**, *126*, 064506−064506.
(94) (a) Balbach, J. J.; Ishii, Y.; Antzutkin, O. N.; Leapman, R. D.; Rizzo, N. W.; Dyda, F.; Reed, J.; Tycko, R. *Biochemistry* **2000**, *39*, 13748−13759. (b) Ma, B.; Nussinov, R. *Proc. Natl. Acad. Sci. U.S.A.* **2002**, *99*, 14126−14131.
(95) Mikros, E.; Benaki, D.; Humpfer, E.; Spraul, M.; Loukas, S.; Stassinopoulou, C.; Pelecanou, M. *Angew. Chem., Int. Ed.* **2001**, *40*, 3603−3065.
(96) Antzutkin, O. N.; Balbach, J. J.; Leapman, R. D.; Rizzo, N. W.; Reed, J.; Tycko, R. *Proc. Natl. Acad. Sci. U.S.A.* **2000**, *97*, 13045−13050.
(97) Chi, E. Y.; Frey, S. L.; Winans, A.; Lam, K. L.; Kjaer, K.; Majewski, J.; Lee, K. Y. *Biophys. J.* **2010**, *98*, 2299−2308.
(98) Bertini, I.; Gonnelli, L.; Luchinat, C.; Mao, J. F.; Nesi, A. *J. Am. Chem. Soc.* **2011**, *133*, 16013−16022.
(99) Lopez del Amo, J. M.; Schmidt, M.; Fink, U.; Dasari, M.; Fandrich, M.; Reif, B. *Angew. Chem., Int. Ed.* **2012**, *51*, 6136−6139.
(100) Wu, C.; Bowers, M. T.; Shea, J. E. *PLoS Comput. Biol.* **2010**, *6*, e1000693.
(101) Qiang, W.; Yau, W.; Luo, Y.; Mattson, M. P.; Tycko, R. *Proc. Natl. Acad. Sci. U.S.A.* **2012**, *109*, 4443−4448.

DOI: 10.1021/cr500638n
Chem. Rev. 2015, 115, 3518−3563

(102) Pellarin, R.; Schuetz, P.; Guarnera, E.; Caflisch, A. *J. Am. Chem. Soc.* **2010**, *132*, 14960−14970.
(103) Paravastu, A. K.; Qahwash, I.; Leapman, R. D.; Meredith, S. C.; Tycko, R. *Proc. Natl. Acad. Sci. U.S.A.* **2009**, *106*, 7443−7448.
(104) Snyder, S. W.; Ladror, U. S.; Wade, W. S.; Wang, G. T.; Barrett, L. W.; Matayoshi, E. D.; Huffaker, H. J.; Krafft, G. A.; Holzman, T. F. *Biophys. J.* **1994**, *67*, 1216−1228.
(105) Lambert, M. P.; Barlow, A. K.; Chromy, B. A.; Edwards, C.; Freed, R.; Liosatos, M.; Morgan, T. E.; Rozovsky, I.; Trommer, B.; Viola, K. L.; Wals, P.; Zhang, C.; Finch, C. E.; Drafft, G. A.; Klein, W. L. *Proc. Natl. Acad. Sci. U.S.A.* **1998**, *95*, 6448−6453.
(106) Kodali, R.; Wetzel, R. *Curr. Opin. Struct. Biol.* **2007**, *17*, 48−57.
(107) Walsh, D. M.; Selkoe, D. J. *J. Neurochem.* **2007**, *101*, 1172−1184.
(108) Roychaudhuri, R.; Yang, M.; Hoshi, M. M.; Teplow, D. B. *J. Biol. Chem.* **2009**, *284*, 4749−4753.
(109) Rangachari, V.; Moore, B. D.; Reed, D. K.; Sonoda, L. K.; Bridges, A. W.; Conboy, E.; Hartigan, D.; Rosenberry, T. L. *Biochemistry* **2007**, *46*, 12451−12462.
(110) Nichols, M. R.; Moss, M. A.; Reed, D. K.; Lin, W.; Mukhopadhyay, R.; Hoh, J. H.; Rosenberry, T. L. *Biochemistry* **2002**, *41*, 6115−6127.
(111) Tay, W. M.; Huang, D.; Rosenberry, T. L.; Paravastu, A. K. *J. Mol. Biol.* **2013**, *425*, 2494−2508.
(112) Sandberg, A.; Luheshi, L. M.; Sollvander, S.; Pereira de Barros, T.; Macao, B.; Knowles, T. P.; Biverstal, H.; Lendel, C.; Ekholm-Petterson, F.; Dubnovitsky, A.; Lannfelt, L.; Dobson, C. M.; Hard, T. *Proc. Natl. Acad. Sci. U.S.A.* **2010**, *107*, 15595−15600.
(113) Hard, T. *FEBS J.* **2011**, *278*, 3884−3892.
(114) Hoyer, W.; Gronwall, C.; Jonsson, A.; Stahl, S.; Hard, T. *Proc. Natl. Acad. Sci. U.S.A.* **2008**, *105*, 5099 5099−5104; 5104..
(115) Klein, W. L. *Neurochem. Int.* **2002**, *41*, 345−352.
(116) Barghorn, S.; Nimmrich, V.; Striebinger, A.; Krantz, C.; Keller, P.; Janson, B.; Bahr, M.; Schmidt, M.; Bitner, R. S.; Harlan, J.; Barlow, E.; Ebert, U.; Hillen, H. *J. Neurochem.* **2005**, *95*, 834−847.
(117) Moore, B. D.; Rangachari, V.; Tay, W. M.; Milkovic, N. M.; Rosenberry, T. L. *Biochemistry* **2009**, *48*, 11796−11806.
(118) Chimon, S.; Shaibat, M. A.; Jones, C. R.; Calero, D. C.; Aizezi, B.; Ishii, Y. *Nat. Struct. Mol. Biol.* **2007**, *14*, 1157−1164.
(119) Matsumura, S.; Shinoda, K.; Yamada, M.; Yokojima, S.; Inoue, M.; Ohnishi, T.; Shimada, T.; Kikuchi, K.; Masui, D.; Hashimoto, S.; Sato, M.; Ito, A.; Akioka, M.; Takagi, S.; Nakamura, Y.; Nemoto, K.; Hasegawa, Y.; Takamoto, H.; Inoue, H.; Nakamura, S.; Nabeshima, Y.; Teplow, D. B.; Kinjo, M.; Hoshi, M. *J. Biol. Chem.* **2011**, *286*, 11555−11562.
(120) Scheidt, H. A.; Morgado, I.; Huster, D. *J. Biol. Chem.* **2012**, *287*, 22822−22826.
(121) Scheidt, H. A.; Morgado, I.; Rothemund, S.; Huster, D.; Fandrich, M. *Angew. Chem., Int. Ed.* **2011**, *50*, 2837−2840.
(122) Doi, T.; Masuda, Y.; Irie, K.; Akagi, K.; Monobe, Y.; Imazawa, T.; Takegoshi, K. *Biochem. Biophys. Res. Commun.* **2012**, *428*, 458−462.
(123) Yu, L.; Edalji, R.; Harlan, J. E.; Holzman, T. F.; Lopez, A. P.; Labkovsky, B.; Hillen, H.; Barghorn, S.; Ebert, U.; Richardson, P. L.; Miesbauer, L.; Solomon, L.; Bartley, D.; Walter, K.; Johnson, R. W.; Hajduk, P. J.; Olejniczak, E. T. *Biochemistry* **2009**, *48*, 1870−1877.
(124) Ahmed, M.; Davis, J.; Aucoin, D.; Sato, T.; Ahuja, S.; Aimoto, S.; Elliott, J. I.; Nostrand, W. E. V.; Smith, S. O. *Nat. Struc. Mol. Biol.* **2010**, *17*, 561−568.
(125) Spencer, R. K.; Li, H.; Nowick, J. S. *J. Am. Chem. Soc.* **2014**, *136*, 5595−5598.
(126) Haupt, C.; Leppert, J.; Ronicke, R.; Meinhardt, J.; Yadav, J. K.; Ramachandran, R.; Ohlenschlager, O.; Reymann, K. G.; Gorlach, M.; Fandrich, M. *Angew. Chem., Int. Ed.* **2012**, *51*, 1576−1579.
(127) (a) Sarkar, B.; Mithu, V. S.; Chandra, B.; Mandal, A.; Chandrakesan, M.; Bhowmik, D.; Madhu, P. K.; Maiti, S. *Angew. Chem., Int. Ed.* **2014**, *53*, 6888−6892. (b) Laganowsky, A.; Liu, C.; Sawaya, M. R.; Whitelegge, J. P.; Park, J.; Zhao, M.; Pensalfini, A.; Soriaga, A. B.; Landau, M.; Teng, P. K.; Cascio, D.; Glabe, C.; Eisenberg, D. *Science* **2012**, *335*, 1228−31.
(128) (a) Wei, G.; Mousseau, N.; Derreumaux, P. *Biophys. J.* **2004**, *87*, 3648−3656. (b) Mousseau, N.; Derreumaux, P. *Acc. Chem. Res.* **2005**, *38*, 885−891.
(129) Melquiond, A.; Mousseau, N.; Derreumaux, P. *Proteins* **2006**, *65*, 180−191.
(130) Song, W.; Wei, G.; Mousseau, N.; Derreumaux, P. *J. Phys. Chem. B* **2008**, *112*, 4410−4418.
(131) Irback, A.; Mitternacht, S. *Proteins* **2008**, *71*, 207−214.
(132) Bellesia, G.; Shea, J. E. *J. Chem. Phys.* **2009**, *130*, 145103.
(133) (a) De Simone, A.; Derreumaux, P. *J. Chem. Phys.* **2010**, *132*, 165103. (b) Hatami, A.; Albay, R., 3rd; Monjazeb, S.; Milton, S.; Glabe, C. *J. Biol. Chem.* **2014**, *289*, 32131−43.
(134) Bitan, G.; Lomakin, A.; Teplow, D. *J. Biol. Chem.* **2001**, *276*, 35176−35184.
(135) Bitan, G.; Kirkitadze, M. D.; Lomakin, A.; Vollers, S. S.; Benedek, G. B.; Teplow, D. B. *Proc. Natl. Acad. Sci. U.S.A.* **2003**, *100*, 330−335.
(136) Roychaudhuri, R.; Yang, M.; Deshpande, A.; Cole, G. M.; Frautschy, S.; Lomakin, A.; Benedek, G. B.; Teplow, D. B. *J. Mol. Biol.* **2013**, *425*, 292−308.
(137) (a) Kloniecki, M.; Jablonowska, A.; Poznanski, J.; Langridge, J.; Hughes, C.; Campuzano, I.; Giles, K.; Dadlez, M. *J. Mol. Biol.* **2011**, *407*, 110−124. (b) Sitkiewicz, E.; Kłoniecki, M.; Poznański, J.; Bal, W.; Dadlez, M. *J. Mol. Biol.* **2014**, *426*, 2871−2885. (c) Chen, Y. R.; Glabe, C. G. *J. Biol. Chem.* **2006**, *281*, 24414−24422.
(138) Liu, R.; McAllister, C.; Lyubchenko, Y.; Sierks, M. R. *J. Neurosci. Res.* **2004**, *75*, 162−171.
(139) (a) Williams, A. D.; Portelius, E.; Kheterpal, I.; Guo, J. T.; Cook, K. D.; Xu, Y.; Wetzel, R. *J. Mol. Biol.* **2004**, *335*, 833−842. (b) Bernstein, S. L.; Wyttenbach, T.; Baumketner, A.; Shea, J. E.; Bitan, G.; Teplow, D. B.; Bowers, M. T. *J. Am. Chem. Soc.* **2005**, *127*, 2075−2084. (c) Masuda, Y.; Uemura, S.; Ohashi, R.; Nakanishi, A.; Takegoshi, K.; Shimizu, T.; Shirasawa, T.; Irie, K. *ChemBioChem* **2009**, *10*, 287−295.
(140) Gu, L.; Ngo, S.; Guo, Z. *J. Biol. Chem.* **2012**, *287*, 9081−9089.
(141) Bramucci, E.; Paiardini, A.; Bossa, F.; Pascarella, S. *BMC Bioinf.* **2012**, *13* (Suppl. 4), S2 DOI: 10.1186/1471-2105-13-S4-S2.
(142) Lazo, N. D.; Grant, M. A.; Condron, M. C.; Rigby, A. C.; Teplow, D. B. *Protein Sci.* **2005**, *14*, 1581−1596.
(143) Chen, W.; Mousseau, N.; Derreumaux, P. *J. Chem. Phys.* **2006**, *125*, 084911.
(144) Chebaro, Y.; Mousseau, N.; Derreumaux, P. *J. Phys. Chem. B* **2009**, *113*, 7668−7675.
(145) (a) Cruz, L.; Rao, J. S.; Teplow, D. B.; Urbanc, B. *J. Phys. Chem. B* **2012**, *116*, 6311−6325. (b) Smith, M. D.; Cruz, L. *J. Phys. Chem. B* **2013**, *117*, 6614−6624.
(146) Doran, T. M.; Anderson, E. A.; Latchney, S. E.; Opanashuk, L. A.; Nilsson, B. L. *J. Mol. Biol.* **2012**, *421*, 315−328.
(147) (a) Tsubuki, S.; Takaki, Y.; Saido, T. C. *Lancet* **2003**, *361*, 1957−1958. (b) Smith, M. D.; Cruz, L. *J. Phys. Chem. B* **2013**, *117*, 14907−14915.
(148) Maji, S. K.; Ogorzalek Loo, R. R.; Inayathullah, M.; Spring, S. M.; Vollers, S. S.; Condron, M. M.; Bitan, G.; Loo, J. A.; Teplow, D. B. *J. Biol. Chem.* **2009**, *284*, 23580−23591.
(149) (a) Ono, K.; Condron, M. M.; Teplow, D. B. *J. Biol. Chem.* **2010**, *285*, 23186−23197. (b) Ono, K.; Condron, M. M.; Teplow, D. B. *Proc. Natl. Acad. Sci. U.S.A.* **2009**, *106*, 14745−14750.
(150) Bitan, G.; Vollers, S. S.; Teplow, D. B. *J. Biol. Chem.* **2003**, *278*, 34882−34889.
(151) (a) Sinha, S.; Lopes, D. H.; Bitan, G. A. *ACS Chem. Neurosci.* **2012**, *3*, 473−481. (b) Xu, W.; Zhang, C.; Derreumaux, P.; Gräslund, A.; Morozova-Roche, L.; Mu, Y. *PLoS One* **2011**, *6*, e24329. (c) Chi, E. Y.; Frey, S. L.; Winans, A.; Lam, K. L.; Kjaer, K.; Majewski, J.; Lee, K. Y. *Biophys. J.* **2010**, *98*, 2299−308. (d) Tycko, R. *Protein Sci.* **2014**, *23*, 1528−39. (e) Adler, J.; Scheidt, H. A.; Krüger, M.; Thomas, L.; Huster, D. *Phys. Chem. Chem. Phys.* **2014**, *16*, 7461−71.
(152) (a) Zhang, S.; Iwata, K.; Lachenmann, M. J.; Peng, J. W.; Li, S.; Stimson, E. R.; Lu, Y.; Felix, A. M.; Maggio, J. E.; Lee, J. P. *J. Struct. Biol.* **2000**, *130*, 130−141. (b) Lim, K. H.; Collver, H. H.; Le, Y. T.;

DOI: 10.1021/cr500638n
Chem. Rev. 2015, 115, 3518−3563

Nagchowdhuri, P.; Kenney, J. M. *Biochem. Biophys. Res. Commun.* **2007**, *353*, 443−449.
(153) Yan, Y.; McCallum, S. A.; Wang, C. *J. Am. Chem. Soc.* **2008**, *130*, 5394−5395.
(154) Rosenman, D. J.; Connors, C. R.; Chen, W.; Wang, C.; Garcia, A. E. *J. Mol. Biol.* **2013**, *425*, 3338−3359.
(155) Yan, Y.; Wang, C. *J. Mol. Biol.* **2006**, *364*, 853−862.
(156) Yan, Y.; Liu, J.; McCallum, S. A.; Yang, D.; Wang, C. *Biochem. Biophys. Res. Commun.* **2007**, *362*, 410−414.
(157) (a) Vivekanandan, S.; Brender, J. R.; Lee, S. Y.; Ramamoorthy, A. *Biochem. Biophys. Res. Commun.* **2011**, *411*, 312−316. (b) Bhowmik, D.; MacLaughlin, C. M.; Chandrakesan, M.; Ramesh, P.; Venkatramani, R.; Walker, G. C.; Maiti, S. *Phys. Chem. Chem. Phys.* **2014**, *16*, 885−9.
(158) Hwang, T. L.; van Zijl, P. C.; Mori, S. *J. Biomol. NMR* **1998**, *11*, 221−226.
(159) Rezaei-Ghaleh, N.; Andreetto, E.; Yan, L.-M.; Kapurniotu, A.; Zweckstetter, M. *PLoS One* **2011**, *6*, e20289.
(160) Bitan, G.; Teplow, D. B. *Acc. Chem. Res.* **2004**, *37*, 357−364.
(161) (a) Hukushima, K.; Nemoto, K. *J. Phys. Soc. Jpn.* **1996**, *65*, 1604−1608. (b) Sugita, Y.; Okamoto, Y. *Chem. Phys. Lett.* **1999**, *314*, 141−151.
(162) Nguyen, P. H.; Okamoto, Y.; Derreumaux, P. *J. Chem. Phys.* **2013**, *138*, 061102.
(163) (a) Laio, A.; Parrinello, M. *Proc. Natl. Acad. Sci. U.S.A.* **2002**, *99*, 12562−12566. (b) Laio, A.; Gervasio, F. L. *Rep. Prog. Phys.* **2008**, *71*, 126601 DOI: 10.1088/0034-4885/71/12/126601. (c) Barducci, A.; Bonomi, M.; Derreumaux, P. *J. Chem. Theory Comput.* **2011**, *7*, 1928−1934.
(164) Kaminski, G. A.; Friesner, R. A.; Tirado-Rives, J.; Jorgensen, W. L. *J. Phys. Chem. B* **2001**, *105*, 6474−6487.
(165) (a) Hornak, V.; Abel, R.; Okur, A.; Strockbine, B.; Roitberg, A.; Simmerling, C. *Proteins: Struct., Funct., Bioinf.* **2006**, *65*, 712−725. (b) Best, R. B.; Hummer, G. *J. Phys. Chem. B* **2009**, *113*, 9004−9015. (c) Lindorff-Larsen, K.; Piana, S.; Palmo, K.; Maragakis, P.; Klepeis, J. L.; Dror, R. O.; Shaw, D. E. *Proteins: Struct., Funct., Bioinf.* **2010**, *78*, 1950−1958.
(166) Piana, S.; Lindorff-Larsen, K.; Shaw, D. E. *Biophys. J.* **2011**, *100*, L47−L49.
(167) Jorgensen, W. L.; Chandrasekhar, J.; Madura, J. D.; Impey, R. W.; Klein, M. L. *J. Chem. Phys.* **1983**, *79*, 926.
(168) Berendsen, H. J. C.; Grigera, J. R.; Straatsma, T. P. *J. Phys. Chem.* **1987**, *91*, 6269−6271.
(169) Horn, H. W.; Swope, W. C.; Pitera, J. W.; Madura, J. D.; Dick, T. J.; Hura, G. L.; Head-Gordon, T. *J. Chem. Phys.* **2004**, *120*, 9665−9678.
(170) (a) Shaw, D. E.; Maragakis, P.; Lindorff-Larsen, K.; Piana, S.; Dror, R. O.; Eastwood, M. P.; Bank, J. A.; Jumper, J. M.; Salmon, J. K.; Shan, Y.; Wriggers, W. *Science* **2010**, *330*, 341−346. (b) Lindorff-Larsen, K.; Piana, S.; Dror, R. O.; Shaw, D. E. *Science* **2011**, *334*, 517−520. (c) Lindorff-Larsen, K.; Maragakis, P.; Piana, S.; Eastwood, M. P.; Dror, R. O.; Shaw, D. E. *PLoS One* **2012**, *7*, e32131. (d) Piana, S.; Lindorff-Larsen, K.; Shaw, D. E. *Proc. Natl. Acad. Sci. U.S.A.* **2012**, *109*, 17845−17850. (e) Lindorff-Larsen, K.; Trbovic, N.; Maragakis, P.; Piana, S.; Shaw, D. E. *J. Am. Chem. Soc.* **2012**, *134*, 3787−3791. (f) Wang, W.; Ye, W.; Jiang, C.; Luo, R.; Chen, H. F. *Chem. Biol. Drug Des.* **2014**, *84*, 253−269.
(171) (a) Sgourakis, N. G.; Yan, Y.; McCallum, S. A.; Wang, C.; Garcia, A. E. *J. Mol. Biol.* **2007**, *368*, 1448−1457. (b) Sgourakis, N. G.; Merced-Serrano, M.; Boutsidis, C.; Drineas, P.; Du, Z.; Wang, C.; Garcia, A. E. *J. Mol. Biol.* **2011**, *405*, 570−583.
(172) Ball, K. A.; Phillips, A. H.; Nerenberg, P. S.; Fawzi, N. L.; Wemmer, D. E.; Head-Gordon, T. *Biochemistry* **2011**, *50*, 7612−7628.
(173) (a) Choy, W. Y.; Forman-Kay, J. D. *J. Mol. Biol.* **2001**, *308*, 1011−1032. (b) Marsh, J. A.; Forman-Kay, J. D. *J. Mol. Biol.* **2009**, *391*, 359−374. (c) Krzeminski, M.; Marsh, J. A.; Neale, C.; Choy, W. Y.; Forman-Kay, J. D. *Bioinformatics* **2013**, *29*, 398−399.
(174) Ball, K. A.; Phillips, A. H.; Wemmer, D. E.; Head-Gordon, T. *Biophys. J.* **2013**, *104*, 2714−2724.
(175) Zhu, M.; De Simone, A.; Schenk, D.; Toth, G.; Dobson, C. M.; Vendruscolo, M. *J. Chem. Phys.* **2013**, *139*, 035101.
(176) Lin, Y.-S.; Bowman, G. R.; Beauchamp, K. A.; Pande, V. S. *Biophys. J.* **2012**, *102*, 315−324.
(177) Lin, Y. S.; Pande, V. S. *Biophys. J.* **2012**, *103*, L47−L49.
(178) (a) Granata, D. Characterizing Structure and Free Energy Landscape of Proteins by NMR-Guided Metadynamics. Ph.D. Thesis, Scuola Internazionale Superiore di Studi Avanzati (SISSA), Trieste, Italy, Oct 21, 2013. (b) Granata, D.; Camilloni, C.; Vendruscolo, M.; Laio, A. *Proc. Natl. Acad. Sci. U.S.A.* **2013**, *110*, 6817−6822.
(179) Chebaro, Y.; Dong, X.; Laghaei, R.; Derreumaux, P.; Mousseau, N. *J. Phys. Chem. B* **2009**, *113*, 267−274.
(180) (a) Maupetit, J.; Tuffery, P.; Derreumaux, P. *Proteins* **2007**, *69*, 394−408. (b) Derreumaux, P. *J. Chem. Phys.* **1997**, *107*, 1941−1947. (c) Derreumaux, P. *J. Chem. Phys.* **1997**, *106*, 5260−5270. (d) Derreumaux, P. *Phys. Rev. Lett.* **2000**, *85*, 206−209. (e) Derreumaux, P.; Mousseau, N. *J. Chem. Phys.* **2007**, *126*, 025101. (f) Derreumaux, P.; Vergoten, G.; Lagant, P. *J. Comput. Chem.* **1990**, *11*, 560−568. (g) Derreumaux, P.; Dauchez, M.; Vergoten, G. *J. Mol. Struct.* **1993**, *295*, 203−221. (h) Thévenet, P.; Shen, Y.; Maupetit, J.; Guyon, F.; Derreumaux, P.; Tufféry, P. *Nucleic Acids Res.* **2012**, *40* (Web Server issue), W288−93. (i) Shen, Y.; Maupetit, J.; Derreumaux, P.; Tufféry, P. *J. Chem. Theory Comput.* **2014**, *10*, 4745−4758.
(181) (a) Irbäck, A.; Mitternacht, S.; Mohanty, S. *PMC Biophys.* **2009**, *2*, 2 DOI: 10.1186/1757-5036-2-2. (b) Mitternacht, S.; Staneva, I.; Härd, T.; Irbäck, A. *Proteins: Struct., Funct., Bioinf.* **2010**, *78*, 2600−2608.
(182) Côté, S.; Derreumaux, P.; Mousseau, N. *J. Chem. Theory Comput.* **2011**, *7*, 2584−2592.
(183) Sterpone, F.; Nguyen, P. H.; Kalimeri, M.; Derreumaux, P. *J. Chem. Theory Comput.* **2013**, *9*, 4574−4584.
(184) (a) Yang, M.; Teplow, D. B. *J. Mol. Biol.* **2008**, *384*, 450−464. (b) Lam, A. R.; Teplow, D. B.; Stanley, H. E.; Urbanc, B. *J. Am. Chem. Soc.* **2008**, *130*, 17413−17422.
(185) Rauscher, S.; Gapsys, V.; Volkhardt, A.; Blau, C.; de Groot, B. L.; Grubmüller, H. *Biophys. J.* **2014**, *106*, 271a.
(186) Jin, M.; Shepardson, N.; Yang, T.; Chen, G.; Walsh, D.; Selkoe, D. J. *Proc. Natl. Acad. Sci. U.S.A.* **2011**, *108*, 5819−5824.
(187) Autiero, I.; Saviano, M.; Langella, E. *Mol. Biosyst.* **2013**, *9*, 2118−2124.
(188) Berhanu, W. M.; Hansmann, U. H. *PLoS One* **2012**, *7*, e41479.
(189) Yu, X.; Zheng, J. *PloS One* **2011**, *6*, e20575.
(190) Ma, B.; Nussinov, R. *J. Biol. Chem.* **2011**, *286*, 34244−34253.
(191) Derreumaux, P. *J. Chem. Phys.* **1999**, *111*, 2301−2310.
(192) Forcellino, F.; Derreumaux, P. *Proteins* **2001**, *45*, 159−166.
(193) Chebaro, Y.; Pasquali, S.; Derreumaux, P. *J. Phys. Chem. B* **2012**, *116*, 8741−8752.
(194) Kalimari, M.; Derreumaux, P.; Sterpone, F. *J. Non-Cryst. Solids* **2015**, *407*, 494−501.
(195) Côté, S.; Laghaei, R.; Derreumaux, P.; Mousseau, N. *J. Phys. Chem. B* **2012**, *116*, 4043−4055.
(196) Laghaei, R.; Mousseau, N.; Wei, G. *J. Phys. Chem. B* **2010**, *114*, 7071−7077.
(197) MacKerell, A. D.; Bashford, D.; Bellott, M.; Dunbrack, R. L.; Evanseck, J. D.; Field, M. J.; Fischer, S.; Gao, J.; Guo, H.; Ha, S.; Joseph-McCarthy, D.; Kuchnir, L.; Kuczera, K.; Lau, F. T.; Mattos, C.; Michnick, S.; Ngo, T.; Nguyen, D. T.; Prodhom, B.; Reiher, W. E.; Roux, B.; Schlenkrich, M.; Smith, J. C.; Stote, R.; Straub, J.; Watanabe, M.; Wiórkiewicz-Kuczera, J.; Yin, D.; Karplus, M. *J. Phys. Chem. B* **1998**, *102*, 3586−3616.
(198) Ferrara, P.; Apostolakis, J.; Caflisch, A. *Proteins* **2002**, *46*, 24−33.
(199) Takeda, T.; Klimov, D. K. *J. Phys. Chem. B* **2009**, *113*, 6692−6702.
(200) Kim, S.; Takeda, T.; Klimov, D. K. *Biophys. J.* **2010**, *99*, 1949−1958.
(201) Lockhart, C.; Kim, S.; Kumar, R.; Klimov, D. K. *J. Chem. Phys.* **2011**, *135*, 035103.

DOI: 10.1021/cr500638n
Chem. Rev. 2015, 115, 3518−3563

(202) Mitternacht, S.; Staneva, I.; Hard, T.; Irback, A. *J. Mol. Biol.* **2011**, *410*, 357−367.
(203) Urbanc, B.; Betnel, M.; Cruz, L.; Bitan, G.; Teplow, D. B. *J. Am. Chem. Soc.* **2010**, *132*, 4266−4280.
(204) Barz, B.; Urbanc, B. *PLoS One* **2012**, *7*, e34345.
(205) Chong, S. H.; Ham, S. *Phys. Chem. Chem. Phys.* **2012**, *14*, 1573−1575.
(206) (a) Yano, A.; Okamoto, A.; Nomura, K.; Higai, S.; Kurita, N. *Chem. Phys. Lett.* **2014**, *595*−*596*, 242−249. (b) Nguyen, P. H.; Mai, L. S.; Derreumaux, P. *J. Chem. Phys.* **2014**, *140*, 094105.
(207) Zhang, T.; Zhang, J.; Derreumaux, P.; Mu, Y. *J. Phys. Chem. B* **2013**, *117*, 3993−4002.
(208) Chebaro, Y.; Jiang, P.; Zang, T.; Mu, Y.; Nguyen, P. H.; Mousseau, N.; Derreumaux, P. *J. Phys. Chem. B* **2012**, *116*, 8412−8422.
(209) Qiu, D.; Shenkin, P. S.; Hollinger, F. P.; Still, W. C. *J. Phys. Chem. A* **1997**, *101*, 3005−3014.
(210) Barz, B.; Olubiyi, O. O.; Strodel, B. *Chem. Commun.* **2014**, *50*, 5373−5375.
(211) Ferrone, F. *Methods Enzymol.* **1999**, *309*, 256−274.
(212) Oosawa, F., Asakura, S. *Thermodynamics of the Polymerization of Protein*; Academic: Waltham, MA, 1975.
(213) Wegner, A. *Nature* **1982**, *296*, 266−267.
(214) Ferrone, F. A.; Hofrichter, J.; Eaton, W. A. *J. Mol. Biol.* **1985**, *183*, 611−631.
(215) Nasica-Labouze, J.; Mousseau, N. *PLoS Comput. Biol.* **2012**, *8*, 1002782.
(216) Irbäck, A.; Jonsson, S.Æ.; Linnemann, N.; Linse, B.; Wallin, S. *Phys. Rev. Lett.* **2013**, *110*, 058101.
(217) Bhattacharyya, A. M.; A. K. Thakur, A. K.; Wetzel, R. *Proc. Natl. Acad. Sci. U.S.A.* **2005**, *102*, 15400−15405.
(218) Fay, N.; Inoue, Y. J.; Bousset, L.; Taguchi, H.; Melki, R. *J. Biol. Chem.* **2003**, *278*, 30199−30205.
(219) Li, M. S.; Co, N. T.; Reddy, G.; Hu, C. K.; Straub, J. E.; Thirumalai, D. *Phys. Rev. Lett.* **2010**, *105*, 218101.
(220) Abeln, S.; Vendruscolo, M.; Dobson, C. M.; Frenkel, D. *PLoS One* **2014**, *9*, e85185 DOI: 10.1371/journal.pone.0085185.
(221) Mompeán, M.; González, C.; Lomba, E.; Laurents, D. V. *J. Phys. Chem. B* **2014**, *118*, 7312−7316.
(222) De Simone, A.; Kitchen, C.; Kwan, A. H.; Sunde, M.; Dobson, C. M.; Frenkel, D. *Proc. Natl. Acad. Sci. U.S.A.* **2012**, *109*, 6951−6956.
(223) Bieler, N. S.; Knowles, T. P. J.; Frenkel, D.; Vacha, R. *PLoS Comput. Biol.* **2012**, *8*, e1002692 DOI: 10.1371/journal.pcbi.1002692.
(224) Lomakin, A.; Teplow, D. B.; Kirschner, D. A.; Benedek, G. B. *Proc. Natl. Acad. Sci. U.S.A.* **1997**, *94*, 7942−7947.
(225) Fawzi, N. L.; Okabe, Y.; Yap, E. H.; Head-Gordon, T. *J. Mol. Biol.* **2007**, *365*, 535−550.
(226) Collins, S. R.; Douglass, A.; Vale, R. D.; Weissman, J. S. *PLoS Biol.* **2004**, *2*, 1582−1590.
(227) Nguyen, P. H.; Li, M. S.; Stock, G.; Straub, J. E.; Thirumalai, D. *Proc. Natl. Acad. Sci. U.S.A.* **2007**, *104*, 111−116.
(228) Takeda, T.; Klimov, D. K. *J. Mol. Biol.* **2007**, *368*, 1202−1213.
(229) Li, M. S.; Klimov, D. K.; Straub, J. E.; Thirumalai, D. *J. Chem. Phys.* **2008**, *129*, 175101 DOI: 10.1063/1.2989981.
(230) Co, N. T.; Li, M. S. *J. Chem. Phys.* **2012**, *137*, 095101 DOI: 10.1063/1.4749257.
(231) (a) Cabriolu, R.; Auer, S. *J. Mol. Biol.* **2011**, *411*, 275−285. (b) Garai, K.; Sahoo, B.; Sengupta, P.; Maiti, S. *J. Chem. Phys.* **2008**, *128*, 045102.
(232) Kashchiev, D.; Cabriolu, R.; Auer, S. *J. Am. Chem. Soc.* **2013**, *135*, 1531−1539.
(233) Baftizadeh, F.; Biarnes, X.; Pietrucci, F.; Affinito, F.; Laio, A. *J. Am. Chem. Soc.* **2012**, *134*, 3886−3894.
(234) Baftizadeh, F.; Pietrucci, F.; Biarnes, X.; Laio, A. *Phys. Rev. Lett.* **2013**, *110*, 168103.
(235) Hilbich, C.; Kisters-Woike, B.; Reed, J.; Masters, C.; Beyreuther, K. *J. Mol. Biol.* **1992**, *228*, 460−473.
(236) Tjernberg, L.; Naslund, J.; Lindqvist, F.; Johansson, J.; Karlstrom, A.; Thyberg, J.; Terenius, L.; Nordstedt, C. *J. Biol. Chem.* **1996**, *271*, 8545−8548.
(237) Kheterpal, I.; Williams, A.; Murphy, C.; Bledsoe, B.; Wetzel, R. *Biochemistry* **2001**, *40*, 11757−11767.
(238) Piana, S.; Laio, A. *J. Phys. Chem. B* **2007**, *111*, 4553−4559.
(239) Nguyen, P. H.; Derreumaux, P. *J. Phys. Chem. B* **2013**, *117*, 5831−5840.
(240) Yang, Y. I.; Gao, Y. Q. *J. Phys. Chem. B* **2015**, *119*, 662−670.
(241) Lu, Y.; Wei, G.; Derreumaux, P. *J. Chem. Phys.* **2012**, *137*, 025101 DOI: 10.1063/1.4732761.
(242) Wei, G.; Mousseau, N.; Derreumaux, P. *Prion* **2007**, *1*, 3−8.
(243) Mousseau, N.; Derreumaux, P. *Front. Biosci.* **2008**, *13*, 4495−516.
(244) Wei, G.; Song, W.; Derreumaux, P.; Mousseau, N. *Front. Biosci.* **2008**, *13*, 5681−92.
(245) Nasica-Labouze, J.; Meli, M.; Derreumaux, P.; Colombo, G.; Mousseau, N. *PLoS Comput. Biol.* **2011**, *5*, e1002051 DOI: 10.1371/journal.pcbi.1002051.
(246) Santini, S.; Wei, G.; Mousseau, N.; Derreumaux, P. *Structure* **2004**, *12*, 1245−55.
(247) Santini, S.; Mousseau, N.; Derreumaux, P. *J. Am. Chem. Soc.* **2004**, *126*, 11509−11516.
(248) Petty, S. A.; Decatur, S. M. *Proc. Natl. Acad. Sci. U.S.A.* **2005**, *102*, 14272−14277.
(249) Kittner, M.; Knecht, V. *J. Phys. Chem. B* **2010**, *114*, 15288−15295.
(250) Whittleston, C. S.; Wales, D. J. *J. Am. Chem. Soc.* **2007**, *129*, 16005−16014.
(251) Sciarretta, K. L.; Gordon, D. J.; Petkova, A. T.; Tycko, R.; Meredith, S. C. *Biochemistry* **2005**, *44*, 6003−6014.
(252) Reddy, G.; Straub, J. E.; Thirumalai, D. *J. Phys. Chem. B* **2009**, *113*, 1162−1172.
(253) Wood, S. J.; Wetzel, R.; Martin, J. D.; Hurle, M. R. *Biochemistry* **1995**, *34*, 724−730.
(254) Larini, L.; Shea, J. E. *Biophys. J.* **2012**, *103*, 576−586.
(255) Grabenauer, M.; Wu, C.; Soto, P.; Shea, J. E.; Bowers, M. T. *J. Am. Chem. Soc.* **2010**, *132*, 532−539.
(256) Liang, C.; Derreumaux, P.; Wei, G. *Biophys. J.* **2007**, *93*, 3353−3362.
(257) Liang, C.; Derreumaux, P.; Mousseau, N.; Wei, G. *Biophys. J.* **2008**, *95*, 510−517.
(258) Qiao, Q.; Bowman, G. R.; Huang, X. *J. Am. Chem. Soc.* **2013**, *135*, 16092−16101.
(259) Wu, C.; Shea, J. E. *PLoS Comput. Biol.* **2013**, *9*, e1003211 DOI: 10.1371/journal.pcbi.1003211.
(260) Cheon, M.; Chang, I.; Mohanty, S.; Luheshi, L. M.; Dobson, C. M.; Vendruscolo, M.; Favrin, G. *PLoS Comput. Biol.* **2007**, *3*, 1727−1738.
(261) (a) Colletier, J. P.; Laganowsky, A.; Landau, M.; Zhao, M.; Soriaga, A. B.; Goldschmidt, L.; Flot, D.; Cascio, D.; Sawaya, M. R.; Eisenberg, D. *Proc. Natl. Acad. Sci. U.S.A.* **2011**, *108*, 16938−16943. (b) Armstrong, A. H.; Chen, J.; McKoy, A. F.; Hecht, M. H. *Biochemistry* **2011**, *50*, 4058−4067.
(262) Kayed, R.; Sokolov, Y.; Edmonds, B.; McIntire, T. M.; Milton, S. C.; Hall, J. E.; Glabe, C. G. *J. Biol. Chem.* **2004**, *279*, 46363−46366.
(263) Quist, A.; Doudevski, L.; Lin, H.; Azimova, R.; Ng, D.; Frangione, B.; Kagan, B.; Ghiso, J.; Lal, R. *Proc. Natl. Acad. Sci. U.S.A.* **2005**, *102*, 10427−10432.
(264) Engel, M. F. M.; Khemtemourian, L.; Kleijer, C. C.; Meeldijk, H. J. D.; Jacobs, J.; Verkleij, A. J.; de Kruijff, B.; Killian, J. A.; Hoppener, J. W. M. *Proc. Natl. Acad. Sci. U.S.A.* **2008**, *105*, 6033−6038.
(265) Kastorna, A.; Trusova, V.; Gorbenko, G.; Kinnunen, P. *Chem. Phys. Lipids* **2012**, *165*, 331−337.
(266) Hung, L. W.; Ciccotosto, G. D.; Giannakis, E.; Tew, D. J.; Perez, K.; Masters, C. L.; Cappai, R.; Wade, J. D. *J. Neurosci.* **2008**, *28*, 11950−11958.

DOI: 10.1021/cr500638n
Chem. Rev. 2015, 115, 3518−3563

(267) Butterfield, S. M.; Lashuel, H. A. *Angew. Chem., Int. Ed.* **2010**, *49*, 5628−5654.
(268) Williams, T. L.; Serpell, L. C. *FEBS J.* **2011**, *278*, 3905−3917.
(269) Connelly, L.; Jang, H.; Arce, F. T.; Capone, R.; Kotler, S. A.; Ramachandran, S.; Kagan, B. L.; Nussinov, R.; Lal, R. *J. Phys. Chem. B* **2012**, *116*, 1728−1735.
(270) Bokvist, M.; Lindstrom, F.; Watts, A.; Grobner, G. *J. Mol. Biol.* **2004**, *335*, 1039−1049.
(271) Zhao, H.; Tuominen, E. K.; Kinnunen, P. K. *Biochemistry* **2004**, *43*, 10302−10307.
(272) Yates, E. A.; Owens, S. L.; Lynch, M. F.; Cucco, E. M.; Umbaugh, C. S.; Legleiter, J. *J. Mol. Biol.* **2013**, *425*, 1915−1933.
(273) Tofoleanu, F.; Buchete, N. V. *J. Mol. Biol.* **2012**, *421*, 572−586.
(274) Nagarathinam, A.; Höflinger, P.; Bühler, A.; Schäfer, C.; McGovern, G.; Jeffrey, M.; Staufenbiel, M.; Jucker, M.; Baumann, F. *J. Neurosci.* **2013**, *33*, 19284−19294.
(275) Shao, H.; Jao, S.; Ma, K.; Zagorski, M. G. *J. Mol. Biol.* **1999**, *285*, 755−773.
(276) Coles, M.; Bicknell, W.; Watson, A. A.; Fairlie, D. P.; Craik, D. J. *Biochemistry* **1998**, *37*, 11064−11077.
(277) Gorbenko, G. P.; Trusova, V. *Adv. Protein Chem. Struct. Biol.* **2011**, *84*, 113−142.
(278) Gorbenko, G. P.; Kinnunen, P. K. *Chem. Phys. Lipids* **2006**, *142*, 72−82.
(279) Lin, H.; Bhatia, R.; Lal, R. *FASEB J.* **2001**, *15*, 2433−2444.
(280) Morita, M.; Hamada, T.; Tendo, Y.; Hata, T.; Vestergaard, M. C.; Takagi, M. *Soft Matter* **2012**, *8*, 2816−2819.
(281) Nag, S.; Sarkar, B.; Chandrakesan, M.; Abhyanakar, R.; Bhowmik, D.; Kombrabail, M.; Dandekar, S.; Lerner, E.; Haas, E.; Maiti, A. *Phys. Chem. Chem. Phys.* **2013**, *15*, 19129−19133.
(282) Benilova, I.; Karran, E.; De Strooper, B. *Nat. Neurosci.* **2012**, *15*, 349−357.
(283) Davis, C. H.; Berkowitz, M. L. *J. Phys. Chem. B* **2009**, *113*, 14480−14486.
(284) Davis, C. H.; Berkowitz, M. L. *Biophys. J.* **2009**, *96*, 785−797.
(285) Davis, C. H.; Berkowitz, M. L. *Proteins* **2010**, *78*, 2533−2545.
(286) Lockhart, C.; Klimov, D. K. *J. Phys. Chem. B* **2014**, *118*, 2638−2648.
(287) Yu, X.; Zheng, J. *J. Mol. Biol.* **2012**, *421*, 561−571.
(288) Miyashita, N.; Straub, J. E.; Thirumalai, D. *J. Am. Chem. Soc.* **2009**, *131*, 17843−17852.
(289) Buchete, N. V.; Tycko, R.; Hummer, G. *J. Mol. Biol.* **2005**, *353*, 804−821.
(290) Buchete, N. V.; Hummer, G. *Biophys. J.* **2007**, *92*, 3032−3039.
(291) Tofoleanu, F.; Brooks, B. R.; Buchete, N. V. Modulation of Alzheimer's Aβ Protofilament−Membrane Interactions by Lipid Headgroups. *ACS Chem. Neurosci.* **2015**, DOI: 10.1021/cn500277f, in press.
(292) Tofoleanu, F.; Buchete, N. V. *Prion* **2012**, *6*, 339−345.
(293) Jang, H.; Ma, B.; Lal, R.; Nussinov, R. *Biophys. J.* **2008**, *95*, 4631−4642.
(294) Jang, H.; Arce, F. T.; Capone, R.; Ramachandran, S.; Lal, R.; Nussinov, R. *Biophys. J.* **2009**, *97*, 3029−3037.
(295) Jang, H.; Arce, F. T.; Ramachandran, S.; Kagan, B. L.; Lal, R.; Nussinov, R. *J. Phys. Chem. B* **2013**, *117*, 11518−11529.
(296) Strodel, B.; Lee, J. W.; Whittleston, C. S.; Whales, D. J. *J. Am. Chem. Soc.* **2010**, *132*, 13300−13312.
(297) Poojari, C.; Kukol, A.; Strodel, B. *Biochim. Biophys. Acta, Biomembr.* **2013**, *1828*, 327−339.
(298) Poojari, C.; Strodel, B. *PLoS One* **2013**, *8*, e78399.
(299) Xu, Y.; Shen, J.; Luo, X.; Zhu, W.; Chen, K.; Ma, J.; Jiang, H. *Proc. Natl. Acad. Sci. U.S.A.* **2005**, *102*, 5403−5407.
(300) Lemkul, J. A.; Bevan, D. R. *Arch. Biochem. Biophys.* **2008**, *470*, 54−63.
(301) Lemkul, J. A.; Bevan, D. R. *Protein Sci.* **2011**, *20*, 1530−1545.
(302) Zhao, L. N.; Chiu, S. W.; Benoit, J.; Chew, L. Y.; Mu, Y. *J. Phys. Chem. B* **2011**, *115*, 12247−12256.
(303) Hoshino, T.; Mahmood, M. I.; Mori, K.; Matsuzaki, K. *J. Phys. Chem. B* **2013**, *117*, 8085−8094.
(304) (a) Manna, M.; Mukhopadhyay, C. *PLoS One* **2013**, *8*, e71308. (b) Devarajan, S.; Sharmika, J. E. *J. Mol. Liq.* **2014**, *195*, 59−64.
(305) Rushworth, J. V.; Hooper, N. M. *Int. J. Alzheimer's Dis.* **2010**, *2011*, 603052.
(306) Pobandt, T.; Knecht, V. *J. Phys. Chem. B* **2014**, *118*, 3507−3516.
(307) (a) Wu, C.; Shea, J. E. *Curr. Opin. Struct. Biol.* **2011**, *21*, 209−220. (b) Shea, J. E.; Urbanc, B. *Curr. Top. Med. Chem.* **2012**, *12*, 2596−2610.
(308) (a) Derreumaux, P. *Methods Mol. Biol.* **2013**, *924*, 585−600. (b) Morriss-Andrews, A.; Brown, F. L.; Shea, J. E. *J. Phys. Chem. B* **2014**, *118*, 8420−32.
(309) Friedman, R. *Biochem. J.* **2011**, *438*, 415−426.
(310) Pellarin, R.; Caflisch, A. *J. Mol. Biol.* **2006**, *360*, 882−892.
(311) Friedman, R.; Pellarin, R.; Caflisch, A. *J. Mol. Biol.* **2009**, *387*, 407−415.
(312) Ayton, S.; Lei, P.; Bush, A. I. *Free Radical Biol. Med.* **2013**, *62*, 76−89.
(313) Leskovjan, A. C.; Lanzirotti, A.; Miller, L. M. *Neuroimage* **2009**, *47*, 1215−1220.
(314) Hureau, C. *Coord. Chem. Rev.* **2012**, *256*, 2164−2174.
(315) Roberts, B. R.; Ryan, T. M.; Bush, A. I.; Masters, C. L.; Duce, J. A. *J. Neurochem.* **2012**, *120*, 149−166.
(316) Faller, P.; Hureau, C. *Chemistry* **2012**, *18*, 15910−20.
(317) Squitti, R. *J. Trace Elem. Med. Biol.* **2012**, *26*, 93−6.
(318) Lee, J.-Y.; Cole, T. B.; Palmiter, R. D.; Suh, S. W.; Koh, J.-Y. *Proc. Natl. Acad. Sci. U.S.A.* **2002**, *99*, 7705−7710.
(319) Drew, S. C.; Barnham, K. J. *Acc. Chem. Res.* **2011**, *44*, 1146−1155.
(320) Faller, P.; Hureau, C.; Berthoumieu, O. *Inorg. Chem.* **2013**, *52*, 12193−206.
(321) Zawisza, I.; Rozga, M.; Bal, W. *Coord. Chem. Rev.* **2012**, *256*, 2297−2307.
(322) Hureau, C.; Dorlet, P. *Coord. Chem. Rev.* **2012**, *256*, 2175−2187.
(323) Xu, L.; Wang, X.; Shan, S. *J. Comput. Chem.* **2013**, *34*, 2524−36.
(324) Azimi, S.; Rauk, A. *Int. J. Alzheimer's Dis.* **2011**, *2011*, 539762.
(325) Eury, H.; Bijani, C.; Faller, P.; Hureau, C. *Angew. Chem., Int. Ed.* **2011**, *50*, 901−905.
(326) Gunderson, W. A.; Hernandez-Guzman, J.; Karr, J. W.; Sun, L.; Szalai, V. A.; Warncke, K. *J. Am. Chem. Soc.* **2012**, *134*, 18330−7.
(327) Parthasarathy, S.; Long, F.; Miller, Y.; Xiao, Y.; McElheny, D.; Thurber, K.; Ma, B.; Nussinov, R.; Ishii, Y. *J. Am. Chem. Soc.* **2011**, *133*, 3390−400.
(328) Hureau, C.; Coppel, Y.; Dorlet, P.; Solari, P. L.; Sayen, S.; Guillon, E.; Sabater, L.; Faller, P. *Angew. Chem., Int. Ed.* **2009**, *48*, 9522−9525.
(329) Miller, Y.; Ma, B. Y.; Nussinov, R. *Coord. Chem. Rev.* **2012**, *256*, 2245−2252.
(330) Xu, L.; Wang, X. J.; Wang, X. C. *ACS Chem. Neurosci.* **2013**, *4*, 1458−1468.
(331) Chassaing, S.; Collin, F.; Dorlet, P.; Gout, J.; Hureau, C.; Faller, P. *Curr. Top. Med. Chem.* **2012**, *12*, 2573−2595.
(332) Alies, B.; Renaglia, E.; Rozga, M.; Bal, W.; Faller, P.; Hureau, C. *Anal. Chem.* **2013**, *85*, 1501−1518.
(333) Jiang, D.; Zhang, L.; Grant, G. P.; Dudzik, C. G.; Chen, S.; Patel, S.; Hao, Y.; Millhauser, G. L.; Zhou, F. *Biochemistry* **2013**, *52*, 547−56.
(334) Alies, B.; Badei, B.; Faller, P.; Hureau, C. *Chemistry* **2012**, *18*, 1161−1167.
(335) Xiao, Z.; Gottschlich, L.; van der Meulen, R.; Udagedara, S. R.; Wedd, A. G. *Metallomics* **2013**, *5*, 501−13.
(336) (a) Viles, J. H. *Coord. Chem. Rev.* **2012**, *256*, 2271−2284. (b) Miller, Y.; Ma, B.; Nussinov, R. *Proc. Natl. Acad. Sci. U.S.A.* **2010**, *107*, 9490−9495. (c) Mithu, V. S.; Sarkar, B.; Bhowmik, D.; Chandrakesan, M.; Maiti, S.; Madhu, P. K. *Biophys. J.* **2011**, *101*, 2825−32. (d) Garai, K.; Sahoo, B.; Kaushalya, S. K.; Desai, R.; Maiti, S. *Biochemistry* **2007**, *46*, 10655−63.

DOI: 10.1021/cr500638n
Chem. Rev. 2015, 115, 3518−3563

(337) Zhu, X.; Su, B.; Wang, X.; Smith, M. A.; Perry, G. *Cell. Mol. Life Sci.* **2007**, *64*, 2202−10.
(338) Cassagnes, L. E.; Herve, V.; Nepveu, F.; Hureau, C.; Faller, P.; Collin, F. *Angew. Chem., Int. Ed.* **2013**, *52*, 11110−3.
(339) La Penna, G.; Hureau, C.; Andreussi, O.; Faller, P. *J. Phys. Chem. B* **2013**, *117*, 16455−67.
(340) James, S. A.; Volitakis, I.; Adlard, P. A.; Duce, J. A.; Masters, C. L.; Cherny, R. A.; Bush, A. I. *Free Radical Biol. Med.* **2012**, *52*, 298−302.
(341) Ceccom, J.; Cosledan, F.; Halley, H.; Frances, B.; Lassalle, J. M.; Meunier, B. *PLoS One* **2012**, *7*, e43105.
(342) Rodriguez-Rodriguez, C.; Telpoukhovskaia, M.; Orvig, C. *Coord. Chem. Rev.* **2012**, *256*, 2308−2332.
(343) Crouch, P. J.; Barnham, K. J. *Acc. Chem. Res.* **2012**, *45*, 1604−11.
(344) Pithadia, A. S.; Lim, M. H. *Curr. Opin. Chem. Biol.* **2012**, *16*, 67−73.
(345) You, H.; Tsutsui, S.; Hameed, S.; Kannanayakal, T. J.; Chen, L.; Xia, P.; Engbers, J. D.; Lipton, S. A.; Stys, P. K.; Zamponi, G. W. *Proc. Natl. Acad. Sci. U.S.A.* **2012**, *109*, 1737−1742.
(346) Snyder, E. M.; Nong, Y.; Almeida, C. G.; Paul, S.; Moran, T.; Choi, E. Y.; Nairn, A. C.; Salter, M. W.; Lombroso, P. J.; Gouras, G. K.; Greengard, P. *Nat. Neurosci.* **2005**, *8*, 1051−1058.
(347) Renner, M.; Lacor, P. N.; Velasco, P. T.; Xu, J.; Contractor, A.; Klein, W. L.; Triller, A. *Neuron* **2010**, *66*, 739−754.
(348) Cisse, M.; Halabisky, B.; Harris, J.; Devidze, N.; Dubal, D. B.; Sun, B.; Orr, A.; Lotz, G.; Kim, D. H.; Hamto, P.; Ho, K.; Yu, G. Q.; Mucke, L. *Nature* **2011**, *469*, 47−52.
(349) Yanagisawa, K.; Ihara, Y. *Neurobiol. Aging.* **1998**, *19* (Suppl. 1), S65−67.
(350) Yerbury, J. J.; Poon, S.; Meehan, S.; Thompson, B.; Kumita, J. R.; Dobson, C. M.; Wilson, M. R. *FASEB J.* **2007**, *21*, 2312−2322.
(351) Narayan, P.; Orte, A.; Clarke, R. W.; Bolognesi, B.; Hook, S.; Ganzinger, K. A.; Meehan, S.; Wilson, M. R.; Dobson, C. M.; Klenerman, D. *Nat. Struct. Mol. Biol.* **2011**, *19*, 79−83.
(352) Stanyon, H. F.; Viles, J. H. *J. Biol. Chem.* **2012**, *287*, 28163−28168.
(353) Likó, I.; Mák, M.; Klement, É.; Hunyadi-Gulyás, É.; Pázmány, T.; Medzihradszky, K. F.; Urbányi, Z. *Neurosci. Lett.* **2007**, *412*, 51−55.
(354) Andreetto, E.; Yan, L.-M.; Tatarek-Nossol, M.; Velkova, A.; Frank, R.; Kapurniotu, A. *Angew. Chem., Int. Ed.* **2010**, *49*, 3081−3085.
(355) Buxbaum, J. N.; Ye, Z.; Reixach, N.; Friske, L.; Levy, C.; Das, P.; Golde, T.; Masliah, E.; Roberts, A. R.; Bartfai, T. *Proc. Natl. Acad. Sci. U.S.A.* **2008**, *105*, 2681−2686.
(356) Coria, F.; Castano, E.; Prelli, F.; Larrondo-Lillo, M.; Van Duinen, S.; Shelanski, M.; Frangione, B. *Lab. Invest.* **1988**, *58*, 454−458.
(357) Dohler, F.; Sepulveda-Falla, D.; Krasemann, S.; Altmeppen, H.; Schluter, H.; Hildebrand, D.; Zerr, I.; Matschke, J.; Glatzel, M. *Brain* **2014**, *137*, 873−876.
(358) Kuperstein, I.; Broersen, K.; Benilova, I.; Rozenski, J.; Jonckheere, W.; Debulpaep, M.; Vandersteen, A.; Segers-Nolten, I.; Van Der Werf, K.; Subramaniam, V.; Braeken, D.; Callewaert, G.; Bartic, C.; D'Hooge, R.; Martins, I. C.; Rousseau, F.; Schymkowitz, J.; De Strooper, B. *EMBO J.* **2010**, *29*, 3408−3420.
(359) Jan, A.; Gokce, O.; Luthi-Carter, R.; Lashuel, H. A. *J. Biol. Chem.* **2008**, *283*, 28176−89.
(360) Gimbel, D. A.; Nygaard, H. B.; Coffey, E. E.; Gunther, E. C.; Lauren, J.; Gimbel, Z. A.; Strittmatter, S. M. *J. Neurosci.* **2010**, *30*, 6367−6374.
(361) Gunther, E. C.; Strittmatter, S. M. *J. Mol. Med.* **2010**, *88*, 331−338.
(362) Chen, S.; Yadav, S. P.; Surewicz, W. K. *J. Biol. Chem.* **2010**, *285*, 26377−26383.
(363) Balducci, C.; Beeg, M.; Stravalaci, M.; Bastone, A.; Sclip, A.; Biasini, E.; Tapella, L.; Colombo, L.; Manzoni, C.; Borsello, T.; Chiesa, R.; Gobbi, M.; Salmona, M.; Forloni, G. *Proc. Natl. Acad. Sci. U.S.A.* **2010**, *107*, 2295−2300.
(364) Calella, A. M.; Farinelli, M.; Nuvolone, M.; Mirante, O.; Moos, R.; Falsig, J.; Mansuy, I. M.; Aguzzi, A. *EMBO Mol. Med.* **2010**, *2*, 306−310.
(365) Kessels, H. W.; Nguyen, L. N.; Nabavi, S.; Malinow, R. *Nature* **2010**, *466*, E3−E4. Laurén, J.; Gimbel, D. A.; Nygaard, H. B.; Gilbert, J. W.; Strittmatter, S. M. *Nature* **2010**, *466*, E4−E5.
(366) Cisse, M.; Sanchez, P. E.; Kim, D. H.; Ho, K.; Yu, G. Q.; Mucke, L. *J. Neurosci.* **2011**, *31*, 10427−10431.
(367) Freir, D. B.; Nicoll, A. J.; Klyubin, I.; Panico, S.; Mc Donald, J. M.; Risse, E.; Asante, E. A.; Farrow, M. A.; Sessions, R. B.; Saibil, H. R.; Clarke, A. R.; Rowan, M. J.; Walsh, D. M.; Collinge, J. *Nat. Commun.* **2011**, *2*, 336.
(368) Barry, A. E.; Klyubin, I.; Mc Donald, J. M.; Mably, A. J.; Farrell, M. A.; Scott, M.; Walsh, D. M.; Rowan, M. J. *J; Neurosci.* **2011**, *31*, 7259−7263.
(369) Um, J. W.; Nygaard, H. B.; Heiss, J. K.; Kostylev, M. A.; Stagi, M.; Vortmeyer, A.; Wisniewski, T.; Gunther, E. C.; Strittmatter, S. M. *Nat. Neurosci.* **2012**, *15*, 1227−1235.
(370) Bate, C.; Williams, A. *J. Biol. Chem.* **2011**, *286*, 37955−37963.
(371) Kudo, W.; Lee, H. P.; Zou, W. Q.; Wang, X.; Perry, G.; Zhu, X.; Smith, M. A.; Petersen, R. B.; Lee, H. G. *Hum. Mol. Genet.* **2012**, *21*, 1138−44.
(372) Nicoll, A. J.; Panico, S.; Freir, D. B.; Wright, D.; Terry, C.; Risse, E.; Herron, C. E.; O'Malley, T.; Wadsworth, J. D.; Farrow, M. A.; Walsh, D. M.; Saibil, H. R.; Collinge, J. *Nat. Commun.* **2013**, *4*, 2416.
(373) Zou, W. Q.; Xiao, X.; Yuan, J.; Puoti, G.; Fujioka, H.; Wang, X.; Richardson, S.; Zhou, X.; Zou, R.; Li, S. *J. Biol. Chem.* **2011**, *286*, 15095−15105.
(374) Ferrer, I.; Blanco, R.; Carmona, M.; Puig, B.; Ribera, R.; Rey, M.; Ribalta, T. *Acta Neuropathol.* **2001**, *101*, 49−56.
(375) Krieger, J.; Fusco, G.; Lewitzky, M.; Simister, P. C.; Marchant, J.; Camilloni, C.; Feller, S. M.; De Simone, A. *Biophys. J.* **2014**, *106*, 1771−1779.
(376) (a) Derreumaux, P. *Biophys. J.* **2001**, *81*, 1657−65. (b) Santini, S.; Claude, J. B.; Audic, S.; Derreumaux, P. *Proteins* **2003**, *51*, 258−65. (c) Santini, S.; Derreumaux, P. *Cell. Mol. Life Sci.* **2004**, *61*, 951−60.
(377) Gallion, S. L. *PLoS One* **2012**, *7*, e49375.
(378) Chebaro, Y.; Derreumaux, P. *J. Phys. Chem. B* **2009**, *113*, 6942−6948.
(379) Barducci, A.; Chelli, R.; Procacci, P.; Schettino, V.; Gervasio, F. L.; Parrinello, M. *J. Am. Chem. Soc.* **2006**, *128*, 2705−2710.
(380) De Simone, A.; Dodson, G. G.; Fraternali, F.; Zagari, A. *FEBS Lett.* **2006**, *580*, 2488−2894.
(381) Cobb, N. J.; Apostol, M. I.; Chen, S.; Smirnovas, V.; Surewicz, W. K. *J. Biol. Chem.* **2014**, *289*, 2643−2650.
(382) Cordeiro, Y.; Kraineva, J.; Ravindra, R.; Lima, L. M.; Gomes, M. P.; Foguel, D.; Winter, R.; Silva, J. L. *J. Biol. Chem.* **2004**, *279*, 32354−32359.
(383) De Simone, A.; Zagari, A.; Derreumaux, P. *Biophys. J.* **2007**, *93*, 1284−1292.
(384) Eghiaian, F.; Daubenfeld, T.; Quenet, Y.; van Audenhaege, M.; Bouin, A. P.; van der Rest, G.; Grosclaude, J.; Rezaei, H. *Proc. Natl. Acad. Sci. U.S.A.* **2007**, *104*, 7414−7419.
(385) Schwarzinger, S.; Horn, A. H.; Ziegler, J.; Sticht, H. *J. Biomol. Struct. Dyn.* **2006**, *23*, 581−590.
(386) Khosravani, H.; Zhang, Y.; Tsutsui, S.; Hameed, S.; Altier, C.; Hamid, J.; Chen, L.; Villemaire, M.; Ali, Z.; Jirik, F. R.; Zamponi, G. W. *J. Cell. Biol.* **2008**, *181*, 551−565.
(387) Sarell, C. J.; Syme, C. D.; Rigby, S. E.; Viles, J. H. *Biochemistry* **2009**, *48*, 4388−4402.
(388) Hu, N. W.; Nicoll, A. J.; Zhang, D.; Mably, A. J.; O'Malley, T.; Purro, S. A.; Terry, C.; Collinge, J.; Walsh, D. M.; Rowan, M. J. *Nat. Commun.* **2014**, *5*, 3374.
(389) Chen, X.; Lin, R.; Chang, L.; Xu, S.; Wei, X.; Zhang, J.; Wang, C.; Anwyl, R.; Wang, Q. *Neuroscience* **2013**, *253*, 435−443.
(390) Kessels, H. W.; Nabavi, S.; Malinow, R. *Proc. Natl. Acad. Sci. U.S.A.* **2013**, *110*, 4033−4038.

DOI: 10.1021/cr500638n
Chem. Rev. 2015, 115, 3518−3563

(391) Mota, S. I.; Ferreira, I. L.; Pereira, C.; Oliveira, C. R.; Rego, A. C. *Curr. Alzheimer Res.* **2012**, *9*, 844−856.
(392) Brito-Moreira, J.; Paula-Lima, A. C.; Bomfim, T. R.; Oliveira, F. B.; Sepulveda, F. J.; De Mello, F. G.; Aguayo, L. G.; Panizzutti, R.; Ferreira, S. T. *Curr. Alzheimer Res.* **2011**, *8*, 552−562.
(393) Sleegers, K.; Lambert, J. C.; Bertram, L.; Cruts, M.; Amouyel, P.; Van Broeckhoven, C. *Trends Genet.* **2010**, *26*, 84−93.
(394) Narayan, P.; Meehan, S.; Carver, J. A.; Wilson, M. R.; Dobson, C. M.; Klenerman, D. *Biochemistry* **2012**, *51*, 9270−9276.
(395) Humphreys, D. T.; Carver, J. A.; Easterbrook-Smith, S. B.; Wilson, M. R. *J. Biol. Chem.* **1999**, *274*, 6875−81.
(396) Wyatt, A. R.; Yerbury, J. J.; Poon, S.; Wilson, M. R. *Curr. Med. Chem.* **2009**, *16*, 2855−2866.
(397) Wyatt, A. R.; Yerbury, J. J.; Wilson, M. R. *J. Biol. Chem.* **2009**, *284*, 21920−21927.
(398) Wyatt, A. R.; Yerbury, J. J.; Berghofer, P.; Greguric, I.; Katsifis, A.; Dobson, C. M.; Wilson, M. R. *Cell. Mol. Life Sci.* **2011**, *68*, 3919−3931.
(399) Biere, A. L.; Ostaszewski, B.; Stimson, E. R.; Hyman, B. T.; Maggio, J. E.; Selkoe, D. J. *J. Biol. Chem.* **1996**, *271*, 32916−32922.
(400) Kuo, Y.-M.; Kokjohn, T. A.; Kalback, W. M.; Luehrs, D.; Galasko, D. R.; Chevallier, N.; Koo, E. H.; Emmerling, M. R.; Roher, A. E. *Biochem. Biophys. Res. Commun.* **2000**, *268*, 750−756.
(401) Seubert, P.; Vigo-Pelfrey, C.; Esch, F.; Lee, M.; Dovey, H.; Davis, D.; Sinha, S.; Schiossmacher, M.; Whaley, J.; Swindlehurst, C. *Nature* **1992**, *359*, 325−327.
(402) Lame, M. E.; Chambers, E. E.; Blatnik, M. *Anal. Biochem.* **2011**, *419*, 133−139.
(403) Stevens, R.; Elmendorf, D.; Gourlay, M.; Stroebel, E.; Gaafar, H. *J. Clin. Microbiol.* **1979**, *10*, 346−50.
(404) Rózga, M.; Kloniecki, M.; Jablonowska, A.; Dadlez, M.; Bal, W. *Biochem. Biophys. Res. Commun.* **2007**, *364*, 714−718.
(405) Bohrmann, B.; Tjernberg, L.; Kuner, P.; Poli, S.; Levet-Trafit, B.; Näslund, J.; Richards, G.; Huber, W.; Döbeli, H.; Nordstedt, C. *J. Biol. Chem.* **1999**, *274*, 15990−15995.
(406) Milojevic, J.; Esposito, V.; Das, R.; Melacini, G. *J. Am. Chem. Soc.* **2007**, *129*, 4282−4290.
(407) Milojevic, J.; Melacini, G. *Biophys. J.* **2011**, *100*, 183−192.
(408) (a) Garg, A.; Manidhar, D. M.; Gokara, M.; Mlleda, C.; Reddy, C. S.; Subramanyam, R. *PLoS One* **2013**, *8* (5), e63805. (b) Raz, Y.; Miller, Y. *PLoS One* **2013**, *8*, e73303.
(409) Mullard, A. *Nat. Rev. Drug Discovery* **2012**, *11*, 657−660.
(410) Pujadas, L.; Rossi, D.; Andrés, R.; Teixeira, C. M.; Serra-Vidal, B.; Parcerisas, A.; Maldonado, R.; Giralt, E.; Crulla, N.; Soriano, E. *Nat. Commun.* **2014**, *5*, 3443 DOI: 10.1038/ncomms4443.
(411) Pratim Bose, P.; Chatterjee, U.; Nerelius, C.; Govender, T.; Norström, T.; Gogoll, A.; Sandegren, A.; Göthelid, E.; Johansson, J.; Arvidsson, P. I. *J. Med. Chem.* **2009**, *52*, 8002−8009.
(412) Amijee, H.; Bate, C.; Williams, A.; Virdee, J.; Jeggo, R.; Spanswick, D.; Scopes, D. I. C.; Mazzitelli, J.; Doig, A. *Biochemistry* **2012**, *51*, 8338−8352.
(413) Hopping, G.; Kellock, J.; Barnwal, R. P.; Law, P.; Bryers, J.; Varani, G.; Caughey, B.; Daggett, V. *Elife* **2014**, *3*, e01681.
(414) Bieschke, J.; Herbst, M.; Wiglenda, T.; Friedrich, R. P.; Boeddrich, A.; Schiele, F.; Kleckers, D.; Lopez del Amo, J. M.; Grüning, B. A.; Wang, Q.; Schmidt, M. R.; Lurz, R.; Anwyl, R.; Schnoegl, S.; Fändrich, M.; Frank, R. F.; Reif, B.; Günter, S.; Walsh, D. M.; Wanker, E. E. *Nat. Chem. Biol.* **2012**, *8*, 93−101.
(415) Richard, T.; Poupard, P.; Nassra, M.; Papastamoulis, Y.; Iglésias, M. L.; Krisa, S.; Waffo-Teguo, P.; Mérillon, J. M.; Monti, J. P. *Bioorg. Med. Chem.* **2011**, *19*, 3152−3155.
(416) Richard, T.; Papastamoulis, Y.; Waffo-Teguo, P.; Monti, J. P. *Biochim. Biophys. Acta, Gen. Subj.* **2013**, *1830* (11), 5068−5074.
(417) Ehrnhoefer, D. E.; Bieschke, J.; Boeddrich, A.; Herbst, M.; Masino, L.; Lurz, R.; Engemann, S.; Pastore, A.; Wanker, E. E. *Nat. Struct. Mol. Biol.* **2008**, *15*, 558−566.
(418) Bieschke, J.; Russ, J.; Friedrich, R. P.; Ehrnhoefer, D. E.; Wobst, H.; Neugebauer, K.; Wanker, E. E. *Proc. Natl. Acad. Sci. U.S.A.* **2010**, *107*, 7710−7715.
(419) Wang, S.-H.; Liu, F. F.; Dong, X. Y.; Sun, Y. *J. Phys. Chem. B* **2010**, *114*, 11576−11583.
(420) Liu, F.-F.; Dong, X. Y.; He, L.; Middelberg, A. P.; Sun, Y. *J. Phys. Chem. B* **2011**, *115*, 11879−11887.
(421) Lopez del Amo, J. M.; Fink, U.; Dasari, M.; Grelle, G.; Wanker, E. E.; Bieschke, J.; Reif, B. *J. Mol. Biol.* **2012**, *421* (4−5), 517−524.
(422) Attanasio, F.; Convertino, M.; Magno, A.; Caflisch, A.; Corazza, A.; Harridas, H.; Esposito, G.; Cataldo, S.; Pignataro, B.; Milardi, D.; Rizzarelli, E. *ChemBioChem* **2013**, *14*, 583−592.
(423) Arai, T.; Araya, T.; Sasaki, D.; Taniguchi, A.; Sato, T.; Sohma, Y.; Kanai, M. *Angew. Chem., Int. Ed.* **2014**, *53*, 8236−8239.
(424) Sato, M.; Murakami, K.; Uno, M.; Nakagawa, Y.; Katayama, S.; Akagi, K.; Masuda, Y.; Takegoshi, K.; Irie, K. *J. Biol. Chem.* **2013**, *288*, 23212−23214.
(425) Palhano, F. L.; Lee, J.; Grimster, N. P.; Kelly, J. W. *J. Am. Chem. Soc.* **2013**, *135*, 7503−7510.
(426) Tomiyama, T.; Kaneko, H.; Kataoka, K. I.; Asano, S.; Endo, N. *Biochem. J.* **1997**, *322*, 859−865.
(427) Pickhardt, M.; Gazova, Z.; von Bergen, M.; Khlistunova, I.; Wang, Y.; Hascher, A.; Mandelkow, E. M.; Biernat, J.; Mandelkow, E. *J. Biol. Chem.* **2005**, *280*, 3628−3635.
(428) Necula, M.; Kayed, R.; Milton, S.; Glabe, C. G. *J. Biol. Chem.* **2007**, *282*, 10311−10324.
(429) Scherzer-Attali, R.; Pellarin, R.; Convertino, M.; Frydman-Marom, A.; Egoz-Matia, N.; Peled, S.; Levy-Sakin, M.; Shalev, D. E.; Caflisch, A.; Gazit, E.; Segal, D. *PLoS One* **2010**, *5*, e11101.
(430) Convertino, M.; Vitalis, A.; Caflisch, A. *J. Biol. Chem.* **2011**, *286*, 41578−41588.
(431) Scherzer-Attali, R.; Convertino, M.; Pellarin, R.; Gazit, E.; Segal, D.; Caflisch, A. *J. Phys. Chem. B* **2013**, *117*, 1780−1789.
(432) Zhang, T.; Xu, W.; Mu, Y.; Derreumaux, P. *ACS Chem. Neurosci.* **2013**, *5*, 148−159.
(433) Brenke, R.; Kozakov, D.; Chuang, G. Y.; Beglov, D.; Hall, D.; Landon, M. R.; Mattos, C.; Vajda, S. *Bioinformatics* **2009**, *25*, 621−627.
(434) McGann, M. *J. Chem. Inf. Model.* **2011**, *51*, 578−596.
(435) Kroth, H.; Ansaloni, A.; Varisco, Y.; Jan, A.; Sreenivasachary, N.; Rezaei-Ghaleh, N.; Giriens, V.; Lohmann, S.; Lopez-Deber, M. P.; Adolfsson, O.; Pihlgren, M.; Paganetti, P.; Froestl, W.; Nagel-Steger, L.; Willbold, D.; Schrader, T.; Zweckstetter, M.; Pfeifer, A.; Lashuel, H. A.; Muhs, A. *J. Biol. Chem.* **2012**, *287*, 34786−34800.
(436) Connors, C. R.; Rosenman, D. J.; Lopes, D. H.; Mittal, S.; Bitan, G.; Sorci, M.; Belfort, G.; Garcia, A.; Wang, C. *Biochemistry* **2013**, *52*, 3995−4002.
(437) Tarus, B.; Nguyen, P. H.; Berthoumieu, O.; Faller, P.; Doig, A. J.; Derreumaux, P. *Eur. J. Med. Chem.* **2015**, *91*, 43−50 DOI: 10.1016/j.ejmech.2014.07.002.
(438) Novick, P. A.; Lopes, D. H.; Branson, K. M.; Esteras-Chopo, A.; Graef, I. A.; Bitan, G.; Pande, V. S. *J. Med. Chem.* **2012**, *55*, 3002−3010.
(439) Stefanova, N. A.; Muraleva, N. A.; Korbolina, E. E.; Kiseleva, E.; Maksimova, K. Y.; Kolosova, N. G. *Oncotarget* **2015**, *6*, 1396−413.
(440) Alzheimer Disease & Frontotemporal Dementia Mutation Database. http://www.molgen.ua.ac.be/admutations/ (accessed Mar 17, 2015).
(441) Rovelet-Lecrux, A.; Tuominen, H.; Majamaa, K.; Campion, D.; Remes, A. M. *J. Neurol., Neurosurg. Psychiatry* **2007**, *78*, 1158−1159.
(442) St George-Hyslop, P. H. *Biol. Psychiatry* **2000**, *47*, 183−199.
(443) Levy, E.; Carman, M. D.; Fernandez-Madrid, I. J.; Power, M. D.; Lieberburg, I.; van Duinen, S. G.; Bots, G. T.; Luyendijk, W.; Frangione, B. *Science* **1990**, *248*, 1124−1126.
(444) Kaden, D.; Harmeier, A.; Weise, C.; Munter, L. M.; Althoff, V.; Rost, B. R.; Hildebrand, P. W.; Schmitz, D.; Schaefer, M.; Lurz, R.; Skodda, S.; Yamamoto, R.; Arlt, S.; Finckh, U.; Multhaup, G. *EMBO Mol. Med.* **2012**, *4*, 647−659.
(445) Nomura, S.; Umeda, T.; Tomiyama, T.; Mori, H. *J. Neurosci. Res.* **2013**, *91*, 1541−1550.
(446) Shimizu, T.; Fukuda, H.; Murayama, S.; Izumiyama, N.; Shirasawa, T. *J. Neurosci. Res.* **2002**, *70*, 451−461.

DOI: 10.1021/cr500638n
Chem. Rev. 2015, 115, 3518−3563

(447) Hashimoto, Y.; Matsuoka, M. *J. Neurochem.* **2014**, *130* (2), 291−300.
(448) Qahwash, I.; Weiland, K. L.; Lu, Y.; Sarver, R. W.; Kletzien, R. F.; Yan, R. *J. Biol. Chem.* **2003**, *278*, 23187−23195.
(449) Moskovitz, J.; Maiti, P.; Lopes, D. H.; Oien, D. B.; Attar, A.; Liu, T.; Mittal, S.; Hayes, J.; Bitan, G. *Biochemistry* **2011**, *50*, 10687−10697.
(450) Harmeier, A.; Wozny, C.; Rost, B. R.; Munter, L. M.; Hua, H.; Georgiev, O.; Beyermann, M.; Hildebrand, P. W.; Weise, C.; Schaffner, W.; Schmitz, D.; Multhaup, G. *J. Neurosci.* **2009**, *29*, 7582−7590.
(451) Kim, W.; Hecht, M. H. *J. Mol. Biol.* **2008**, *377*, 565−574.
(452) Kim, W.; Hecht, M. H. *Proc. Natl. Acad. Sci. U.S.A.* **2006**, *103*, 15824−15829.
(453) Sandebring, A.; Welander, H.; Winblad, B.; Graff, C.; Tjernberg, L. O. *PLoS One* **2013**, *8*, e55847.
(454) Conicella, A. E.; Fawzi, N. L. *Biochemistry* **2014**, *53*, 3095−105.
(455) Messa, M.; Colombo, L.; del Favero, E.; Cantù, L.; Stoilova, T.; Cagnotto, A.; Rossi, A.; Morbin, M.; Di Fede, G.; Tagliavini, F.; Salmona, M. *J. Biol. Chem.* **2014**, *289*, 24143−24152.
(456) Liu, Y. W.; He, Y. H.; Zhang, Y. X.; Cai, W. W.; Yang, L. Q.; Xu, L. Y.; Kong, Q. P. *Neurobiol. Aging* **2014**, *35*, 935.e11−e12.
(457) Bamne, M. N.; Demirci, F. Y.; Berman, S.; Snitz, B. E.; Rosenthal, S. L.; Wang, X.; Lopez, O. L.; Kamboh, L. I. *Neurobiol. Aging* **2014**, *35*, 1779e15−e16.
(458) Benilova, I.; Gallardo, R.; Ungureanu, A. A.; Castillo Cano, V.; Snellinx, A.; Ramakers, M.; Bartic, C.; Rousseau, F.; Schymkowitz, J.; De Strooper, B. *J. Biol. Chem.* **2014**, *289*, 30977−30989.
(459) Maloney, J. A.; Bainbridge, T.; Gustafson, A.; Zhang, S.; Kyauk, R.; Steiner, P.; van der Brug, M.; Liu, Y.; Ernst, J. A.; Watts, R. J.; Atwal, J. K. *J. Biol. Chem.* **2014**, *289*, 30990−31000.
(460) Coskuner, O.; Wise-Scira, O.; Perry, G.; Kitahara, T. *ACS Chem. Neurosci.* **2013**, *4*, 310−320.
(461) Baumketner, A.; Krone, M. G.; Shea, J.-E. *Proc. Natl. Acad. Sci. U.S.A.* **2008**, *105*, 6027−6032.
(462) Huet, A.; Derreumaux, P. *Biophys. J.* **2006**, *91*, 3829−3840.
(463) Okamoto, A.; Yano, A.; Nomura, K.; Higai, S.; Kurita, N. *J. Mol. Graphics Modell.* **2014**, *50*, 113−124.
(464) Viet, M. H.; Nguyen, P. H.; Ngo, S. T.; Li, M. S.; Derreumaux, P. *ACS Chem. Neurosci.* **2013**, *4*, 1446−1457.
(465) Viet, M. H.; Nguyen, P. H.; Derreumaux, P.; Li, M. S. *ACS Chem. Neurosci.* **2014**, *5*, 646−657.
(466) Truong, P. M.; Viet, M. H.; Nguyen, P. H.; Hu, C. K.; Li, M. S. *J. Phys. Chem. B* **2014**, *118*, 8972−8981.
(467) Takeda, T.; Klimov, D. K. *J. Phys. Chem. B* **2009**, *113*, 11848−11857.
(468) Lu, Y.; Wei, G.; Derreumaux, P. *J. Phys. Chem. B* **2011**, *115*, 1282−1288.
(469) Brown, A. M.; Lemkul, J. A.; Schaum, N.; Bevan, D. R. *Arch. Biochem. Biophys.* **2014**, *545*, 44−52.
(470) Yano, A.; Okamoto, A.; Nomura, K.; Higai, S.; Kurita, N. *Chem. Phys. Lett.* **2014**, *595*, 242−249.
(471) Anand, P.; Nandel, F. S.; Hansmann, U. H. *J. Chem. Phys.* **2008**, *128*, 165102.
(472) Anand, P.; Nandel, F. S.; Hansmann, U. H. *J. Chem. Phys.* **2008**, *129*, 195102.
(473) Nguyen, P. H.; Tarus, B.; Derreumaux, P. *J. Phys. Chem. B* **2014**, *118*, 501−510.
(474) Meral, D.; Urbanc, B. *J. Mol. Biol.* **2013**, *425*, 2260−2275.
(475) Gillman, A. L.; Jang, H.; Lee, J.; Ramachandran, S.; Kagan, B. L.; Nussinov, R.; Teran Arce, F. *J. Phys. Chem. B* **2014**, *118*, 7335−7344.
(476) Lee, J.; Gillman, A. L.; Jang, H.; Ramachandran, S.; Kagan, B. L.; Nussinov, R.; Teran Arce, F. *Biochemistry* **2014**, *53*, 4704−4714.
(477) Zhuravlev, P. I.; Reddy, G.; Straub, J. E.; Thirumalai, D. *J. Mol. Biol.* **2014**, *426*, 2653−2666.
(478) Liang, C.; Ni, R.; Smith, J. E.; Childers, W. S.; Mehta, A. K.; Lynn, D. G. *J. Am. Chem. Soc.* **2014**, *136*, 15146−14149.
(479) Baell, J.; Walters, M. A. *Nature* **2014**, *513*, 481−483.
(480) Ingólfsson, H. I.; Thakur, P.; Herold, K. F.; Hobart, E. A.; Ramsey, N. B.; Periole, X.; de Jong, D. H.; Zwama, M.; Yilmaz, D.; Hall, K.; Maretzky, T.; Hemmings, H. C., Jr; Blobel, C.; Marrink, S. J.; Koçer, A.; Sack, J. T.; Andersen, O. S. *ACS Chem. Biol.* **2014**, *9*, 1788−1798.
(481) Lesné, S. E.; Sherman, M. A.; Grant, M.; Kuskowski, M.; Schneider, J. A.; Bennett, D. A.; Ashe, K. H. *Brain* **2013**, *136*, 1383−1398.
(482) Hamilton-Brown, P.; Bekard, I.; Ducker, W. A.; Dunstan, D.; Dave, E. *J. Phys. Chem. B* **2008**, *112*, 16249−16251.
(483) Dunstan, D.; Hamilton-Brown, P.; Asimakis, P.; Duckerand, W.; Bertolini, J. *Protein Eng., Des Sel* **2009**, *22*, 741−746.
(484) Lee, C.; Bird, S.; Shaw, M.; Jean, L.; Vaux, D. J. *J. Biol. Chem.* **2012**, *287*, 38006−38019.
(485) Gruebele, M.; Thirumalai, D. *J. Chem. Phys.* **2013**, *139*, 121701.
(486) Esbjörner, E. K.; Chan, F.; Rees, E.; Erdelyi, M.; Luheshi, L. M.; Bertoncini, C. W.; Kaminski, C. F.; Dobson, C. M.; Kaminski Schierle, G. S. *Chem. Biol.* **2014**, *21*, 732742.
(487) Li, C.; Charlton, L. M.; Lakkavaram, A.; Seale, C.; Wang, G.; Young, G. B.; MacDonald, J. M.; Pielak, G. J. *J. Am. Chem. Soc.* **2008**, *130*, 6310−6311.
(488) Li, C.; Liu, M. *FEBS Lett.* **2013**, *587*, 1008−1011.
(489) Lu, P.; Bai, X. C.; Ma, D.; Xie, T.; Yan, C.; Sun, L.; Yang, G.; Zhao, Y.; Zhou, R.; Scheres, S. H.; Shi, Y. *Nature* **2014**, *512*, 166.
(490) Dominguez, L.; Foster, L.; Meredith, S. C.; Straub, J. E.; Thirumalai, D. *J. Am. Chem. Soc.* **2014**, *136*, 9619−9626.

DOI: 10.1021/cr500638n
Chem. Rev. 2015, 115, 3518−3563